AD-A045 649 AIR FORCE MATERIALS LAB WRIGHT-PATTERSON AFB OHIO F/G 20/3
LUMINESCENCE AND HALL EFFECT OF ION IMPLANTED LAYERS IN ZNO.(U)
OCT 76 B J PIERCE
UNCLASSIFIED AFML-TR-75-161 NL

1 OF 2
AD A045649

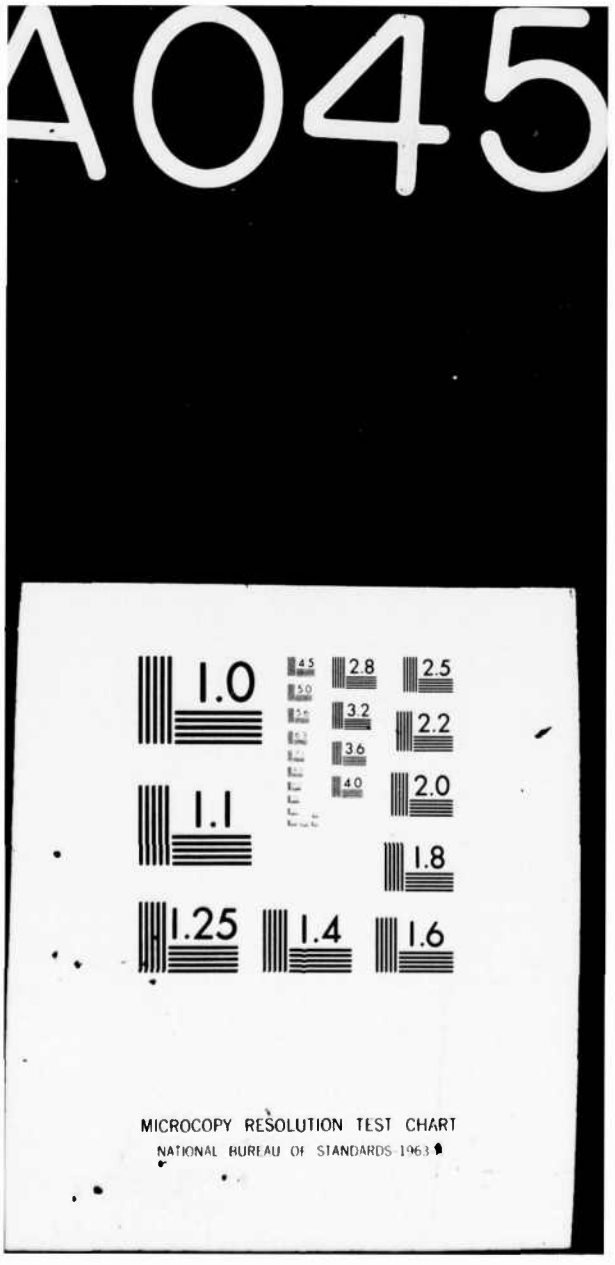
A045
1.0
1.1
1.25
1.4
1.6
2.8
2.5
2.2
2.0
1.8
MICROCOPY RESOLUTION TEST CHART
NATIONAL BUREAU OF STANDARDS 1963

(14) AFML-TR-75-161

13 2

(6) # LUMINESCENCE AND HALL EFFECT OF ION IMPLANTED LAYERS IN ZnO

Laser and Optical Materials Branch
Electromagnetic Materials Division

(10) Bruce J. Pierce

(16) 7367

(11) Oct[redacted]76

(12) 177p.

(17) ϕ3

TECHNICAL REPORT AFML-TR-75-161

(9) Final Report, [redacted] Sep[redacted]70 - Sep[redacted]74,

Approved for Public Release; Distribution Unlimited

61102F

AIR FORCE MATERIALS LABORATORY
AIR FORCE WRIGHT AERONAUTICAL LABORATORIES
AIR FORCE SYSTEMS COMMAND
WRIGHT-PATTERSON AIR FORCE BASE, OHIO 45433

012 320

NOTICE

When Government drawings, specifications, or other data are used for any purpose other than in connection with a definitely related Government procurement operation, the United States Government thereby incurs no responsibility nor any obligation whatsoever; and the fact that the government may have formulated, furnished, or in any way supplied the said drawings, specifications, or other data, is not to be regarded by implication or otherwise as in any manner licensing the holder or any other person or corporation, or conveying any rights or permission to manufacture, use, or sell any patented invention that may in any way be related thereto.

This technical report has been reviewed and is approved for publication.

PATRICK M. HEMENGER

BRUCE J. PIERCE

WILLIAM G.D. FREDERICK, Chief
Laser & Optical Materials Branch
Electromagnetic Materials Division

Copies of this report should not be returned unless return is required by security considerations, contractual obligations, or notice on a specific document.

AIR FORCE/56780/28 September 1977 — 150

UNCLASSIFIED

SECURITY CLASSIFICATION OF THIS PAGE (When Data Entered)

REPORT DOCUMENTATION PAGE	READ INSTRUCTIONS BEFORE COMPLETING FORM
1. REPORT NUMBER: AFML-TR-75-161	2. GOVT ACCESSION NO.
3. RECIPIENT'S CATALOG NUMBER	
4. TITLE (and Subtitle): LUMINESCENCE AND HALL EFFECT OF ION IMPLANTED LAYERS IN ZNO	5. TYPE OF REPORT & PERIOD COVERED: AFIT Dissertation
6. PERFORMING ORG. REPORT NUMBER	
7. AUTHOR(s): Bruce J. Pierce, Captain USAF	8. CONTRACT OR GRANT NUMBER(s)
9. PERFORMING ORGANIZATION NAME AND ADDRESS: Air Force Materials Laboratory, WPAFB, Ohio 45433	10. PROGRAM ELEMENT, PROJECT, TASK AREA & WORK UNIT NUMBERS: 7367-0383
11. CONTROLLING OFFICE NAME AND ADDRESS: Air Force Materials Laboratory, WPAFB, Ohio 45433	12. REPORT DATE: October 1976
	13. NUMBER OF PAGES: 178
14. MONITORING AGENCY NAME & ADDRESS(if different from Controlling Office): Air Force Institute of Technology (AFIT-EN) WPAFB, Ohio 45433	15. SECURITY CLASS. (of this report): Unclassified
	15a. DECLASSIFICATION/DOWNGRADING SCHEDULE

16. DISTRIBUTION STATEMENT (of this Report)

Approved for public release, distribution unlimited.

DDC RECEIVED OCT 26 1977 B

17. DISTRIBUTION STATEMENT (of the abstract entered in Block 20, if different from Report)

18. SUPPLEMENTARY NOTES

19. KEY WORDS (Continue on reverse side if necessary and identify by block number)

Luminescence
Hall Effect
Ion Implantation
Zinc Oxide

20. ABSTRACT (Continue on reverse side if necessary and identify by block number)

An experimental investigation was conducted on implanted layers of Li, Na, N, P, and Ne in ZnO substrates. The primary experimental method used was cathodoluminescence, and it was found that it was possible to probe an implanted layer by varying the beam voltage of the exciting electrons. A comparison of calculated implantation profiles with semi-quantitative electron profiles showed that fair agreement existed between these theoretical profiles and the depth-resolved cathodoluminescence results. The electrical

→ next page

DD FORM 1 JAN 73 1473 EDITION OF 1 NOV 65 IS OBSOLETE

UNCLASSIFIED

SECURITY CLASSIFICATION OF THIS PAGE (When Data Entered)

properties of the implanted layers were obtained using the van der Pauw technique, and a photoluminescence system incorporating a nitrogen laser was used to perform time-resolved spectroscopy. Optical evidence of a shallow acceptor center in ZnO was revealed for the first time in the cathodoluminescent spectra obtained from implanted samples of ZnO, however, no evidence of type conversion and pn-junction formation was found in the electrical measurements. Cathodoluminescence was obtained over a temperature range of 10°K to 300°K and the electrical properties were measured between 77°K and 373°K. Photoluminescence was recorded using sample temperatures in the range 4.2°K to 300°K.

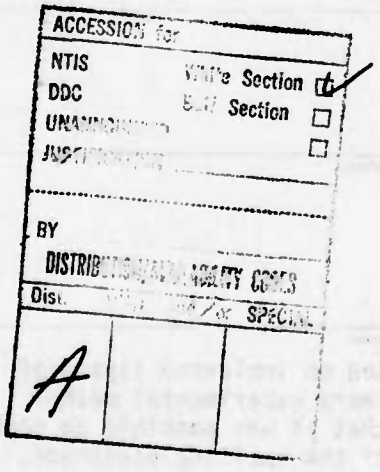

FOREWORD

This report was prepared by Captain Bruce J. Pierce, Laser and Optical Materials Branch, Electromagnetic Materials Division, Air Force Materials Laboratory, Wright-Patterson Air Force Base, Ohio. The work was performed in support of Project 7367 and Task 736703.

This report was submitted as the thesis requirement for the Degree of Doctor of Philosophy to the School of Engineering of the Air Force Institute of Technology and was published as AFIT report DS-PH:74-01.

The author would like to thank the members of the Air Force Materials Laboratory who supported this study and Dr. P. M. Hemenger for many informative discussions. Also thanks goes to Mr. Bok Kyoon Shin of the Systems Research Laboratory for providing the data used to derive the implantation profiles and to Mrs. E. Anne Buvinger of the Air Force Avionics Laboratory for allowing the use of the RF system to deposit quartz layers.

The author is also indebted to Dr. R. L. Hengehold, for much help and guidance in the completion of this study and to Mr. R. V. Bertke for his assistance in sample preparation and for performing the electrical measurements.

TABLE OF CONTENTS

SECTION		PAGE
I	INTRODUCTION	1
II	PREVIOUS RESULTS AND THEORY	5
	1. Ion Implantation	6
	a. Electronic Stopping	7
	b. Nuclear Stopping	9
	c. Projected Range	9
	2. Channeling	14
	3. Radiation Damage and Annealing	15
	a. Displacement Threshold	15
	b. Measurement of Displacement Threshold	16
	c. Displacement Cascades	17
	d. Replacement Collisions	18
	e. Spike Phenomena	18
	f. Annealing	19
	g. Previous Results: Damage and Annealing in Implanted Layers	19
	4. Excitation of Luminescence by Energetic Electrons	23
	a. Electron Stopping Curves	25
	b. Previous Results: Depth-Resolved Cathodoluminescence	31
	5. Luminescence	32
	a. Luminescence Mechanisms	33
	b. Trapping Effects	37
	c. ZnO Luminescence	38
	d. Previous Results: Luminescence of Ion Implanted Layers	43

TABLE OF CONTENTS (CONT'D)

SECTION		PAGE
II	6. Electrical Properties	45
	a. van der Pauw Method	46
	b. Interpretation of Data	49
	c. Electrical Properties of ZnO	50
	d. Previous Results: Electrical Properties of Ion Implanted Layers	51
III	DESCRIPTION OF EXPERIMENT	54
	1. Sample Preparation	54
	a. Polishing	55
	b. Etching	55
	c. Annealing	56
	d. Sputtering	58
	e. Implant Conditions	58
	2. Cathodoluminescence System	60
	a. Sample Environment	62
	b. Excitation Source	65
	c. Signal Processing	68
	3. Photoluminescence System	69
	a. Configuration of Photoluminescence System	73
	b. Sample Holder and Temperature Control	73
	c. Signal Electronics	74
	d. van der Pauw System	74

TABLE OF CONTENTS (CONT'D)

SECTION		PAGE
IV	RESULTS AND DISCUSSION	77
	1. Physical Appearance of Implanted Layers	77
	2. Cathodoluminescence Results	78
	a. Cathodoluminescence of Virgin Crystals	78
	b. Cathodoluminescence of Baked Samples	86
	c. Cathodoluminescence of Unimplanted Annealed Samples	93
	d. Probing by Cathodoluminescence	98
	e. Results Produced by Li Implants	100
	f. Results Produced by P Implants	108
	g. Results of Hot Implants: The Red Peak	112
	3. Electrical Results	115
	a. Electrical Properties of Baked Samples	119
	b. Electrical Properties of Implanted Samples	123
	c. Photoluminescence Results	129
	d. Summary of Results	137
V	CONCLUSIONS AND RECOMMENDATIONS	139
	1. Conclusions	139
	2. Recommendations	140
APPENDIX A:	PENETRATION OF VARIOUS IONS IN ZnO	143
APPENDIX B:	PENETRATION OF ELECTRONS IN ZnO	153
REFERENCES		154

LIST OF ILLUSTRATIONS

FIGURE		PAGE
1	Ranges of Implanted Ions	6
2	Variation in Stopping Powers with Ion Velocity	8
3	Implant Profiles for Room Temperature Implants	11
4	Implant Profiles for 475°C (Hot) Implants	12
5	Illustration of a Multiple Energy Implant	13
6	Cathodoluminescence Brightness Contours	24
7	Electron Energy Loss Curves	26
8	Universal Electron Stopping Curve	28
9	Single Electron Excitation Profiles	29
10	Current-Corrected Excitation Profiles	30
11	Luminescence Transitions	34
12	Typical ZnO Luminescence Spectrum	39
13	van der Pauw Sample Geometry	47
14	Cathodoluminescence System	61
15	Cathodoluminescence Sample Holder	63
16	Gun Bias System	67
17	Photoluminescence System	71
18	van der Pauw System	76
19	Cathodoluminescence of an Unbaked, Unimplanted Sample	79
20	Cathodoluminescence of an Unbaked, Unimplanted Sample	80
21	Cathodoluminescence of Unimplanted, Unbaked Sample (Variable Temperature)	84
22	Variable Temperature Cathodoluminescence of an Unbaked, Unimplanted Sample	85
23	Cathodoluminescence of a Zn-Baked Sample	87

LIST OF ILLUSTRATIONS (CONT'D)

FIGURE		PAGE
24	Cathodoluminescence of a Zn-Baked Sample	88
25	Comparison of Cathodoluminescence in Baked Samples	90
26	Cathodoluminescence of a Vacuum-Baked Sample	91
27	Cathodoluminescence of a Vacuum-Baked Sample	92
28	Annealed, Unbaked, Unimplanted Samples	95
29	Probing of a 275 keV Li Implant	99
30	Compilation of Electron Profiles with 275 keV Li Profile	101
31	Cathodoluminescence of a Low Dose Li Implant After a 475°C Anneal for Two Hours	102
32	Cathodoluminescence of a Low Dose Li Implant	103
33	Cathodoluminescence of a Ne Implant	107
34	Cathodoluminescence of P Implant - UV Bands	109
35	Cathodoluminescence of P Implants	110
36	Cathodoluminescence of a Hot P Implant After a Two-Hour Anneal at 900°C	113
37	Comparison of Hot Implants: UV and Violet Bands	114
38	Comparison of Hot Implants in the Visible Portion of the Spectrum	114
39	Resistivity and Carrier Concentration in an Unbaked Unimplanted Sample	116
40	Hall Mobility of Unbaked, Unimplanted Sample	117
41	Resistivity and Carrier Concentration of a Vacuum-Baked Sample	120
42	Resistivity and Carrier Concentration of a Zn-Baked Sample	135
43	Hall Mobility of a Zn-Baked Sample	136

LIST OF ILLUSTRATIONS (CONT'D)

FIGURE		PAGE
44	Resistivity and Carrier Concentration in a Hot Li Implant After a Two-Hour Anneal at 475°C	125
45	Hall Mobility in a Hot Li Implant After a Two-Hour Anneal at 475°C	126
46	Resistivity and Carrier Concentration in a Hot Li Implant After a Two-Hour Anneal at 900°C	127
47	Hall Mobility in a Hot Li Implant After a Two-Hour Anneal at 900°C	128
48	Resistivity and Carrier Concentration in a Hot P Implant After a Two-Hour Anneal at 475°C	130
49	Hall Mobility in a Hot P Implant After a Two-Hour Anneal at 475°C	131
50	Resistivity and Carrier Concentration in a Hot P Implant After a Two-Hour Anneal at 900°C	132
51	Hall Mobility in a Hot P Implant After a Two-Hour Anneal at 900°C	133
52	Decays of Photoluminescence at Various Wavelengths in an Unimplanted, Unannealed Sample	135
53	Time-Resolved Spectrum of a Hot Li Implant	136

LIST OF TABLES

TABLE		PAGE
1	Sample of Computer Data for Li in ZnO	14
2	Implant Conditions	59
3	Operating Parameters of the Nitrogen Laser	70
4	Comparison of Bound Exciton Lines in Unimplanted Unannealed ZnO	81
5	UV Bands of Unimplanted Unannealed ZnO	82
6	Comparison of Violet Emission Bands	111

SUMMARY

Semiconducting compounds composed of elements from group IIB and VIA of the periodic table have long been investigated because they offer great potential as a source of wide bandgap semiconductor materials. In describing the present state of knowledge concerning defect centers in II-VI compounds, Dr. G. D. Watkins wrote (Reference 18):

> "There is, therefore, quite a bit of experimental information that bears rather directly on intrinsic lattice defects in II-VI compounds. Ultimately of course, all of this information will fit together and a coherent self consistent picture must emerge. However, at present, it is certainly not unfair to say that this is not the case. Very little is actually known with any certainty. In fact, much of the experimental results often appear contradictory and defy simple interpretation."

The study of ion implantation in II - VI compounds represents a fresh approach to doping these materials in a controlled manner, however, the damage attendant with the implantation process creates native defects which may obscure the properties of the implanted ions. The investigation of ion implanted ZnO described herein, answers many of the questions which arise concerning the properties of implanted layers in ZnO, yet as in past studies of II - VI compounds, it appears to also raise some questions in regard to the formation of defect centers.

SECTION I

INTRODUCTION

For a number of years the Air Force Materials Laboratory (AFML) has supported research in various aspects of Electronic Materials. A portion of the effort has been expended in an investigation of the properties of materials suitable for optoelectronic devices. One class of materials which received considerable attention was that consisting of the II-VI compounds, i.e. those compounds composed of elements from groups IIB and VIA of the periodic table. Of particular interest were those compounds (CdS, ZnS, ZnSe, and ZnO) which have wide band gaps with energies corresponding to wavelengths of light in the visible portion of the spectrum. Since these compounds have direct gaps and, for the most part, readily form solid solutions with one another it should be possible to fabricate a variety of highly efficient Light Emitting Diodes and pn-junction lasers from such materials - using solid solutions to tailor the device to any desired wavelength within the visible range.

Unfortunately, despite years of effort by many workers throughout university, industrial, and government laboratories, no method of routinely obtaining type conversion and pn-junction structures had been developed. The as-grown substrates were always highly resistive or n-type, and conventional doping techniques failed to provide low resistivity p-type material because of the production of compensating donor centers. Whether these compensating centers are primarily due to impurities or native defects is a matter which is still unresolved, however, because of this self-compensation mechanism it is not likely that p-type material can be produced by conventional doping methods.

There exists in the literature, preliminary data which indicate that some measure of type conversion can be achieved in II-VI compounds through the use of ion implantation (References 132, 133, 136, 137). Since implantation is a nonequilibrium process and since the damage produced by implants appears to anneal at temperatures well below

diffusion temperatures, there is a possibility of achieving doping without self-compensation occurring. Thus, it was decided that a program would be initiated to evaluate the use of ion implantation as a means of doping II-VI compounds. This dissertation presents the results from a study of ion implanted layers in single crystals of ZnO. The primary investigative technique used was cathodoluminescence - excitation of luminescence by bombarding the sample with an energetic beam of electrons. Since the luminescence is produced at varying depths within the sample according to the energy of the exciting electrons, it was possible to profile an implant by varying the beam voltage. The electrical properties of some of the implants were determined by use of the van der Pauw technique for measuring the Hall effect, and in addition, some of the samples were examined using time-resolved spectroscopy, observing the photoluminescence excited in these samples by the pulsed 3371 Å radiation from a nitrogen laser.

ZnO was chosen as the material to be implanted because it has a wide energy gap, 3.3435 eV at 1.2°K (Reference 1), which makes it a suitable candidate for a single substrate that may be used for a variety of optoelectronic devices covering the entire visible portion of the spectrum.

The ions chosen for implantation were those which had potential as acceptor atoms: Li, Na, N and P. These ions were implanted using a total fluence (dose) in the range of 10^{11}-10^{16} ions/cm^2 and employing beam energies of 30 keV to 1 MeV, while the substrate was held either at room temperature or at 475°C. Ions of Ne were implanted under conditions identical to those used for Na in an effort to separate effects due to chemical doping from those due to radiation damage by an inert ion of similar mass. This resulted in the production of a large number of samples. Because of the time required to evaluate the variety of samples available, no attempt was made to study the effects of any particular implant in great detail.

Two large, hydrothermally grown, single crystals of ZnO were purchased from the Airtron Corporation in order to complete the study. ZnO single crystals are clear and transparent (the fundamental absorption edge being in the ultraviolet portion of the spectrum) and crystallize in the wurtzite (hexagonal) structure with lattice constants "a" = 3.249858 ± 6 x 10^{-6} Å and "c" = 5.206619 ± 2 x 10^{-6} Å (Reference 2). The density of this material is 5.642 ± .012 g/cm^3 (Reference 2). The bonding in ZnO is approximately 62% ionic (Reference 3), and ZnO is thus a strongly polar semiconductor possessing good piezoelectric properties which have led to its use in a variety of functions relating to acoustoelectric devices (References 4, 5, 6) as well as optoelectronic devices (References 7, 8).

The ZnO substrates were prepared at the AFML by cutting them from single crystal boules with a diamond wire saw, polishing them, and chemically etching them. Some samples were subjected to annealing in various atmospheres, after which they received a second etch. These heat treatments were either aimed at correcting or producing stoichiometric excesses of one of the elements comprising the crystal or were an attempt to rid the samples of unwanted impurities by solvent extraction. All heat treatments were performed in evacuated quartz ampoules. Once the substrates had been prepared they were sent to KSW Electronics, Inc. where the implantation of selected impurity ions was performed. After implantation the surface was usually protected, for the purposes of subsequent handling or annealing, by a layer of SiO_2 applied by the RF sputtering of a quartz target, which was accomplished at the Air Force Avionics Laboratory (AFAL). The SiO_2 was etched off the sample surface by using a 50% solution of HF prior to all measurements.

Cathodoluminescent spectra were recorded as the sample was bombarded by an electron beam of energy 1-25 keV with currents in the range 0 - 5 μ A. The sample was maintained at a temperature in the range 10 - 300°K. Electrical data were obtained using the van der Pauw technique for temperatures between 77°K and 400°K, and photoluminescence was produced at sample temperatures ranging from 4.2°K to 300°K. The results of these measurements are presented and discussed in Section IV.

Section II provides details of theory and selected results from prior studies of ZnO and other materials which are useful in interpreting the data obtained during the course of this investigation. The third section presents the details of the experimental systems and procedures used to obtain the data. Section V gives conclusions based upon the analysis of the data and provides recommendations for future studies of ion implanted ZnO.

SECTION II

PREVIOUS RESULTS AND THEORY

In investigating materials with potential application for optoelectronic devices there are two factors of utmost concern. These are the optical and electrical properties of centers which exist in the material of interest. The centers may be the result of doping with selected ions to achieve a desired device structure, or they may be induced by foreign impurity ions which have been accidentally incorporated during the growth and subsequent processing of the substrate under investigation. Another type of center which is of particular importance in a compound semiconductor, such as ZnO, is one arising from a native defect. Vacant lattice sites or the presence of lattice atoms at the interstices may significantly alter the optical and electrical properties of a compound semiconductor. Thus, one expects numerous changes to occur in these properties for samples of ZnO which have been implanted with various ions. The nature of the stopping processes which cause an energetic ion to come to rest are such that the target solid sustains radiation damage thus producing large changes in stoichiometry. Some of the damage may be eliminated through annealing or through implants performed with the substrate maintained at elevated temperatures, and a substantial fraction of the implanted impurity ions may substitute for atoms of the constituent element of one of the sublattices. But, some of the impurity ions will remain at the interstices or will substitute for lattice atoms comprising the other sublattice.

A discussion of the implant process which includes penetration, damage, and annealing is presented in Section II.1. Computer-generated profiles for the various implants performed as a part of this investigation are also contained in this section. Since cathodoluminescence was used to probe the ion implanted layers, it is necessary to consider the creation of excess electron-hole pairs formed in ZnO by bombardment with energetic electrons. A semiquantitative method for determining excess pair concentration profiles is discussed and adapted to ZnO

targets in Section II.4. Following this is a brief discourse on luminescence, in which particular emphasis is placed on prior studies in ZnO and on studies which have employed luminescence to examine implanted layers. The final subsection provides a description of electrical properties and the van der Pauw technique, which makes the measurement of these properties possible when thin ion implanted layers are to be investigated.

1. ION IMPLANTATION

During the process of ion implantation of impurity atoms into a particular substrate material the impurity atoms are ionized and accelerated to high energies before they are allowed to impinge on the substrate. After striking the solid, the energetic ions are gradually slowed by collision interactions with the atomic electrons and nuclei of the solid and finally come to rest at some depth from the bombarded surface. The total distance the moving ion travels before coming to rest is its "range", R; and the "projected range", R_p, is the projection of that distance along the direction of incidence. These ranges are illustrated in Figure 1.

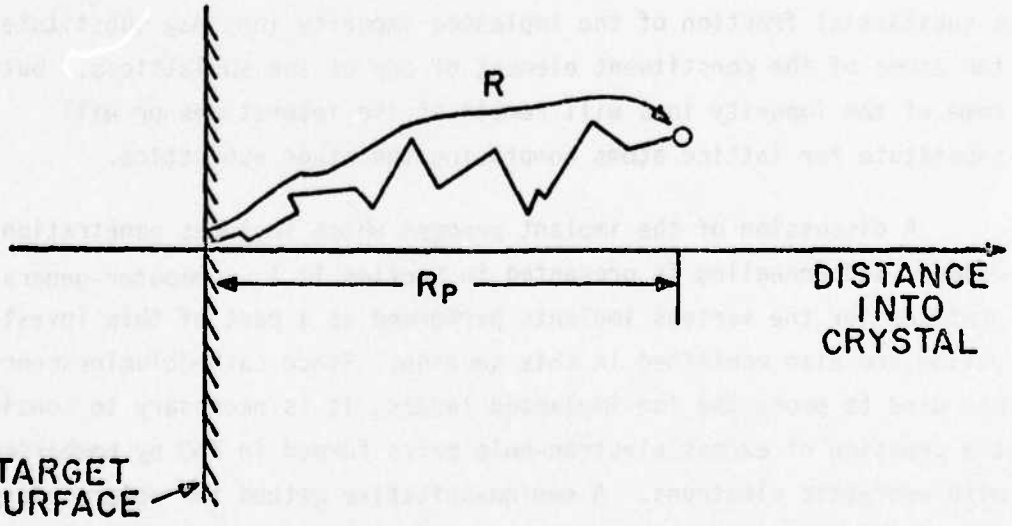

Figure 1. Ranges of Implanted Ions

The average rate of energy loss with distance is given by Reference 9.

$$-\frac{dE}{dx} = N\,[\,S_n(E) + S_e(E)] \qquad (1)$$

where

E is the energy of the moving ion at point x along its path

$S_n(E)$ is the nuclear stopping power

$S_e(E)$ is the electronic stopping power

N is the average number of target atoms per unit volume.

It has been assumed in Equation 1 that the electronic and nuclear stopping processes are independent. This is the usual assumption which is made in determining the range of charged particles in amorphous materials. Initially, the moving atom suffers primarily inelastic (ionizing) collisions with the atomic electrons of the target material until it slows down to a point such that $E = E_c$ given by Reference 10

$$E_c = \frac{1}{8}\left(\frac{M}{m}\right) I \qquad (2)$$

where

M is the mass of the moving ion

m is the electron mass

I corresponds to the energy of the fundamental absorption edge.

For energies where $E < E_c$ the moving ion suffers primarily elastic collisions with the target nuclei, and it is in this range that most of the displacements of lattice atoms are created (Reference 10). In the real physical situation E_c is not a precisely defined quantity, and there is some overlap between the two stopping regimes as illustrated in Figure 2 (Reference 11).

a. Electronic Stopping

When the energetic ion first strikes the target solid it is highly ionized, and as it slows down it gradually acquires electrons (Reference 12). In essence, those electrons having an orbital velocity less than the velocity of the moving ion are stripped away from it by

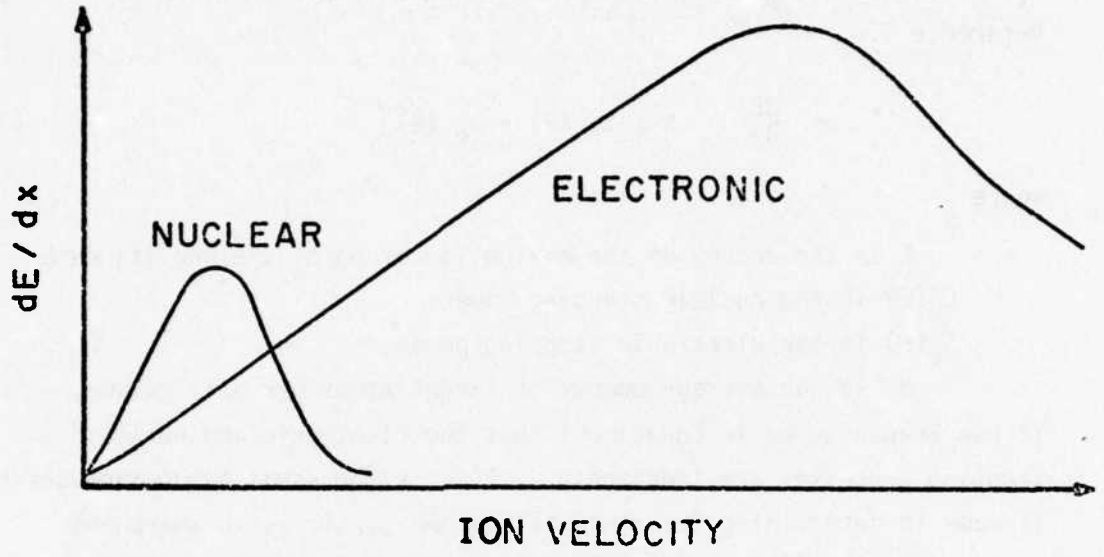

Figure 2. Variation in Stopping Powers with Ion Velocity

interactions with the bound atomic electrons in the target. The mathematical treatment of this interaction and the calculation of S_e (E) is a difficult problem. Two different approaches to this problem have been formulated and are commonly used in computations of the range of implanted ions. The first approach is one taken by Lindhard, Scharff, and Schiott (LSS). In this model it is assumed that the nucleus of the moving ion (neglecting its electrons) is stopped by a free electron gas composed of the electrons in the target (Reference 9). Energy is lost through collisions with individual electrons and through excitation of plasma resonance in the free electron gas. A second approach, due to Firsov, is a more physical one in which the attempt by the moving ion to form a molecule with the stationary ion is considered (Reference 9). Electrons transferred from the moving ion to the stationary one lose momentum and energy, while those transferred in the other direction gain momentum and energy - all at the expense of the moving ion.

Both the above models predict a monotonically increasing dependence of S_e (E) on the atomic number, Z_1, of the projectile ion. Actually, the value of S_e (E) is an oscillatory function of Z_1, as measured by Eisen (References 9, 13). The reason for the failure of the previous

theories is that they do not properly account for the electrons of the moving ion. The Firsov model assumes all the electrons take part in the interaction while, as mentioned previously, LSS ignores them entirely. Recent calculations (References 9, 13) have corrected this deficiency through a modification of the Firsov model, and the implant profiles contained in this dissertation were computed with the oscillations in S_e (E) taken into account.

b. Nuclear Stopping

The derivation of S_n (E) is more straightforward than that of S_e (E). The expression for nuclear stopping is

$$S_n(E) = \int_0^\infty T_n(E, p)\, 2\pi\, p\, dp \tag{3}$$

where T_n is the energy transferred from the moving ion to the stationary one during the elastic collision and p is the impact parameter in a Rutherford description of the collision. The maximum energy transfer occurs for a head-on collision and is given as (Reference 9)

$$T_m = \frac{4\, M_1\, M_2}{(M_1 + M_2)^2}\, E \tag{4}$$

Once T_n (E,p) is known then Equation 3 can be used to calculate S_n (E). The crux of the calculation is choosing a potential to describe the interaction between the moving ion and the target atom. The LSS theory is based on the Thomas - Fermi model of the atom (References 14, 15), and this is the most commonly used method for finding S_n (E).

c. Projected Range

The average total range, R, for an ion with initial energy E_o may be found by integrating Equation 1 to get

$$R = \int_0^R dx = \frac{1}{N} \int_0^{E_o} \frac{dE}{[S_n(E) + S_e(E)]} \tag{5}$$

However, the average projected range, $\overline{R_p}$, is much more useful for device design and comparison with experiment. It is clear from Figure 1 that an ion which has negotiated a tortuous path from the surface of the target solid to find itself at rest at a distance R_p from that surface could have arrived at its present location by any of an infinite variety of paths. It is also clear that not all ions with total range, R, will have the same projected range, R_p. Hence, it is logical that R_p is a statistical entity, and it can be shown that the profile of implanted ions may be described by a Gaussian distribution at a mean projected range, $\overline{R_p}$, with a standard deviation, $\overline{\Delta R_p}$ (Reference 9).

The technique for numerically determining $\overline{R_p}$ and $\overline{\Delta R_p}$, based on the LSS theory, has been outlined by Johnson and Gibbons (Reference 16) and has been widely used to date. Mr. Bok Kyoon Shin of the Systems Research Laboratory, under contract to the Aerospace Research Laboratory, has adapted this technique and written a computer program which takes into account the oscillation in electronic stopping power discussed previously. The author is indebted to Mr. Shin for providing the data necessary to determine the profiles of various energetic ions in randomly aligned ZnO substrates. An abbreviated sample of the data provided is shown in Table 1. All of the data is presented in Appendix A. Using these data and the relation for concentration of implanted ions

$$N(x) = \frac{\phi}{\sqrt{2\pi}\,\overline{\Delta R_p}} \exp\left[- \frac{(x - \overline{R_p})^2}{2\,(\Delta R_p)^2} \right] \qquad (6)$$

where ϕ is the implant dose, one may obtain the theoretical profile of the concentration of implanted ions at various depths within the substrate. The profiles for the various implants examined as part of this investigation are shown in Figures 3, 4, and 5.

TABLE 1

SAMPLE OF COMPUTER DATA FOR LI IN ZnO

KEV	PR RANGE	DELTA	HALF	ONE	FOUR	E NUCLEAR
20.	328.7	386.4	456.0	898.9	1657.8	8.0
50.	2007.9	732.9	864.8	1572.0	3144.1	12.6
100.	3696.0	999.6	1179.5	2144.1	4288.3	16.2
200.	6428.5	1247.0	1471.5	2674.9	5349.8	19.6
500.	12344.3	1501.8	1772.1	3221.3	6442.6	23.4

KEV: Beam Energy in keV

PR RANGE: Projected Range (Angstroms)

DELTA: Standard Deviation in R_p

HALF: Distance from R_p at which concentration is equal to one-half the peak concentration

ONE: Distance from R_p at which concentration is one-tenth of the peak concentration

FOUR: Distance at which concentration is 10^{-4} of peak

E NUCLEAR: Energy available for nuclear stopping processes

2. CHANNELING

Up to this point the discussion of penetration depths has considered only amorphous targets. When a crystalline solid is used, anomalously large ranges for the implanted ions may be discovered. These anomalous penetration depths are due to the phenomenon known as "channeling," which occurs when the impinging ions are incident on a crystalline target along a direction corresponding to relatively open structure (channels) in the lattice. An ion moving along a channel suffers only minor collisions with the lattice atoms that form the channel and thus penetrates much further into the crystal than an ion which is incident along a random direction. In order for an ion to be channeled it must strike the substrate within a narrow angle (critical angle) of an open direction. This critical angle is dependent upon the energy of the incident ions, but for most cases it is within a few degrees of the channeling direction (Reference 13). Thus, it is possible to approximate

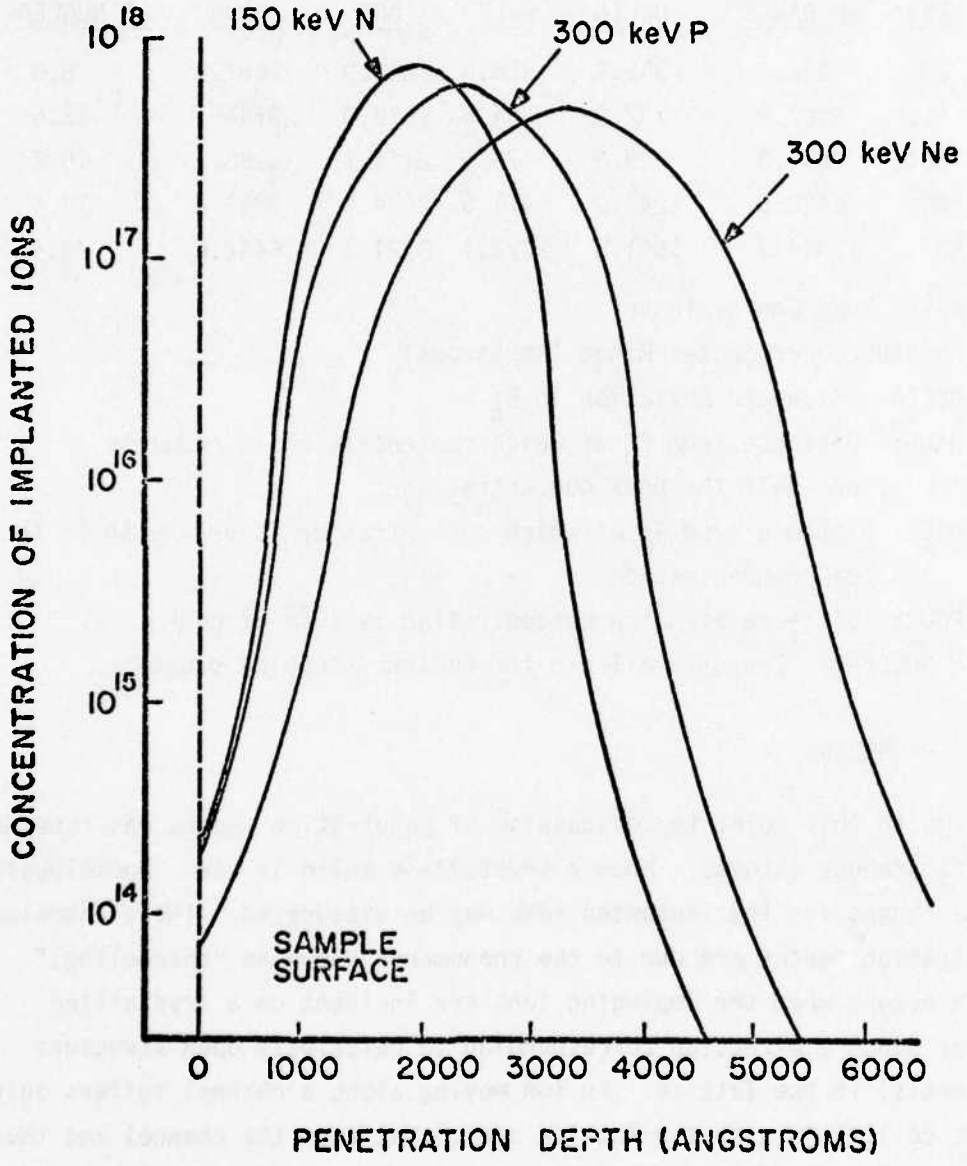

Figure 3. Implant Profiles for Room Temperature Implants

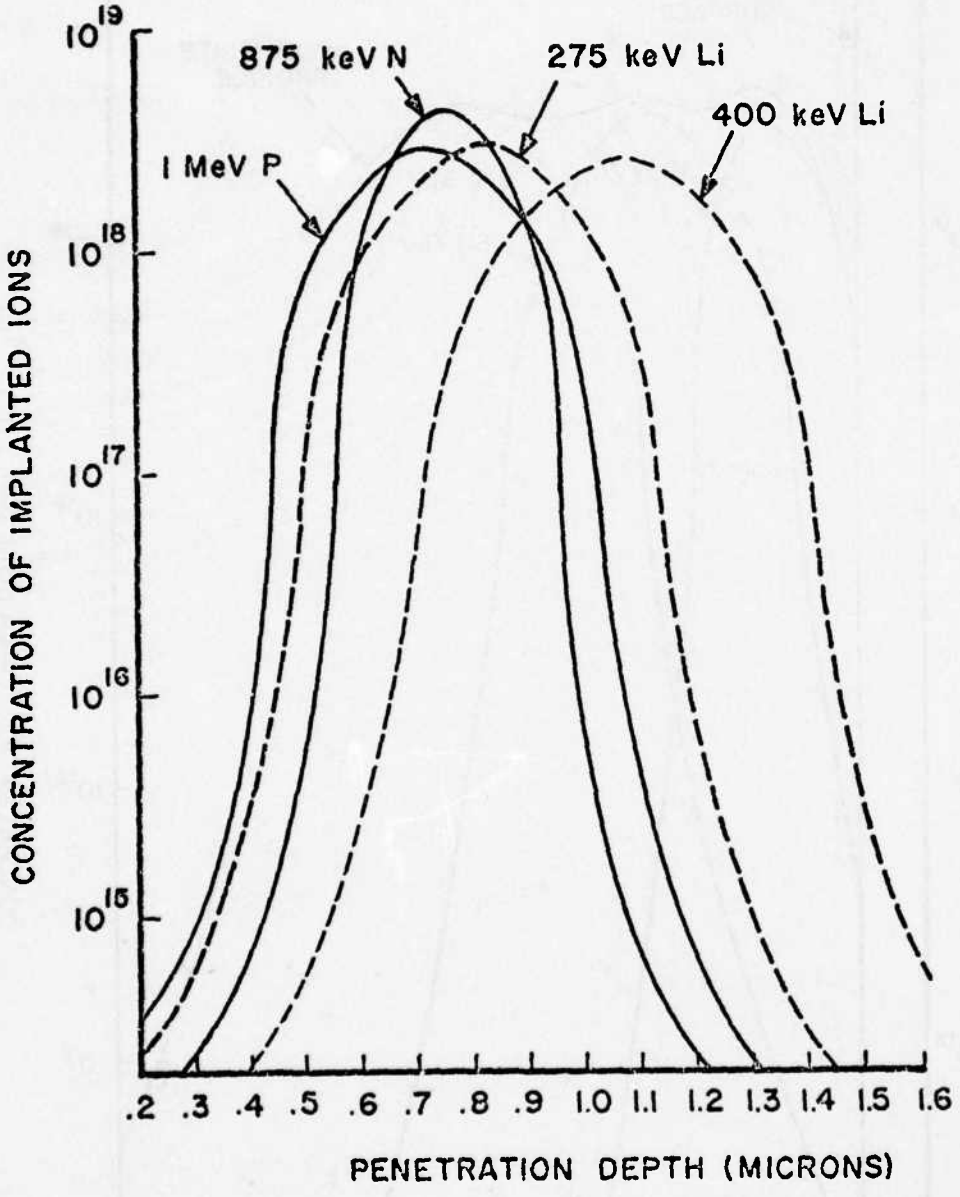

Figure 4. Implant Profiles for 475°C (Hot) Implants

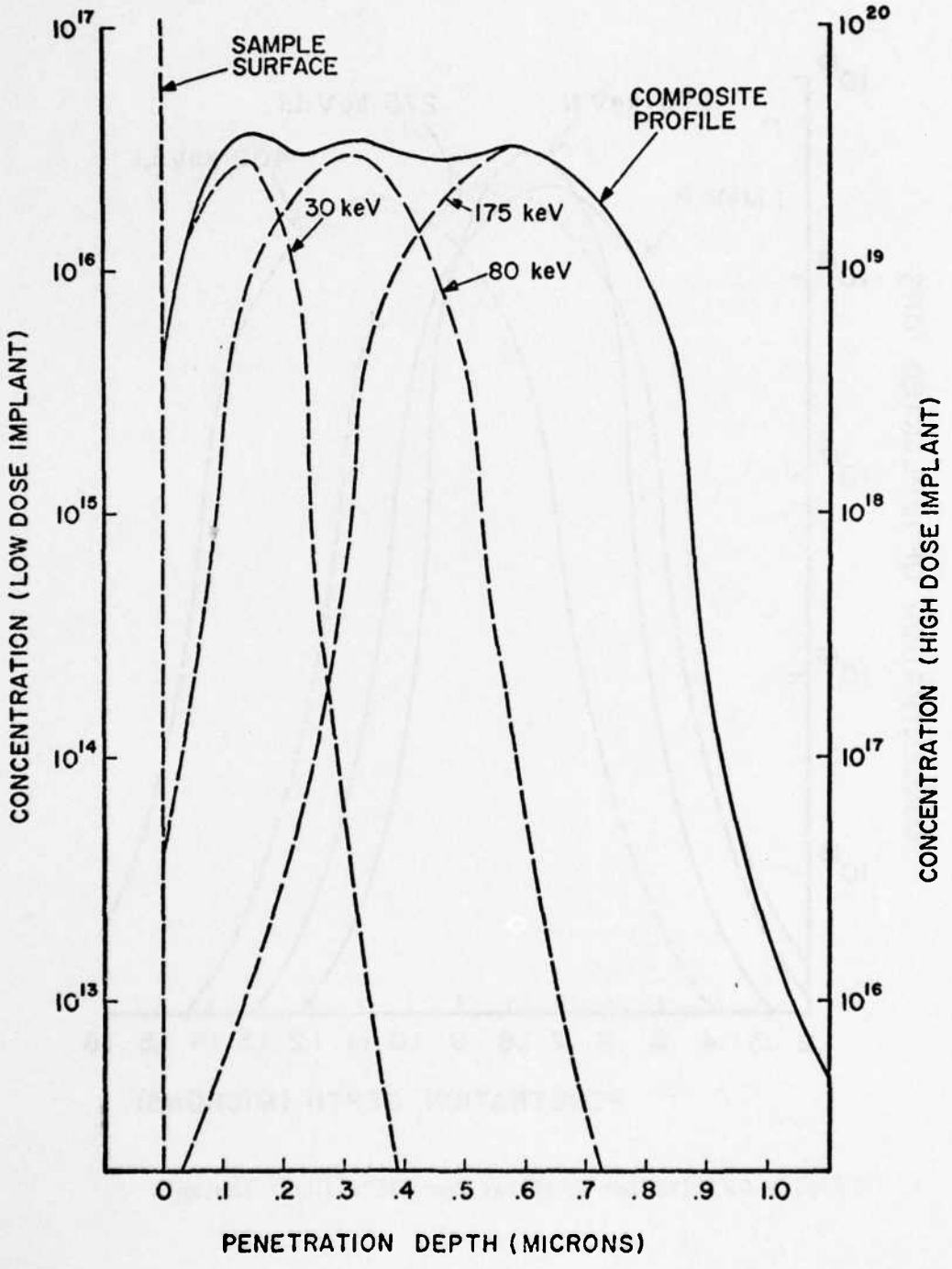

Figure 5. Illustration of a Multiple Energy Implant

the amorphous case with a crystalline target by randomly aligning the substrate, and this was accomplished for all ZnO samples used in this investigation.

The phenomenon of channeling also forms the basis for a method which may be used to locate impurity ions within a crystalline target (Reference 17). Normally, a high energy (1.0-2.0 MeV) beam of He ions is used. A solid state detector is positioned near the path of the incident He ions, and the energy of the He ions backscattered by the target is measured. Several crystallographic directions are examined (the <1,1,0>, <1,1,1>) and the random direction (misaligned from a channeling direction) are used for Si targets. Information concerning the lattice location of implanted ions and the extent of damage produced by the implant can be obtained by comparing the backscattered spectra observed for the various directions of incidence. If the amount of damage is low and if the implanted ions occupy lattice sites, then the number of backscattered He ions with high energy will be drastically lower for the channeling directions than it will be for the random direction. This method works best when the implanted ion has a larger mass then the lattice atoms.

3. RADIATION DAMAGE AND ANNEALING

Radiation damage is created when an energetic projectile imparts enough energy to a lattice atom to cause that atom to be displaced from its normal site. The removal of a single lattice atom is a mild form of radiation damage resulting in the production of a simple defect or "vacancy." Much more severe forms of damage may be created by ion implantation. Such defects as "spikes" where large numbers of lattice atoms are simultaneously affected by a single energetic ion are common occurrences during implants.

a. Displacement Threshold

The energy required to displace an atom of a crystal from its normal lattice site is the "displacement energy," E_d. In real crystals E_d is not a precisely defined entity (Reference 10). It is easier, for example, for a struck atom to depart from its lattice site along an open

crystallographic direction (channel) than it is for that same atom to be ejected along a direction in which its nearest neighbor lies in its path. Besides lattice effects, another factor which affects E_d is the temperature of the solid. At higher temperatures the lattice atoms possess thermal energy so that less energy is required to displace them (Reference 10). Thus, E_d is a quantity with a probabilistic nature. Transfer of an amount of energy slightly less than E_d may cause a displacement in some cases, while in other cases transfer of an energy slightly larger than E_d might not eject the struck atom. Although it is clear that the threshold for displacement is not sharply defined, most theoretical descriptions of radiation damage ignore this complication and assume it is precisely defined.

b. Measurement of the Displacement Threshold

In order to assess the effects of radiation damage produced in crystals by ion implantation, it is useful to know the value of E_d for the target and to have some background information on the production and emanation of damage in the material under investigation. Ion implantation usually creates gross damage, but under certain implant conditions or after annealing at some temperatures, it is possible that simple defects may dominate the properties of the implanted layer. Bombardment of the target by a high energy beam of electrons is the best method for producing simple defects so that the properties of these centers may be investigated. Once a particular result (e.g., a certain luminescence peak) has been attributed to a simple defect center, the production of that result may be studied as a function of the beam energy of the bombarding electrons. In this manner a threshold energy may be established and correlated to the displacement energy, E_d. Studies of this nature have been performed on the II-VI compounds and a review of the recent literature has been presented by Watkins (Reference 18).

The displacement threshold of 600 keV for ZnO determined by Vehse, et al. (Reference 19) and included in "Table 1" of the aforementioned review article (Reference 18) has recently been disputed by Meese and Locker (References 20, 21). Vehse, et al. investigated the coloration of

ZnO single crystal samples induced by bombardment with energetic electrons or by baking the samples in Zn vapor. The degree of coloration was determined by monitoring the absorption coefficient at 4100 Å, and the increase in absorption was attributed to the formation of Zn interstitials. Later work by Feldman and Appleton (References 22, 23) employed the channeling technique to examine ZnO samples which had been colored by baking in Zn vapor, and these workers found no evidence of interstitial Zn centers (within the limit of their experiment which was conservatively estimated as having the capability of detecting a concentration of interstitial Zn in excess of $6 \times 10^{18}/cm^3$ (Reference 22)).

In addition, Smith and Vehse (Reference 24) used ESR to evaluate electron (bombarded ZnO and observed the ESR spectrum of a single donor trapped at an oxygen vacancy (F^+ center)). This seems to indicate that the coloration is due to the formation of oxygen vacancies (F centers) rather than Zn interstitials. Recently, Meese and Locker (References 20, 21) observed two thresholds in electron-bombarded ZnO. The lower energy threshold at 310 keV was attributed to the formation of oxygen vacancies, and the higher energy threshold at 900 keV was correlated with Zn vacancy production. This assignment leads to a single displacement energy of 57 eV for either Zn or O atoms in ZnO.

c. Displacement Cascades

When the bombarding particles are heavy ions, as in the case of implantation, there is a probability that a relatively large amount of energy will be transferred to a single lattice atom. The maximum amount is given by Equation 4 with the value of E equal to the energy available for nuclear stopping processes, as given in Table 1. The struck atom becomes a primary "knock-on" and because it has received a large amount of energy, it is capable of striking additional lattice atoms to produce secondary knock-ons, etc. The shower of displaced atoms produced by the primary knock-on is a "displacement cascade" (Reference 10). An approximate expression for the number of atoms displaced in a cascade by an ion with energy $\bar{E}$ has been derived by Sigmund and is given as (Reference 17)

$$N_d = .42 \frac{\bar{E}}{E_d} \qquad (7)$$

d. Replacement Collisions

A replacement collision occurs whenever the moving atom is left with energy less than E_d and less than the energy imparted to the struck atom if the energy of the struck atom exceeds some threshold value, E_r. A simplified calculation which assumes hard sphere collisions between atoms of equal mass gives the following relation for the number, N_r, of replacement collisions (Reference 25)

$$N_r = .5N_d \left[1 + \ln\left(E_d/E_r\right) / \ln\left(\tfrac{4}{3}\right)\right] \qquad (8)$$

Since E_r is likely to be much less than E_d, then N_r is likely to be much larger than N_d. In the case of a monatomic solid a replacement collision has no effect on the overall disorder, but it can play an important role in a compound semiconductor.

e. Spike Phenomena

Up to this point the assumption has been made that the moving ion interacts with only one lattice atom at a time. This is not always the case, and reactions involving a moving ion which simultaneously excites a number of adjacent lattice atoms have been evolved (Reference 10). Such reactions are referred to as "spikes." If a lattice atom is struck but not displaced, it oscillates about its equilibrium position until its motion is damped out. During the damping process it transfers energy to its neighboring atoms, which are also caused to oscillate, until finally the energy is dissipated. This may be described as a sudden transfer of heat to the affected portion of the lattice (Reference 10), and the phenomenon is known as a "thermal spike." Temperatures as high as 1000°K may endure for sometime on the order of 10^{-11} sec (Reference 13). While there is little chance of displacement production in a thermal spike, there is a good chance that replacement collisions will occur and produce additional disorder in compound semiconductors (Reference 10). Due to the heating within a thermal spike the lattice expands in a localized area thereby creating a region of high stress. This stress can lead to further dislocations which are caused by plastic deformations referred to as "plastic spikes" (Reference 12).

The severest form of damage which may occur along the track of a moving ion is called a "displacement spike," and this spike consists of a region composed of high density of vacancies surrounded by a region composed of a high density of interstitials. The vacancies are created in a time which is so short that the lattice has not had time to relax, and for each vacancy created a nearby interstitial is also formed (Reference 10). The net effect of a displacement spike is the creation of a region of high disorder, which is surrounded by considerable strains (Reference 10).

f. Annealing

Annealing is a heat treatment performed on an implanted sample to renew the crystalline structure of the substrate material. In most semiconductors the simple defects (interstitials and vacancies) are mobile at temperatures much lower than that required for annealing (Reference 13). Some of these mobile defects will recombine and annihilate each other, and some will become trapped and immobilized (Reference 12). It is also possible for the defects to cluster and form extended defects such as "dislocations," "stacking faults," or "line defects" (Reference 10). It then becomes necessary to anneal these extended defects in order to restore the crystalline structure (Reference 13). The "isochronal" technique is usually employed in the investigation of implanted layers. In applying this method one monitors the physical properties of interest between annealing steps at successively higher temperatures (the sample being held at each temperature for a fixed time period).

g. Previous Results: Damage and Annealing in Implanted Layers

In the past decade the ion implantation technology in silicon substrates has rapidly advanced, and implantation is now a routine processing step in the manufacture of a number of devices. A large body of literature exists concerning implants in Si, and no attempt will be made to review this literature. Only a few of the features of damage due to implants in Si will be discussed herein. In the case of compound semiconductors belonging to the III-V and II-VI class the implantation process is far less well understood than it is in Si. Results obtained

in these materials will be emphasized (with particular attention being paid to the II-VI compounds). The primary purpose of this section is the presentation of past work which displays features of damage and annealing studies. A discussion of prior efforts which were predominantly luminescence or electrical studies is reserved for later sections where these properties are presented in detail.

A number of workers have employed electron microscopy techniques (References 13, 17) to study the disorder produced in Ge and Si targets by implantation. It was found that low dose implants create regions of high disorder surrounding the track of an implanted ion, and these essentially amorphous regions are believed to be produced by displacement cascades or spikes. The number of such amorphous zones produced is dependent upon the implant dose, and the mean diameter and depth are dependent upon the substrate temperature and beam voltage. The mean diameter of damage regions created by 100 keV oxygen implants at room temperature is 70 Å in Ge and 40 Å in Si. The same implant in Ge at 30°K produces 90 Å zones. As the dose increases the damage zones begin to overlap until a noncrystalline amorphous layer is produced (Reference 13). The production of this amorphous layer is accompanied by a change in the color of the sample surface, which takes on a "milky white" appearance (Reference 13). For a given beam energy, the dose required to produce an amorphous layer is dependent upon the mass of the implant ions (Reference 17).

It has been found that much of the damage produced by implants in Si can be annealed at temperatures below 600°C (Reference 17). With doses lower than that required to produce the amorphous layer, reordering occurs at 380°C for a series of ten-minute-isochronal anneals. A similar annealing procedure leads to reordering of the amorphous layer at 570°C (Reference 17) unless a very high dose is used, in which case considerably higher temperatures are required (Reference 17). It is believed that the amorphous layer is restructured by the mechanism of epitaxial recrystallization onto the undamaged Si below (Reference 13).

If the dose is high enough the concentration of implanted ions will exceed the solubility limit, and in this case the epitaxial recrystallization process is hindered. A room temperature implant of 40 keV Sb ions in Si to a dose of $2.6 \times 10^{15}/cm^2$ shows little recovery at anneal temperatures as high as 800°C (Reference 13). When the implant dose is not sufficient to produce an amorphous layer, post annealing residual damage remains in the form of loops, which are believed to be clusters of interstitials (Reference 13). If the dose is sufficient enough to create the amorphous layer, the residual damage takes the form of a dense array of small misoriented regions, which becomes denser near the surface as the epitaxial recrystallization proceeds (Reference 13).

Part of the difficulty associated with investigating implants in compound semiconductors arises because of the existence of two sublattices (Reference 26) and because it is hard to distinguish between the effects of chemical doping and residual damage. This is because many of the features concerning dopants and other basic properties are not well understood in these materials (Reference 27). A tabulation of implants in compound semiconductors has been provided by Stephen (Reference 13), but it should be pointed out that this table is not complete.

Carter and coworkers (References 28, 29, 30) have carefully studied the effects of Te implants into GaP substrates. The channeling effect, using 2 MeV helium ions, was employed to investigate the location of the implanted ions within the lattice and the damage incurred by the lattice as a result of the implantation. Implants of Te were performed at an energy of 40 KeV using doses as high as $5 \times 10^{15}/cm^2$ with substrate temperatures up to 500°C. For room temperature implants, it was found that a dose higher than $10^{14}/cm^2$ produced a saturation of lattice disorder. This is analogous to the amorphous layer produced in Si, but there is some evidence that the layer in GaP is composed of microcrystallites. When the damage layer had been saturated, annealing above 500°C was required to restructure the implant; but when the damage incurred was 50% of that required to produce saturation then an anneal

of 300°C was sufficient for reordering to occur. It was estimated that a 20 keV room temperature implant displaced 370 Ga atoms per implanted ion. This should be compared to calculated values of 540 atoms/ion and 440 atoms/ion for the Ga and P sublattices, respectively. The level of damage decreased as the substrate temperature was increased, and for the case of 40 keV Te ions implanted to a dose of $5 \times 10^{15}/cm^2$ into a 500°C GaP substrate, the damage produced was 20% of that incurred for the same implant into a room temperature substrate.

The damage induced by implants in ZnS, ZnSe, and CdS was studied by Olley, et al. (Reference 31) using optical absorption and electron microscopy. ZnS and ZnSe were implanted at room temperature with 100 keV Zn ions to a dose of either $5 \times 10^{13}/cm^2$ or $5 \times 10^{14}/cm^2$. The lower dose produced 10 - 30 Å diameter clusters which formed dislocation loops after a one-hour anneal at 500°C. An additional five-hour anneal at 500°C produced a phase change from the wurtzite to the zincblende structure. The high dose produced a tangle of dislocation loops which showed little change after a six-hour anneal at 500°C.

The CdS samples were implanted at room temperature with 20 keV and 100 keV Ag ions and with 100 keV He ions to doses greater than $1 \times 10^{15}/cm^2$. It was found that marked annealing occurred in 30 minutes at 400°C, in comparison with much longer times required at 300°C or 350°C. Restructuring of the lattice was observed directly by electron microscopy and indirectly by the renewal of the exciton structure in the optical absorption spectrum (as the diameter of the damage centers became smaller than that of the exciton complexes). Implants in CdS were also examined by Armitage (Reference 32) using the channeling technique. In this work room temperature implants of S, Ne, Bi, and P were performed at 200 keV to doses of $10^{13}/cm^2$, $10^{14}/cm^2$, and $10^{15}/cm^2$. It was found that no amorphous layer was produced and that considerable reduction of lattice disorder occurred after annealing in vacuum at 600°C for 20 minutes.

Hutchby and coworkers (References 33, 34, 35) have employed optical reflection and channeling to evaluate implants of F,Cl,Br, and I into CdS. All ions were implanted at 40 keV into room temperature CdS samples with doses in the range 10^{14} - $10^{17}/cm^2$. No evidence of the formation of an

an amorphous layer was observed, except possibly for the case of a $1 \times 10^{17}/cm^2$ F implant. Isochronal anneals indicated that a significant reordering occurred between 200 and 300°C for F and Cl, whereas it occurred between 100 and 250°C and between 400 and 500°C for Br implants. In the case of I no step was observed, and disorder was continuously reduced between 100 and 500°C.

4. EXCITATION OF LUMINESCENCE BY ENERGETIC ELECTRONS

When energetic electrons strike a solid the energy is gradually dissipated, and the electrons finally come to rest after penetrating some distance into the solid. This penetration depth may be correlated to the initial energy of the incident electrons. The idea that one may obtain information on the depth distribution of cathodoluminescent centers by varying the voltage of the excitation beam was first expressed by Makarov (Reference 36). Barnes, et al. (Reference 37) first reported the use of cathodoluminescence for probing ion implanted layers in CdS, and the details of this semiquantitative technique were published by Norris, Barnes, and Beezhold (Reference 38). The actual luminescence profiles in various phosphors have been studied using microphotography by Ehrenberg and coworkers (References 39, 40). Contours of brightness levels of the luminescence produced by electrons of various energies in polystyrene and KI are shown in Figure 6. Notice that the contours show little evidence of spreading out in KI which has a density about 60% of that of ZnO, whereas in the lower density polystyrene the contours are considerably spread. Thus, one expects relatively uniform luminescence contours in single crystals of ZnO bombarded by electrons which have energies in the range available for this study.

The energy lost by an electron in traversing a solid is given mainly to the production of bremsstrahlung and the excitation and ionization of the atomic electrons through elastic collisions. For the case of interest,

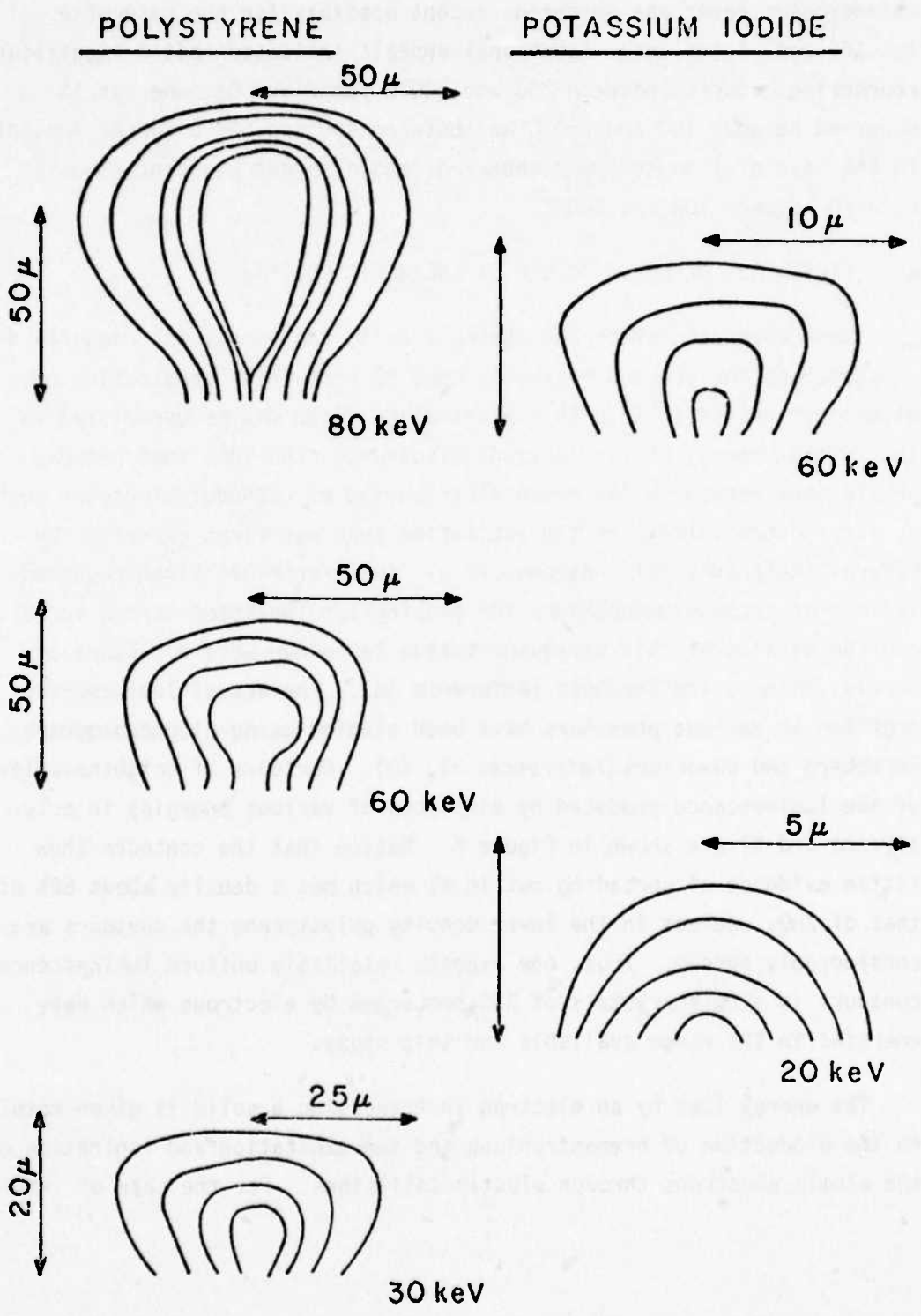

Figure 6. Cathodoluminescence Brightness Contours (Reference 40)

1-25 keV electrons, the radiation losses are negligible; and nearly all the energy is lost via the latter process. For low energy incident electrons the stopping power (Reference 10) is given by:

$$-\frac{dE}{dx} = \frac{4\pi e^4}{mv^2} N_o Z \ln\left[\frac{mv^2}{2\bar{I}}\sqrt{\frac{e}{2}}\right] \qquad (9)$$

where the "e" under the ln is the fundamental constant: the base of the natural logarithms

Z is the atomic number of the target solid

N_o is the number density of atoms in the solid

$\bar{I}$ is the average energy required to ionize an electron from an atom in the solid.

a. Electron Stopping Curves

Experimentally determined stopping curves which show energy deposition vs depth are available for several materials with normal incidence of the electron beam. As shown in Figure 7, there is little difference between the normalized stopping curve of very high energy electrons in polystyrene (Reference 41) and that obtained with significantly lower energies in air (Reference 42) (the only difference being a shift of the maximum toward greater depths with increasing energy). In fact, the data show the remarkable result that the normalized stopping curve, $\frac{dE}{dx}$ vs. x, is approximately a universal curve that may be scaled for the material of interest, in this case ZnO, simply by using the density. For the purposes of this investigation one requires the stopping curves for low energy electrons incident on ZnO at a 45° angle. The only data available are those for high energy electrons incident on polystyrene at a 45° angle (Figure 7), however, using the assumption that the stopping curves are universal it is possible to scale this polystyrene curve for use with ZnO.

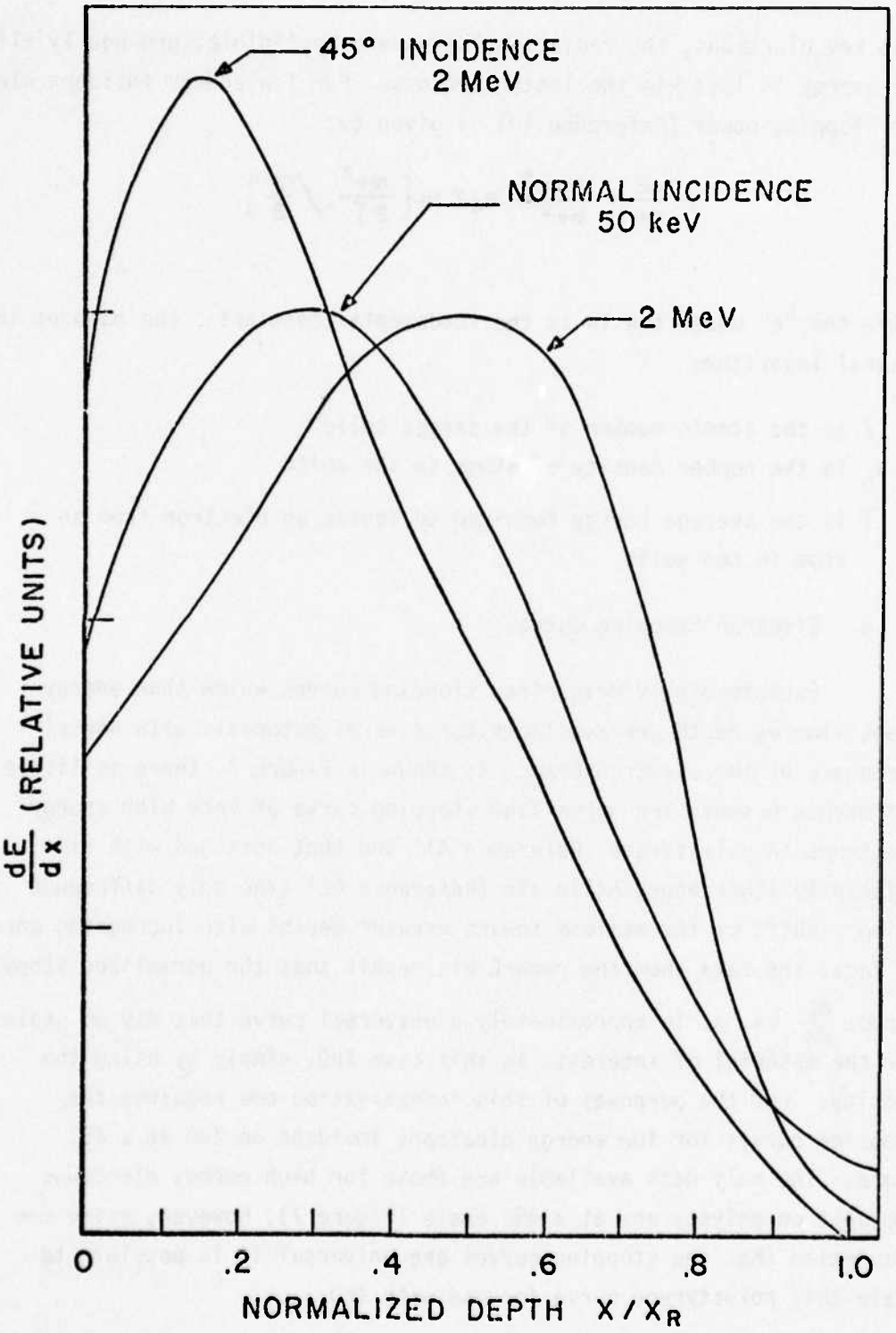

Figure 7. Electron Energy Loss Curves

Figure 8 shows the range vs. energy data for low energy electrons at normal incidence in air. Only the values between 5 - 50 keV are experimentally determined (Reference 42). The remainder of the curve is an extrapolation. Nearly identical results are obtained for the same energy range of normally incident electrons in silicon (Reference 38), and this also indicates the universality of electron stopping in a variety of materials. Referring again to Figure 7, one sees that the penetration of 2 MeV electrons in polystyrene at 45°-incidence is within 10% of the penetration of 2 MeV electrons which are normally incident. At this point the assumption is made that the depth of 45°-incident electrons is equivalent to that of normally incident electrons. Once this assumption has been made the stopping curves for 45°-incident 1-25 keV electrons in ZnO can be generated using Figure 8 and the density of ZnO to scale Figure 7. The data on penetration depths using a density of 5.642 g/cm^3 (Reference 2) for ZnO have been tabulated and placed in Appendix B.

A series of one-electron stopping curves for electrons of various energies incident at 45° in ZnO is shown in Figure 9. Following the method of Norris et al. (Reference 38), the maximum of the stopping curve is arbitrarily scaled to be $\frac{E_B}{X_R}$; where E_B is the beam energy and X_R is the penetration depth as obtained from Appendix B. Notice that I_B, the beam current, is taken to be one unit. In order to account for variations in beam current a second series of stopping curves is shown in Figure 10. For this case the peak of the curve has arbitrarily been scaled as $\frac{I_B E_B}{X_R}$, and these curves have been obtained with $\frac{I_B E_B}{X_R}$ = constant. It should be noted that this results in a constant intensity of excitation at the surface and at a depth in the ZnO substrates, which is dependent upon the beam voltage.

For purposes of luminescence the crucial concern is the generation of electron-hole pairs, which may then recombine radiatively. The energy required to produce an electron-hole pair is denoted herein by E_p. The value of E_p is a constant for a given semiconductor and is

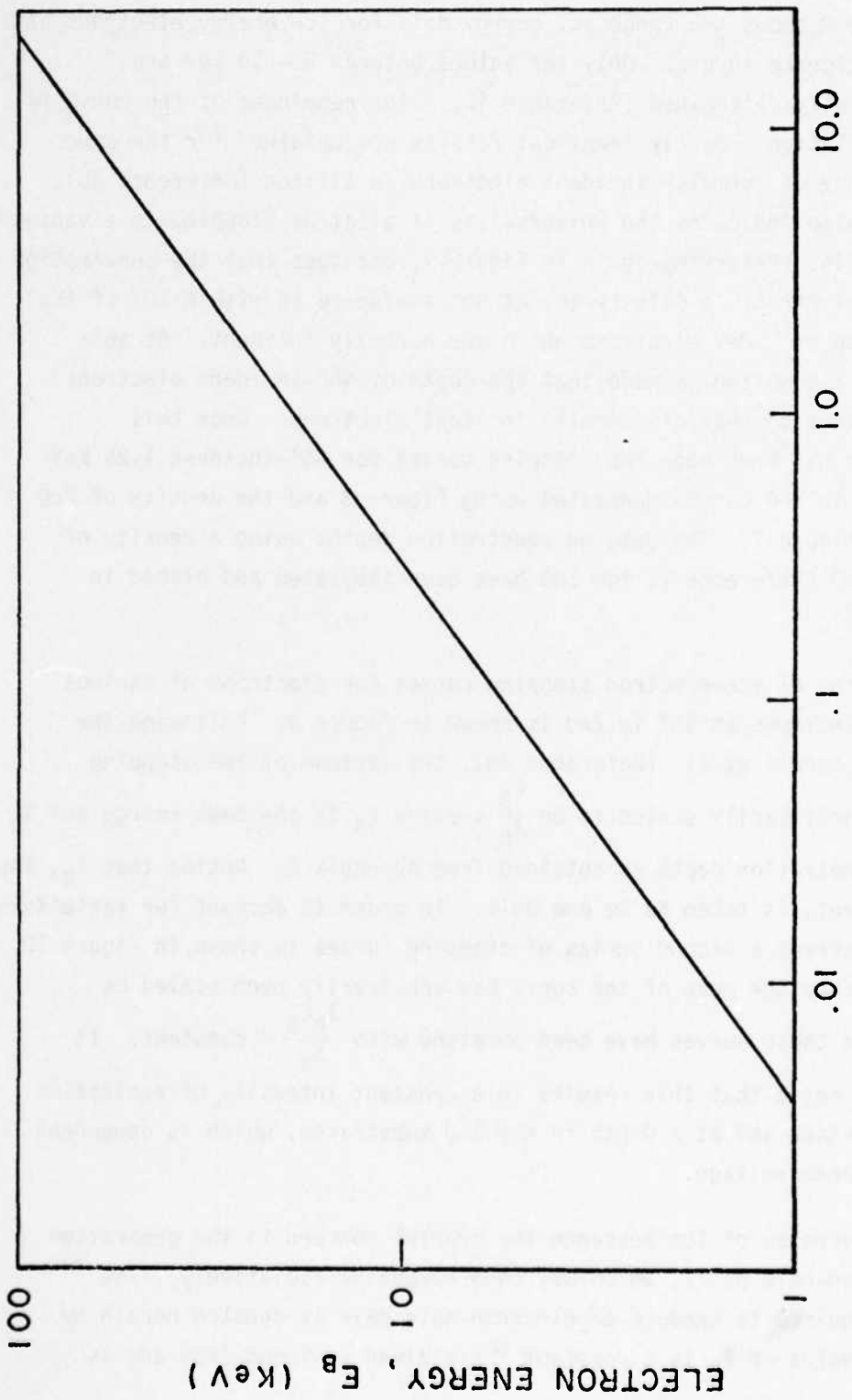

Figure 8. Universal Electron Stopping Curve

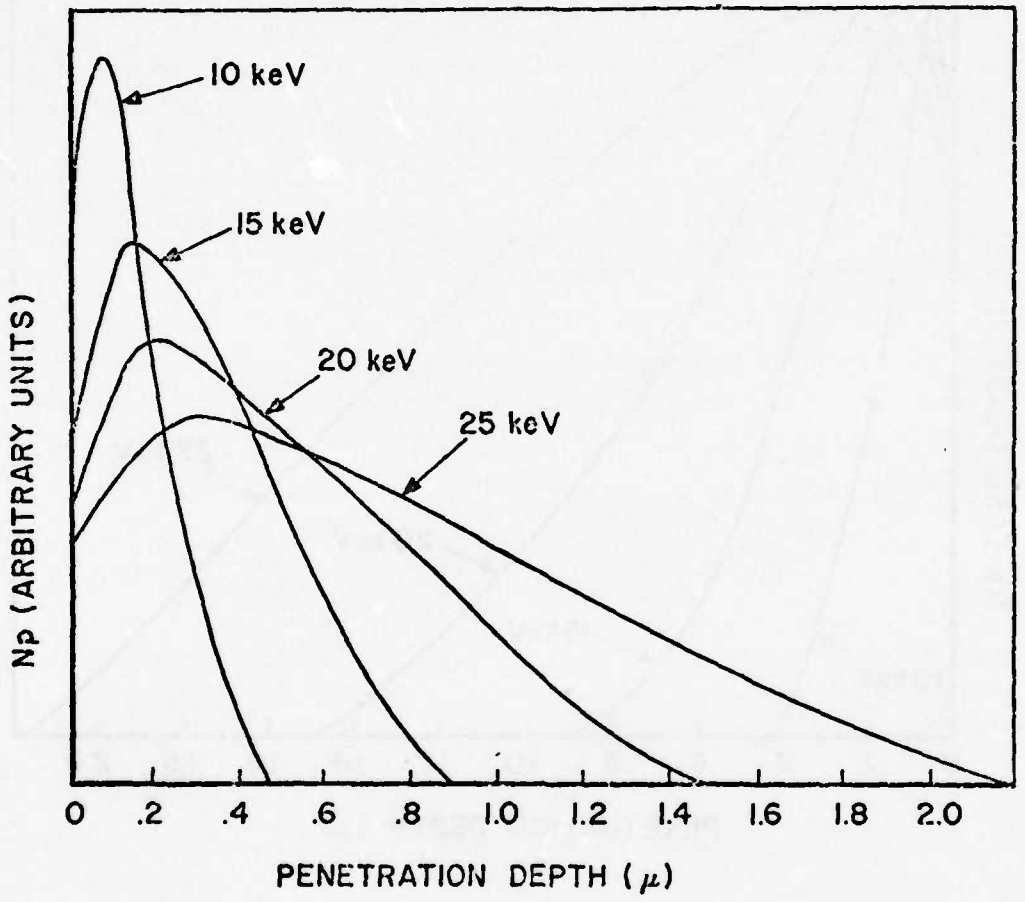

Figure 9. Single Electron Excitation Profiles

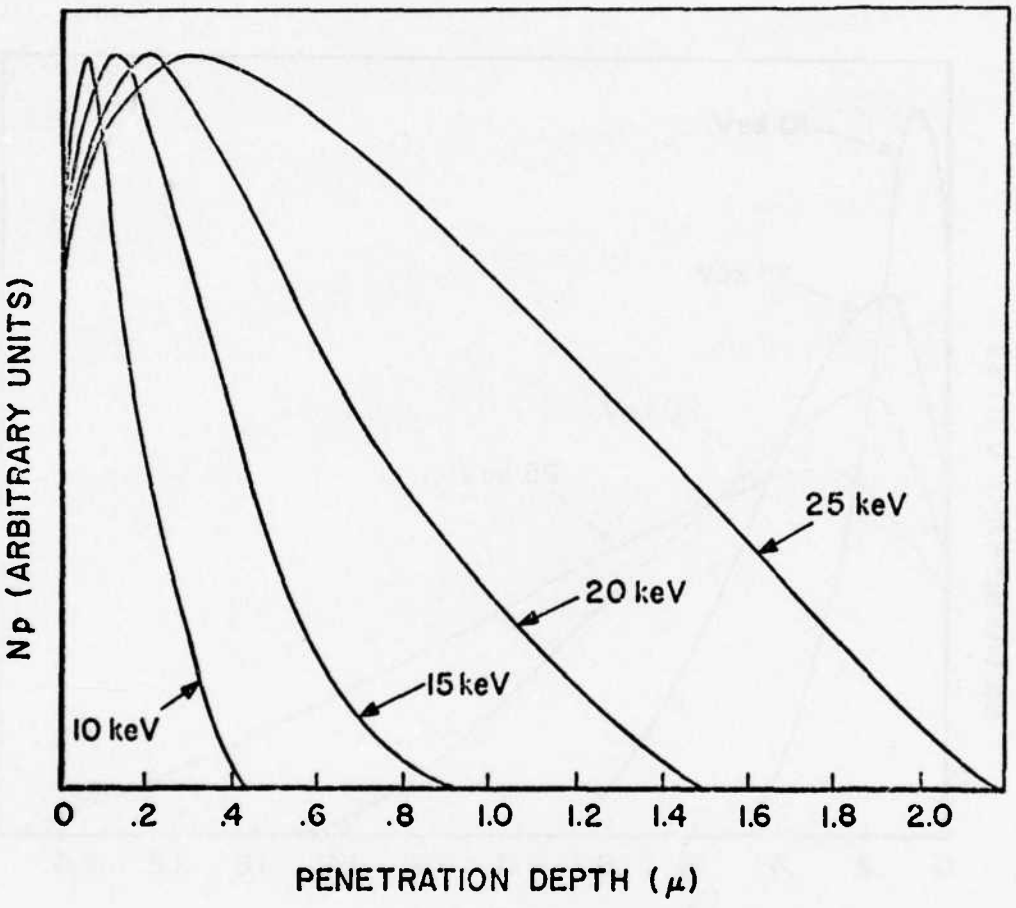

Figure 10. Current-Corrected Excitation Profiles

independent of E_B so long as E_B is much greater than the semiconductor bandgap energy, E_G, (Reference 43), which is certainly true for this investigation. The number of pairs created, N, is given approximately by $N = \frac{E_B}{E_P}$ (Reference 44) for normally incident electrons. It is not unreasonable to assume that a similar relation holds for electrons incident at a 45°-angle. Since the stopping curve, $\frac{dE}{dx}$ vs. x, provides a measure of energy lost to ionization processes, then the stopping curves in Figure 10 also display profiles of electron-hole pair creation at various depths in ZnO (for excitation at 45°-incidence with the beam currents and voltages shown).

It should be emphasized that the method described herein for probing ion implanted layers using cathodoluminescence is only a semiquantitative technique. Assuming that the profile of energy deposited in a material by high energy electrons is a universal curve which can be scaled for any material, and assuming that the penetration depth of 45°-incident electrons is equal to that of normally incident electrons one can generate a scaled set of curves for ZnO. In the scaling process the peak value of electron stopping has arbitrarily been taken equivalent to $\frac{I_B E_B}{X_R}$. These curves then represent the concentration of electron-hole pairs created at various depths within the ZnO samples for given beam energies and currents. Also, it should be pointed out that in the previous analysis no account was taken of ambipolar diffusion of electron-hole pairs. This would result in a greater proportion of the luminescence originating from deeper within the sample. However, based on the analysis of Gergely (References 45, 46) for ZnS, ambipolar diffusion is not expected to contribute a large error in this investigation. In fact, as the data reveal, there is fair agreement between the implant depth expected and that determined from cathodoluminescent probing using the method described.

b. Previous Results: Depth-Resolved Cathodoluminescence

Depth-resolved cathodoluminescence was first used in a study of CdS which had been implanted with Ar, Cu, Cl, He, and H ions (Reference 36). The implants were performed at 90°K, and subsequent annealing took place

at 350°K. Cathodoluminescence was obtained at 90°K over the range 1-20 keV using currents as high as 10 uA. The familiar CdS red band (Reference 47) near 7200 Å became much more intense after implantation and annealing, and it was possible to probe through the region of the crystal where the red band dominated the spectrum. Probing was accomplished by increasing the energy of the exciting electrons, and good qualitative agreement was obtained between the expected electron energy profiles (determined by the method just described) and the theoretical profile of damage created by the implant under investigation. Since the red peak had previously been attributed to S displacements in radiation damage studies (Reference 47) of CdS, the results showed that the depth-resolved cathodoluminescence method could be very useful in evaluating implanted layers. Similar success was achieved in a further application of the method to room temperature implants in GaAs, ZnS, and CdS (Reference 38).

5. LUMINESCENCE

Luminescence in a semiconductor occurs as the result of the recombination of electrons and holes in the material with the simultaneous emission of a photon. It has been studied extensively because the luminescence produced by a semiconductor is a sensitive indicator of the concentrations and types of defect centers (both impurities and native defects) which are present within the material. Luminescence is relatively easy to excite, especially at low temperatures, and the two common sources for the creation of excess electron-hole pairs are light (photoluminescence) and energetic electrons (cathodoluminescence). The light source employed for photoluminescence measurements is generally at a wavelength whose corresponding energy is sufficient to excite an electron from the valence band to the conduction band via optical absorption, and in the case of ZnO a source in the ultraviolet region of the spectrum below approximately 3600 Å is required. During the past decade the luminescence produced in II-VI compounds has been the subject of a number of review articles (References 48, 49, 50, 51, 52); and, in addition, Garlick (Reference 53) and Dean (Reference 54) have discussed recombination mechanisms applicable to all semiconductors.

a. Luminescence Mechanisms

The transition mechanisms which prevail in II-VI compounds are illustrated in Figure 11, which depicts schematically the recombination processes that are possible in a direct-gap semi-conductor containing a single shallow donor (ionization energy E_D), a single shallow acceptor (ionization energy E_A), and a single deep center (ionization energy E_R) near the middle of the gap. The first transition shown in Figure 11 represents the recombination of a free electron from the conduction band with a free hole in the valence band. Such a transition is never observed in luminescence because it is highly improbable that momentum conservation can be satisfied. The second transition depicts the case of a free exciton, which is occasionally observed in the luminescent spectrum as a relatively broad peak very close in energy to the bandgap (Reference 49). This transition produces a photon of energy (Reference 54)

$$E = E_G - \left(\frac{M_R^* e^4}{2\hbar^2 \epsilon^2 n^2}\right) - \frac{\hbar^2 \vec{k}^2}{2(M_e^* + M_h^*)} \tag{10}$$

where

$\vec{k} = \vec{k_e} + \vec{k_h}$

M_e^*, M_h^* are the effective masses of the electron and hole

M_{r*} is the reduced effective mass

n is the principal quantum number for the hydrogenic states of the exciton

ϵ is the static dielectric constant of the semiconducting medium

The last term in Equation 10 is the kinetic energy of the center of mass of the free exciton, and the width of the luminescence peak is attributable to the variation in energy due to this term. Since the momentum of the free exciton and the momentum of the emitted photon must be exactly the same for momentum conservation to be obeyed, this transition is not highly probable. It is more likely that it will be observed through a phonon replica peak produced when the free exciton collapse creates a photon and a lattice phonon simultaneously. Such a transition gives

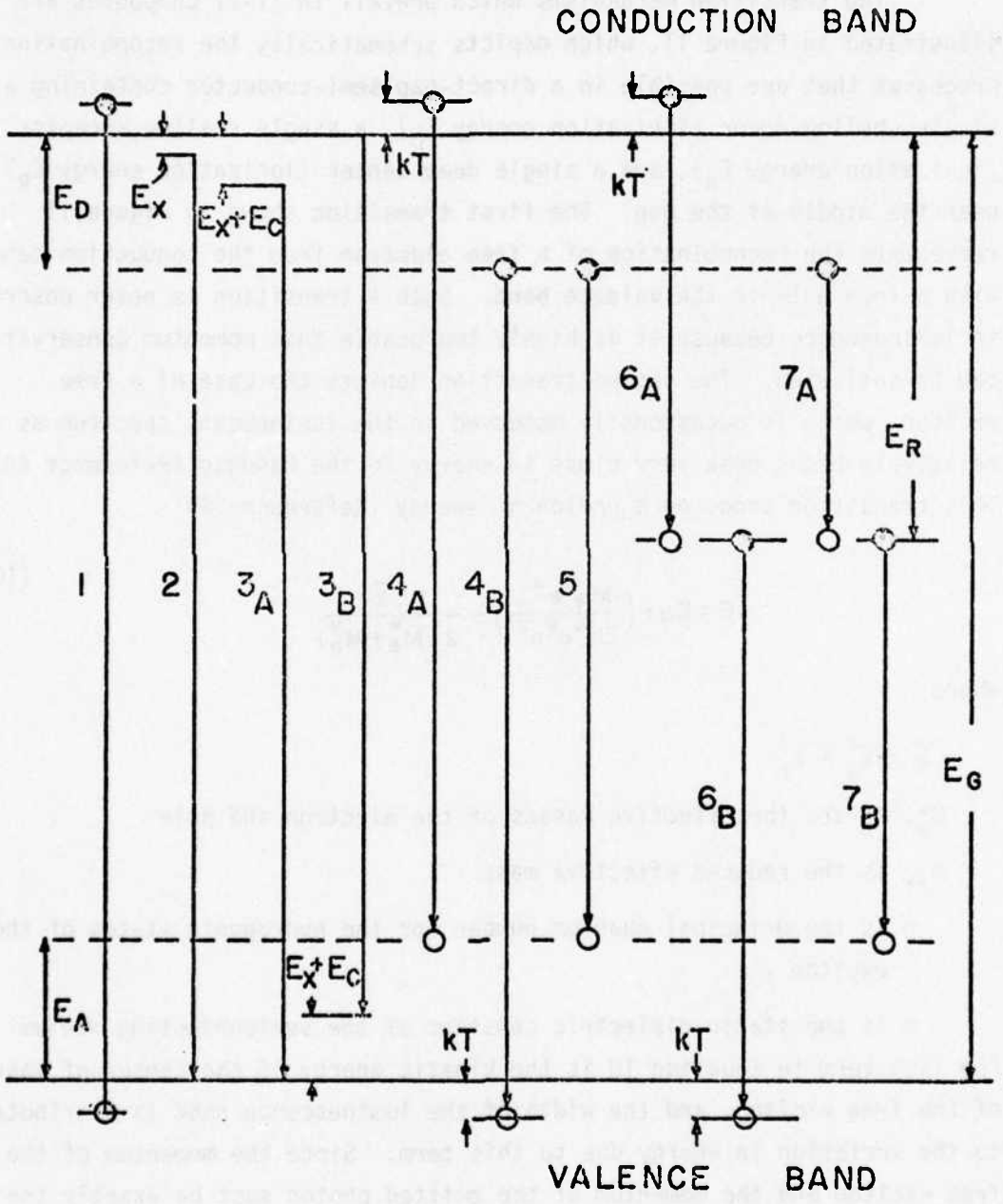

Figure 11. Luminescence Transitions

rise to a peak at lower energy by the amount required to create the phonon, and is more probable because momentum is easily conserved in the three-body process (Reference 54).

Lampert (Reference 55) first postulated the existence of bound exciton complexes and pointed out the analogy between these complexes and the various molecular and polyelectron complexes of hydrogen. The existence of such a complex was confirmed by Haynes (Reference 56) who observed sharp line structure in the luminescent spectrum of Si at 25°K, which he attributed to the collapse of an exciton bound to an ionized donor. Shifts in the sharp line spectrum obtained by doping with various group V impurities were correlated to the expected changes in ionization energy of the donors used. A detailed review of the properties of bound exciton complexes in II-VI compounds has been given by Halsted (Reference 49). Transitions 3A and 3B in the accompanying figure represent an exciton bound respectively to a donor center or an acceptor center. The transition energy is given by

$$E = E_G - E_X - E_C \tag{11}$$

where

E_X is the free exciton binding energy given by the second term on the right in Equation 10

E_C is the binding energy of the exciton complex.

Thus, a sharp line due to a bound exciton transition will occur at a longer wavelength than a free exciton peak, and the spacing in energy will amount to E_C (Reference 57).

The transition illustrated by 4A and 4B is a free-bound transition involving a free electron (hole) and a hole (electron) trapped at an acceptor (donor) center. The transition energy for the case of a free electron-bound hole recombination is given by (Reference 54)

$$E = E_G - E_A + kT \tag{12}$$

where kT is the thermal energy of the free electron. Compared to a luminescence line created by a bound exciton transition, a peak due to a free-bound transition will be a good deal broader because of the thermal distribution of free electrons, as indicated in Equation 12.

The fifth transition depicted in Figure 11 is the bound-bound transition (recombination of an electron bound at a donor and a hole bound at an acceptor). The transition energy in this case is given by (Reference 54)

$$E = E_G - (E_A + E_D) + \frac{e^2}{\epsilon R} \qquad (13)$$

where the last term accounts for the Coulomb interaction between the hole and electron as screened by the dielectric medium of the crystal lattice. The above expression is valid for distant pairs (R large compared to the lattice spacing); and since R is a discrete number corresponding to the spacing of the various donor-acceptor pairs in the crystal lattice, one expects to observe a series of sharp emission lines correlated to these discrete values of R. Series of sharp lines which could be fit to the above model were first observed in GaP (Reference 58) and have since been found in a number of semiconductors, including ZnSe (Reference 59) and CdS (Reference 60).

In many cases the discrete donor-acceptor pair lines are not resolvable, and the evidence of this transition is a rather broad peak which is the envelope of the unresolved sharp lines. However, the recombination probability is greater for those pairs which are more closely spaced in the lattice (i.e. those that have small values of R and a correspondingly larger transition energy as denoted in Equation 13) (Reference 61). As the excitation intensity is increased the pairs with large R and small transition probability will become saturated, and the luminescence will arise predominantly from transitions between the more closely spaced pairs. Thus, as the intensity of excitation is increased the envelope of donor-acceptor pair recombinations will shift toward higher energy (shorter wavelength). After the excitation source producing the luminescence has been extinguished the luminescence will decay at differing rates depending upon the transition probabilities. Hence, the near pairs will decay

first-producing a shift of the envelope toward lower energy (longer wavelength) as a function of time after excitation. The donor-acceptor mechanism had been proposed by Prener and Williams (Reference 62) to explain the properties of luminescence in ZnS phosphors. Confirmation of the model using intensity and time-resolved techniques was found in GaP by Gross and Nedzvetsky (Reference 63) and Thomas, et al. (Reference 61). A similar time-resolved effect was observed in CdS by the latter authors, and it was later examined in detail by Colbow (Reference 64).

The first five transitions have involved shallow, effective mass states which lie within approximately .1 eV of the band edges. These states may be treated using hydrogenic models, because the interaction potential varies slowly over the dimension of the unit cell (Reference 65). Transitions 6 and 7 of Figure 11 indicate free-bound and bound-bound recombinations involving a deep center near the middle of the bandgap. Prediction of the properties of deep centers is made difficult by the fact that these are highly localized, tightly bound states which are strongly affected by interactions with the crystal lattice. Usually, they are not localized enough to be accurately described by the tight-binding approximation (Reference 54). Two approximation techniques have been evolved to describe deep centers. The first method is a semi-classical approach which utilizes the local modes of the lattice to perturb the atomic wavefunctions of the impurity ion. The details of this "configuration coordinate" method and its use for interpreting luminescence results are discussed by various authors (References 66, 67, 68, 69). An alternative description of deep centers in semiconductors has recently been evolved by Messmer and Watkins (References 70, 71, 72, 73, 74). This model employs Molecular Orbital theory and has been applied successfully for various deep impurity centers in diamond.

b. Trapping Effects

The population of the various impurity levels at any given temperature, in the absence of an excitation source, is determined solely by the Fermi - Dirac statistical distribution for that temperature.

When an excitation source is present a single Fermi level is no longer sufficient to determine the occupation levels for hole and electron states, and separate quasi-Fermi levels for holes and electrons may be established for the case of quasi-equilibrium produced by continuous excitation (Reference 75). The two types of center which are of interest are a trapping center and a recombination center. A trapping center is one which captures a hole or electron, but the probability is great that the captured carrier will be thermally freed to its respective band. When a hole or electron is captured at a recombination center the probability is great that it will recombine with a carrier of the opposite type (Reference 75). In most cases centers near the band edges (shallow centers) will act as traps except at very low temperatures, whereas centers near the middle of the gap (deep centers) will act as recombination centers except at very high temperatures (Reference 75). Hence, the luminescence due to bound excitons or bound-bound transitions will decrease as the temperature is increased, because the number of trapped carriers will become progressively smaller. Likewise, as the carriers are freed the number of free-bound and free exciton transitions will increase. In general, however, the total luminescent intensity will decrease as the temperature increases because the large number of free carriers which are thermally ejected from the traps leads to a greater probability of nonradiative transition via the Auger process (Reference 54). In addition, at higher temperatures there are more vibronic states which may interact with the excited electronic state of a deep center and cause a relaxation of this state by nonradiative means (Reference 69).

c. ZnO Luminescence

A typical luminescence spectrum obtained from a ZnO platelet by Reynolds, et al. (Reference 76) is shown in Figure 12. This luminescence, consisting of a series of peaks in the ultraviolet and a broad band in the visible portion of the spectrum, is characteristic of the low temperature luminescence of ZnO (References 77, 78, 79). Depending upon the previous history of the sample, the broad visible band may lie in the green, as shown in Figure 12, or may shift to the yellow (References 80, 81), yellow-orange (Reference 82), or red (References 83, 84, 85)

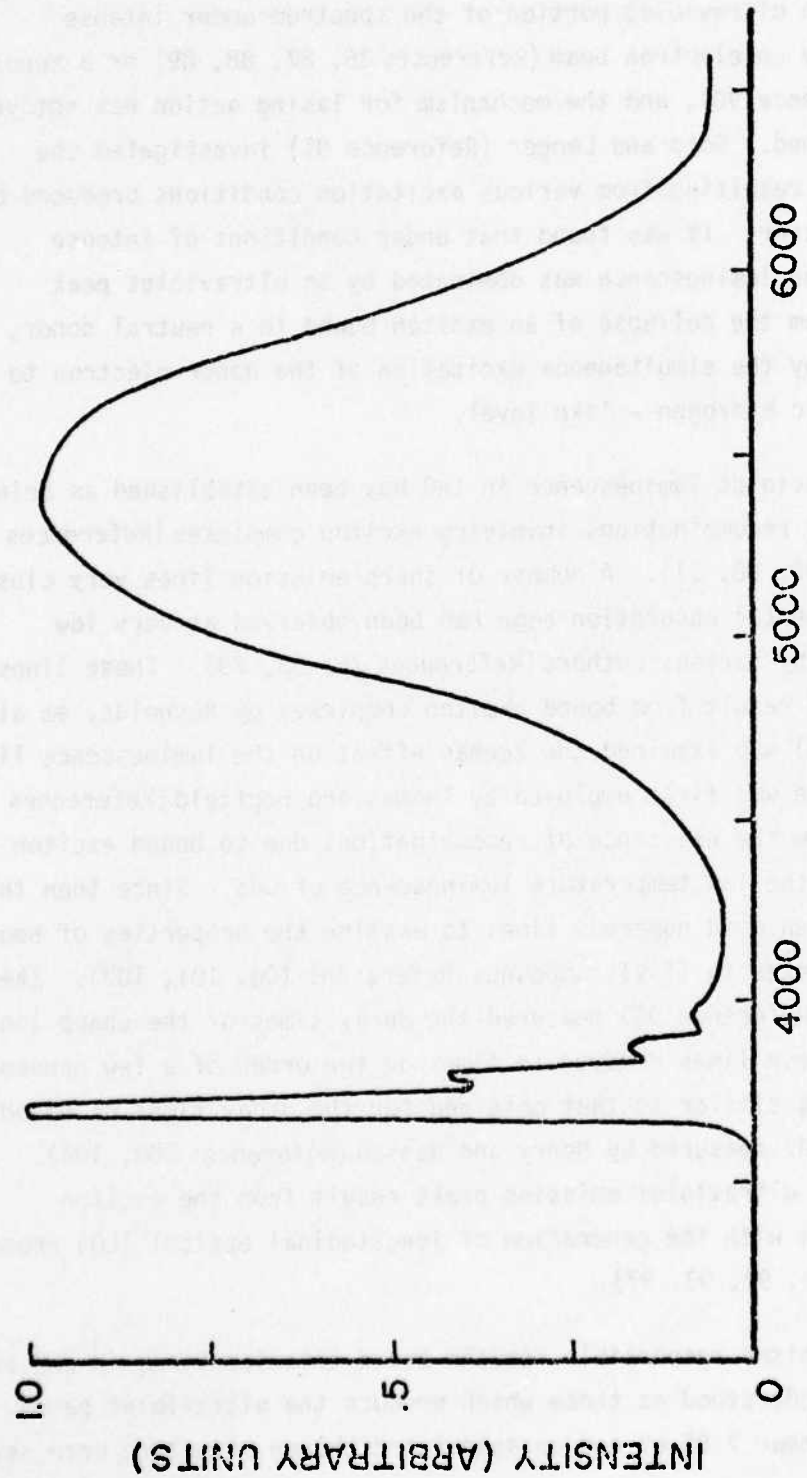

Figure 12. Typical ZnO Luminescence Spectrum (Reference 76)

region of the visible spectrum. ZnO single crystals exhibit lasing action in the ultraviolet portion of the spectrum under intense excitation by an electron beam (References 86, 87, 88, 89) or a xenon laser (Reference 90), and the mechanism for lasing action has not yet been determined. Goto and Langer (Reference 91) investigated the luminescence resulting from various excitation conditions produced by a nitrogen laser. It was found that under conditions of intense excitation the luminescence was dominated by an ultraviolet peak resulting from the collapse of an exciton bound to a neutral donor, accompanied by the simultaneous excitation of the donor electron to a more energetic hydrogen - like level.

The ultraviolet luminescence in ZnO has been established as being the result of recombinations involving exciton complexes (References 76, 92, 93, 94, 95, 96, 97). A number of sharp emission lines very close to the fundamental absorption edge had been observed at very low temperatures by various authors (References 76, 93, 79). These lines were shown to result from bound exciton complexes by Reynolds, et al. (Reference 76) who examined the Zeeman effect on the luminescence lines. This technique was first employed by Thomas and Hopfield (References 98, 99) to confirm the existence of recombinations due to bound exciton complexes in the low temperature luminescence of CdS. Since then the method has been used numerous times to examine the properties of bound exciton complexes in II-VI compounds (References 100, 101, 102). Skettrup and Lidholt (Reference 94) measured the decay times of the sharp lines and found that these lines decayed in times on the order of a few nanoseconds. This result is similar to that obtained for the decay times of bound excitons in CdS measured by Henry and Nassau (References 103, 104). The remaining ultraviolet emission peaks result from the exciton recombinations with the generation of longitudinal optical (LO) phonons (References 79, 92, 93, 97).

The mechanisms responsible for the broad emission bands in ZnO are not as well understood as those which produce the ultraviolet bands. A sharp line near 2.85 eV and an associated phonon structure were seen

in the green region of the visible spectrum by Solbrig and Mollwo (Reference 79). This structure was also reported by Dingle (Reference 105) who was able to resolve two lines at 2.85908 eV and 2.85897 eV in samples which contained Cu as an impurity (as determined spectrographically). Time-resolved measurements at low temperature revealed that the entire green band decayed exponentially within 440 ± 10 nanoseconds, and this is similar to the decay time of 158 nanoseconds for the green band measured by Skettrup and Lidholt (Reference 94). It was also found that the ratio of intensity of the two sharp lines was 2.25 ± .05 and that the ratio remained the same over the region of 1.6°K to 20.4°K. Since the ratio of naturally occurring copper isotopes (Cu^{63}/Cu^{65}) is 2.24 it appeared that the two sharp lines were produced by the same center, which occurred at slightly different energies in accordance with a particular copper isotope. This argument was supported by the Zeeman data, which showed that the two lines behaved identically in the presence of a magnetic field. The values for the g factors obtained from the Zeeman data were in excellent agreement with the values obtained from Cu-doped ZnO crystals investigated by ESR (Reference 106). This offered convincing evidence that the emission was due to a Cu center, and it was proposed that this center was a Cu++ ion substitutionally located at a Zn lattice site with the transition occurring between an excited state and the highly shielded, localized ground state of the center.

Schirmer and Zwingel (Reference 81) investigated the properties of the yellow band which they were able to produce in single crystals in ZnO by doping with Li. A similar yellow luminescence had been observed by other workers in ZnO powders which had been baked in an oxygen stream (Reference 80). Both the green and yellow luminescence were observed in powders obtained by burning high purity zinc and then baking the resultant ZnO powders in air for an hour at 1000°C. The green band became more intense as the powders were heated at progressively higher temperatures in an argon atmosphere, whereas the yellow band became more intense as the powders were heated in oxygen. The yellow band was attributed to the formation of a native defect.

Schirmer and Zwingel employed thermoluminescence to study the yellow band in crystals doped with Li by diffusion or by incorporation during growth to concentrations as high as 200 ppm (Reference 81). The luminescence was excited at low temperatures using the light from a high pressure Hg lamp, and the samples were subsequently heated at a rate of .08°K/sec. in the absence of excitation. Peaks in the luminescent intensity were observed at 35°K and 120°K. It was also found that the green emission decayed very rapidly after the excitation was removed, whereas the yellow band exhibited a rather long after glow. Both the observed thermoluminescence and the long afterglow exhibited the same spectral distribution consisting of a .5 eV wide band with a peak at 2.02 eV. A study of the polarization of the yellow emission showed that it exhibited some degree of polarization and that the amount of polarization was dependent both on temperature and decay time - the ratio, $P = I_{||}/I_{\perp}$, decreased as the temperature increased above 33.5°K and also, as the temperature increased the degree of polarization, $P' = \frac{I_{||} - I_{\perp}}{I_{||} + I_{\perp}}$, obtained a maximum value in progressively shorter time intervals after the removal of excitation. It was shown that this behavior could be correlated with results obtained from ESR studies of the paramagnetic Li center in ZnO (Reference 108), and it was concluded that the yellow luminescence resulted from the incorporation of Li + ions on Zn lattice sites. The increase in polarization with time after excitation was attributed to the relaxation of a hole (initially trapped at a non-axial bond) from the non-axial to the more stable axial position. Further evidence for this interpretation was provided by studying the luminescent decay in samples doped with Li^6 and Li^7. The Li^7 emission polarized parallel to the c-axis was stronger than that due to Li^6 over a range of decay times from 1 minute to 30 minutes. This was to be expected because of the lighter mass of Li^6 which led to faster decay of the polarized luminescence. In a more recent paper (Reference 107) Zwingel proposed that the yellow luminescence arises from a pair recombination between shallow donors, previously existing in the ZnO crystals, and deep acceptors, approximately .8 eV above the valence band, which were incorporated by doping with Li.

Osiko (Reference 83) observed a red band in ZnO powders heated in oxygen at temperatures in the range 1100 to 1200°C and attributed this red band to the excess of oxygen. In a similar experiment on ZnO powders (Reference 84) the red band was attributed to the oxidation of metallic zinc present on the surface of the samples. Recently, Lauer (Reference 85) observed the red band (1.70 eV) in both phosphors and single crystal samples of Airtron hydrothermal ZnO. The 1.70 eV band was found to exist as a lower intensity sideband on the 2.02 eV emission band in samples which had been baked in O_2 at 900 - 1000°C. Unlike the green band which could only be excited with light near the edge, the 2.02 eV and 1.70 eV bands could be excited with light of lower energy. It was found that the red band decayed much more rapidly than the yellow band, and it was shown that the centers responsible for the red band were present in the bulk of the crystal as well as on the surface. The red band was attributed to a free-bound transition between electrons in the conduction band and holes trapped at a center approximately 1.6 eV above the valence band edge. It was postulated that this center arose from the formation of a Zn vacancy or possibly from Na occupying Zn lattice sites.

d. Previous Results: Luminescence of Ion Implanted Layers

Merz, et al. (Reference 109) and Feldman, et al. (Reference 110) have implant Bi into GaP under varying conditions and studied the results using channeling and by observing the well-known luminescence produced by the Bi isoelectronic center. The results of the channeling measurements showed that: each 100 keV Bi ion produced 13,400 displacements (slightly more than one-half the total were P displacements), annealing occurred at 450°C for low dose ($<2 \times 10^{13}/cm^2$) implants and occurred at 750°C for implants with higher doses, a protective coating of SiO_2 was necessary for the high temperature anneals (up to 900°C), for doses of $7.5 \times 10^{13}/cm^2$ 25% of the Bi ions moved to the surface, and ten times more Bi ions were found by channeling to be substitutional on P sites than were indicated by the optical activity observed in photoluminescence. For 200 keV implants it was discovered that the maximum intensity of the isoelectronic Bi photoluminescence peak was obtained using an implant

with a dose of 3.5 x $10^{12}/cm^2$ ($10^{18}/cm^3$) which had been annealed at 900°C. The quenching of the photoluminescence in higher dose samples was presumed to be caused by residual damage.

Eisen and coworkers (References 112, 113) have employed the channeling technique and photoluminescence to study the properties of H, C, O, and Te implants in GaAs. The H, C, and O implants were performed at room temperature; and it was found an anneal of 600°C was required to restore the photoluminescence, which had been quenched by the implant. It was observed that the GaAs surface was extremely reactive to O, and this affected the photoluminescence. A luminescence peak due to acceptor centers induced by As vacancies was observed after implantation or after annealing at high temperature, and it was discovered that the production of As vacancies upon annealing could be inhibited by a protective coating of SiO_2. The channeling measurements revealed an annealing step at 300°C for low dose implants and a second step at 600°C for high dose implants. The Te implants were performed at room temperature and at 150°C; and, in addition, both Si_3N_4 and SiO_2 were evaluated as a protective coating. Photoluminescent measurements revealed that the optimum luminescent intensity was obtained for implants which were performed at 150°C and subsequently annealed above 750°C with a protective coating of Si_3N_4.

The properties of CdS crystals which had been implanted at room temperature with various doses of Li, Na, and Ne were studies by Tell, et al. (Reference 113). Implants were performed at three successive energies with the same dose at each energy. The energies for the Li implant were 35, 90, and 200 keV at a dose of 1 x $10^{13}/cm^2$ for each step. The implants of Na and Ne were both performed at energies of 60, 150, and 270 keV. Na samples were prepared using doses of 2 x $10^{12}/cm^2$, 1 x $10^{13}/cm^2$, and 5 x $10^{13}/cm^2$, and Ne samples were prepared using doses of 2 x $10^{12}/cm^2$ and 1 x $10^{13}/cm^2$. Photoluminescence was obtained from samples which had been isochronally annealed for a one-hour time period at temperatures as high as 400°C in an S ambient. Convincing evidence was obtained showing that the I_1 lines (excitons bound to neutral acceptors) and the green edge emission (donor-acceptor pair emission bands)

in CdS involve alkali metal acceptor centers. This concurred with earlier results using conventional doping techniques (References 60, 114, 115). As expected the Ne implants were significantly different from the Na implants performed with the same energies and doses and annealed in a similar manner. This indicated that the Ne implant simply produced damage, whereas the Na implant contributed chemically active dopant ions.

The broadband or deep center luminescence was studied as a function of annealing temperature for ZnSe samples which had been implanted at room temperature with 90 keV ions of N, Br, and Ar. The dose used for these implants was $10^{15}/cm^2$, and the photoluminescence investigation was performed by Santiago, Ehret, Woody, and Park (Reference 116). An as-grown sample showed a single peak at 6400 Å, but after heating in vacuum at 400°C for 15 minutes a peak appeared at 5400 Å. Subsequent heating at temperatures above 900°C in molten Zn caused the 5400 Å peak to be quenched, indicating that the peak was associated with Zn vacancies. Implants of Ar enhanced the 5400 Å band slightly upon annealing in vacuum, probably due to an increase in the number of Zn vacancies induced by the implant. The N implants induced no new bands for any of the annealing sequences used, however, the 6400 Å and 5400 Å bands drew closer together as the annealing temperature was increased up to 400°C which indicated an interaction between the centers responsible for the luminescence. Similar complexing was observed for the case of the Br implant; and, in addition, a new peak at 6200 Å, which had previously been attributed to Br doping in ZnSe, appeared after annealing above 620°C. It seemed likely that the 6400 Å peak, which was believed to be due to Se vacancies, obscured the major portion of any luminescence produced by optically active centers due to N or Br.

6. ELECTRICAL PROPERTIES

The determination of the electrical properties of Ge and Si, and a knowledge of how impurities affect the electrical properties of these materials has led to great technological advances as well as to a basic understanding of semiconductors. Measurements of the Hall effect in Si and Ge over a wide range of temperatures provided the key to these

developments (for a complete review and discussion see (Reference 117). The Hall effect measurement determines the density and type of charge carriers (i.e. whether holes or electrons) and also the resistivity of the substrate. If the semiconductor is very pure or if the temperature is high enough, the conduction will be dominated by electrons and holes which are thermally generated by exciting electrons directly from the valence band to the conduction band. Due to the wide bandgap of ZnO, intrinsic conduction is relatively unimportant in ZnO at normal temperatures, and the electrical properties are dominated by extrinsic (impurity) effects.

a. van der Pauw Method

When measuring the Hall effect in an isotropic solid of uniform thickness, it is best to use a rectangular bar having a length at least four times the width (Reference 117). This provides for the simplest treatment of the measured values of resistivity, carrier concentration, and Hall mobility. Current is passed through the ends of the bar and the voltages necessary to determine the parameters of interest are measured at points along the sides of the bar. When the electrical properties of an ion implanted layer are to be measured, the fact that the layer is so thin precludes measurement by the standard technique; and it is desirable to have a means of performing Hall effect measurements by contacting the surface of the thin implanted layer. The van der Pauw technique (Reference 118) provides just such a method. The method was derived by van der Pauw using conformal mapping techniques and applies for any flat sample of arbitrary shape. Only four contacts are required; and they are made to the surface of the thin layer under investigation, subject to the following assumptions: the contacts are sufficiently small (essentially ideal point contacts), the contacts are placed at the circumference of the sample, and the sample is of homogeneous thickness with a simply-connected surface (Reference 118).

The sample geometry used in this study is shown in Figure 13. In each of the six configurations shown in the figure, the voltage between V_1 and V_2 is measured and recorded after the current through the battery

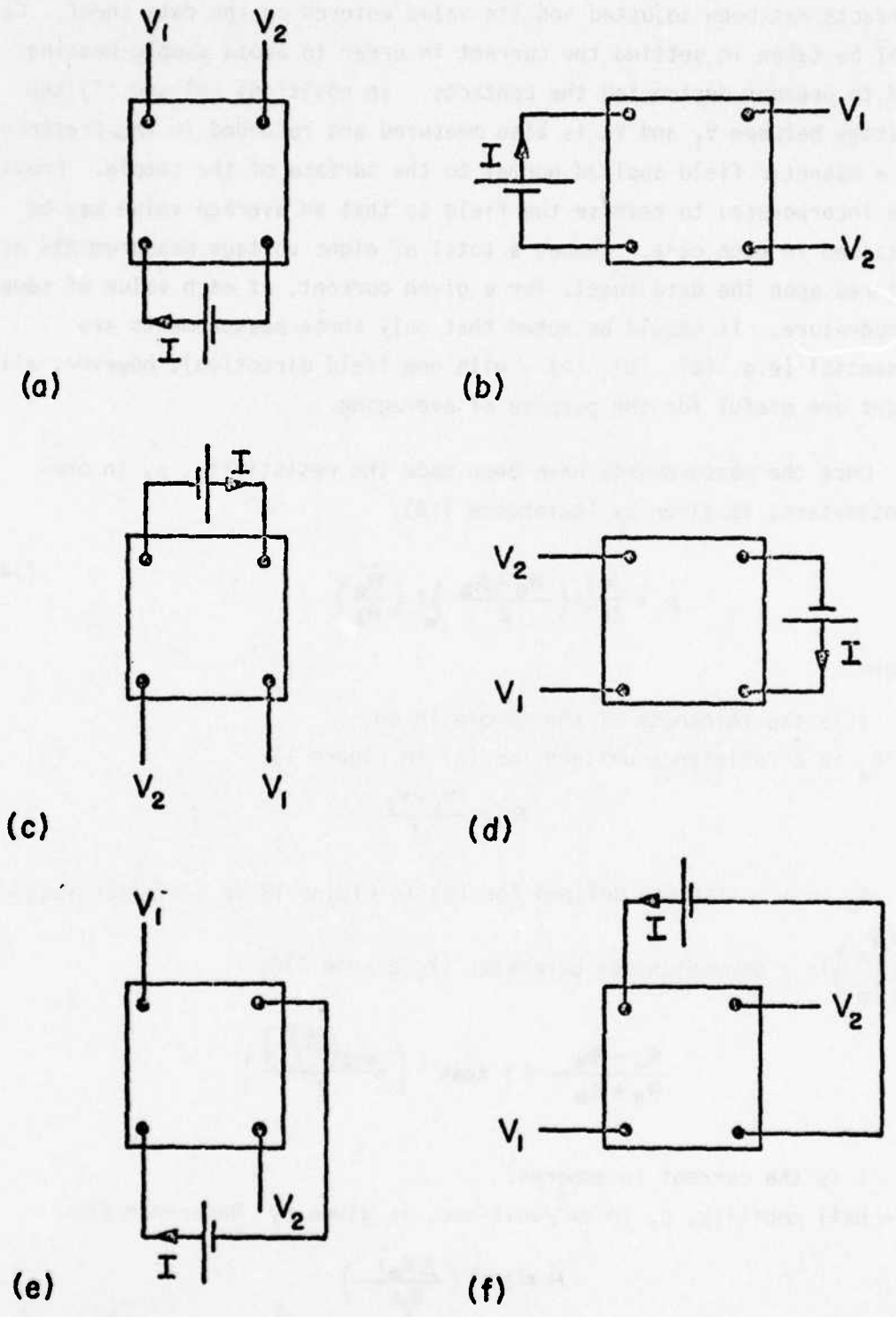

Figure 13. van der Pauw Sample Geometry

contacts has been adjusted and its value entered on the data sheet. Care must be taken in setting the current in order to avoid sample heating and to prevent destroying the contacts. In positions (e) and (f) the voltage between V_1 and V_2 is also measured and recorded in the presence of a magnetic field applied normal to the surface of the sample. Provisions are incorporated to reverse the field so that an average value may be obtained in each case. Hence, a total of eight voltage measurements are entered upon the data sheet, for a given current, at each value of sample temperature. It should be noted that only three measurements are essential (e.g. (a), (b), (e) - with one field direction), however, all eight are useful for the purpose of averaging.

Once the measurements have been made the resistivity, ρ, in ohm-centimeters, is given by (Reference 119).

$$\rho = \frac{\pi t}{\ln 2}\left(\frac{R_a + R_b}{2}\right) f\left(\frac{R_a}{R_b}\right) \tag{14}$$

where

t is the thickness of the sample in cm.

R_a is a resistance defined for (a) in Figure 13

$$R_a = \frac{V_1 - V_2}{I}$$

R_b is a resistance defined for (b) in Figure 13 in a similar fashion

$f\left(\frac{R_a}{R_b}\right)$ is a dimensionless parameter (Reference 118)

$$\frac{R_a - R_b}{R_a + R_b} = f \cosh^{-1}\left[\frac{\exp\left(\frac{\ln 2}{f}\right)}{2}\right]$$

I is the current in amperes.

The Hall mobility, μ, in cm^2/volt-sec, is given by Reference 119

$$\mu = 10^8\left(\frac{\Delta R_e t}{B\rho}\right) \tag{15}$$

where

B is the magnetic field in gauss

ΔR_e is the change in the value of the resistance, R_e, (defined similarly to R_a) of position (e) when the magnetic field is applied normal to the surface.

Finally, the carrier density, n, in number of carriers/cm^3 is computed from Reference 119

$$n = \frac{1}{\rho e \mu} \qquad (16)$$

where e is the charge on the electron in coulombs. A computer program has been written which processes the data for any given temperature, T, in °K, and provides plots of: $\text{Log}_{10}\rho$, $\text{Log}_{10}n$, and μ vs. $\frac{1000}{T}$; and also $\text{Log}_{10}\mu$ vs. Log_{10} T over the range of temperature for which data have been collected on a particular sample.

b. Interpretation of Data

Once the data have been collected it is necessary to compare the results with a theoretical model to determine the effects produced by various impurities. Assuming a single donor and single acceptor impurity with ionization energies, E_D and E_A, concentrations, N_d and N_a, and occupation numbers, n_d and n_a, respectively; one may obtain from the standard expressions for semiconductor statistics (Reference 120).

$$\frac{n_o(n_o+N_a-p_a-p_o)}{N_d-N_a-n_o+p_o+p_a} = \frac{N_c}{2} e^{-E_D/kT}$$

In the above expression the sample has been considered to be n-type, n_o and p_o are the concentrations of electrons in the conduction band and holes in the valence band respectively, and N_c is the conduction band density of states given by:

$$N_c = 2\left(\frac{2\pi M_n^* kT}{h^2}\right)^{3/2}$$

For the case of a purely n-type material the expression becomes

$$\frac{2n_o^2}{(N_d - n_o)N_c} = e^{-E_o/kT} \qquad (17)$$

When compensation becomes important, but p_o is still very small, the expression may be written as

$$\frac{2n_o(n_o + N_a)}{(N_d - N_a - n_o)N_c} = e^{-E_D/kT}$$

The expressions given by Equations 17 and 18 may be used to fit the data of the plot of Log_{10} n vs. $\frac{1000}{T}$ obtained from the van der Pauw measurements. The slope of the curve over a range of values of T provides a measure of the ionization energy, E_D, of the center responsible for donating the electrons in that range of temperatures. A similar analysis holds for p-type samples if an appropriate change of variables is made.

c. Electrical Properties of ZnO

As-grown crystals of ZnO are normally n-type and exhibit conductivities which typically range from .01 ohm^{-1} cm^{-1} to 5 ohm^{-1} cm^{-1} (Reference 121). In an effort to determine the cause of this conductivity, studies were made on ZnO crystals doped with H (Reference 121), Zn (Reference 122), In (Reference 123), and Li (Reference 124). The conductivity of the doped crystals was monitored at various pressures of doping atmosphere and over a wide range of diffusion temperatures. The data obtained were used in an analysis of the diffusion coefficient for the particular impurity being studied. It was found that baking ZnO in H using pressures of .01 to 114 atmospheres over the temperature range of 450 to 700°C produced an increase of conductivity with higher pressures and temperatures. This increase in conductivity was due to an increase in the number of donors, which was attributed to the formation of OH^- centers. A similar increase in conductivity was observed for samples baked in Zn vapor over the temperature range of 300 to 750°C, and this effect was attributed to interstital Zn. It was shown that interstitial Zn was not responsible for the initial conductivity

of the samples, which was thought to be due to impurities; and it is interesting to note that no coloration of the crystals, as described earlier, was observed. Samples of ZnO which had been coated with indium nitrate were baked at temperatures in the range of 800 to 1300°C, and an increase in conductivity was observed at first. This initial increase was followed by a decrease in conductivity as the ZnO became saturated with In which formed precipitates thereby decreasing the number of induced donor centers. All measurements were performed in one atmosphere of oxygen.

In the case of Li it was found that the conductivity could be varied over a wide range. Samples which had been coated with evaporated Li were baked in a Zn atmosphere at temperatures in the range 300 to 600°C, and these samples exhibited increased conductivity due to interstitial Li donors. When a heavily doped sample was subsequently heated in air to temperatures as high as 700°C the conductivity was drastically lowered, and this effect was attributed to the formation of Li acceptor centers with an activation energy of 1.5 eV.

Hutson (References 125, 126) performed Hall effect studies on samples of ZnO doped with Zn, Li, and H which were similar to those described previously. Measurements were obtained over the temperature range from 55°K to 300°K. Both H and Zn readily formed donor centers with an ionization energy of .051 eV for concentrations below $5 \times 10^{16}/cm^3$ as determined by an analysis employing Equation 17. In the case of Li it was necessary to use Equation 18 because some of the Li ions substituted for Zn in the lattice to form compensating acceptor centers. The ionization energy of the interstitial Li donor centers was found to be .044 eV.

d. Previous Results: Electrical Properties of Ion Implanted Layers

The van der Pauw technique has been very successfully applied to measurements of the Hall effect in Si implants (References 127, 128) (see also Reference 17: Chapter 5). More recently, it has been used to study implants of Cd, Zn, S, Si, and C (References 129, 130) which produce type

conversion in various GaAs substrates. Hemenger and Dobbs (Reference 131) of the AFML employed the same system (Reference 119) which was used in this study of ZnO to measure the electrical properties of sulfur-doped GaP samples which had been implanted at room temperature to a dose of $10^{16}/cm^2$ with 250 keV Zn ions. Type conversion was achieved after a 30-minute anneal at 900°C in an evacuated ampoule, and the surface was protected during the anneal by a 1000 Å layer of SiO_2 which had been deposited on the surface by the R.F. sputtering of a quartz target.

A major difficulty in determining the Hall effect in II-VI compounds is that samples having very high resistivities are often encountered, and special care must be taken in the performance of the measurements (Reference 119). For this reason a number of authors (References 132, 133, 134, 135, 136, 137, 138, 139) have employed other means to examine implanted layers in II-VI compounds. These included: I-V characteristics, C-V characteristics, photoelectric properties, thermal probe measurements, and electroluminescence.

Conventional measurements of the Hall effect were made by Chernow et al. (Reference 140) for CdS implanted with Bi and by Shin et al. (Reference 141) in Al implanted ZnSe. It was found that room temperature, high dose ($10^{16}/cm^2$) implants of 25 keV Bi ions in CdS produced a p-type layer with no subsequent annealing required. The layer was estimated to be 3000 Å thick with a hole mobility of approximately 3 cm^2/v-sec and a resistivity between 1Ω cm and 500Ω cm. Temperature dependent conductivity measurements indicated an activation energy of .015 eV. The Al implants in ZnSe were performed at room temperature into undoped high resistivity (10^8Ω cm) n-type samples. A 90 keV implant to a dose of $10^{15}/cm^2$ produced a degenerately doped n-type layer having low mobility (less than 1 cm^2/v-sec).

There has only been one reported study of ion implantation in ZnO (Reference 142). Implants of H, P, V, N, O, Ar, and Ne were made at room temperature into both low resistivity (1.0Ω/□) and high resistivity (2×10^7Ω/□) substrates of Li-doped, n-type ZnO. Beam energies as high as 300 keV were employed at dose levels of 10^{12}-$10^{16}/cm^2$, and annealing was performed isochronally for periods of one hour in evacuated ampoules at temperatures between 100 and 500°C. The van der Pauw technique was used

to measure the Hall effect in the implanted layers (contacts being formed by the evaporation of Al). Implants of P and V to a dose of $5 \times 10^{15}/cm^2$ produced a large reduction in the resistivity of the high resistivity substrates, and the result was unaffected by the annealing temperatures used. A similar Ar implant into high resistivity ZnO produced no change. Identical implants performed in low resistivity substrates resulted in an increase in resistivity subsequent to implantation, however, the resistivity was found to decrease to its initial value for annealing treatments at 500°C. A sharp annealing step was observed at 300°C. Similar results were obtained for low resistivity substrates which had been implanted with N, O, H, and Ne.

SECTION III

DESCRIPTION OF EXPERIMENT

In order to determine the optical and electrical properties of the centers induced in ZnO by the implantation of various ions, several experimental methods were employed. The primary investigative technique used was the method of depth-resolved cathodoluminescence, which has been previously described; and the system employed to produce and record this luminescence is described in detail in this section. Since the luminescence and electrical properties were significantly affected by the physical condition of the ZnO samples, great care had to be taken in preparing the samples. The methods of sample preparation and a complete tabulation of implant conditions are presented prior to the description of the cathodoluminescence system. A brief exposition of the photoluminescence system and van der Pauw Hall effect system is also included in this section.

1. SAMPLE PREPARATION

The samples used for this investigation were cut, using a diamond wire saw, from two large single crystal boules of ZnO obtained from the Airtron Corporation. These crystals were grown by the hydrothermal method (References 143, 144, 145, 146), in which high purity ZnO powders were dissolved in a basic solution, usually an aqueous solution of KOH; and large single crystals were nucleated by epitaxial deposition on a seed crystal. The nucleation occurred in a sealed autoclave under pressures as high as 1700 atmospheres, and the growth temperature was in the range of 300 to 400°C. In order to suppress dendrite formation, a small amount (0 - 2.0 molal) of LiOH was added to the solution. The addition of LiOH resulted in Li doping to levels as high as 10 ppm. One of the boules used for this investigation was a "C-plane" crystal in which the c-axis was normal to the large (0,0,0,1) faces of the boule, while the second was an "A-plane" crystal having the c-axis parallel to its large (1,0,1,0) faces. All of the rough-cut samples were in the shape of 10 mm squares approximately 1 mm thick. After the samples were cut they were polished and etched. Following this they usually were implanted, had a protective coating of approximately 2500 Å of SiO_2 deposited by RF sputtering, and

were then annealed. After which the SiO_2 was removed by a 30-second etch in 50% HF. The details of polishing, etching, annealing, sputtering, and the variety of implant ions and conditions used will be described in the sections that follow.

a. Polishing

All samples were polished after they had been cut. Since ZnO is a relatively hard semiconductor the polishing operation presented no particular difficulties. The initial stage of the operation was accomplished on two automatic Lapmaster machines using first 5μ and then 1μ grit. Following the initial stage the samples were polished by hand on a Buechler rotary wheel using .03μ grit in distilled water. This procedure provided a smooth flat surface, and normally only a few fine scratches could be observed upon closer examination with a microscope.

During the polishing operation the samples were affixed, using black wax, to standard mounting rings provided with the Lapmaster machines. The length of time required for polishing a group of samples depended somewhat upon variations in thickness of the saw cuts, but usually four-eight hours was sufficient to achieve the desired result. Samples were removed from the rings by heating on a hot plate to melt the black wax, the residue of which was then dissolved by soaking the samples overnight in toluene. Following this they were successively rinsed in acetone, methyl alcohol, and distilled water.

b. Etching

It was found that in order to obtain a high degree of luminescence in the ZnO samples after they had been cut and polished, it was necessary to follow the polishing procedure with an etch. A variety of etches were evaluated by examining the physical appearance of the samples under a microscope and by observing the visible luminescence of the samples when they were placed in liquid nitrogen and irradiated by a mercury lamp. Based on the indications obtained in this manner it was discovered that a ten-minute etch in a 90°C, 50% solution of NaOH gave the best results. This etching procedure was then used for all samples after they had been

cut and polished and for all unimplanted samples after they had been given various heat treatments. No attempt was made to establish an etching procedure for the implanted layers.

c. Annealing

It was apparent, from a review of the literature of implants in II-VI compounds and other semiconductors, that it was highly desirable to be able to anneal both the implanted and some unimplanted samples in a controlled atmosphere. Since there was little in the literature concerning the luminescent properties of ZnO single crystals subjected to carefully controlled heat treatments, it was necessary to establish a base line in order to be able to distinguish effects due to implants from those simply due to annealing unimplanted crystals. Toward this end, a system and set of procedures was established for sealing samples in quartz ampoules under carefully controlled conditions.

The sample to be heat treated was placed in a clean, 1/2" ID, quartz ampoule, which was then necked down by heating with a torch. Following this, the ampoule was connected to a vacuum system consisting of a mechanical pump, air-cooled diffusion pump, and liquid nitrogen cold trap. Connection was made through a ground glass seal, and two valves provided for isolating the ampoule from the vacuum system or for introducing ultra high purity (UHP) argon to flush the ampoule. The ampoule was then evacuated to a pressure of less than 10μ using the mechanical pump, after which it was flushed three times by successively introducing a pressure of one atmosphere of UHP argon and reevacuating with the mechanical pump to a pressure of less than 10μ. When the flushing procedure had been completed the high vacuum valve was open to initiate pumping with the diffusion pump. After the ampoule had been evacuated to a pressure of less than 1×10^{-7} torr, it was sealed by heating the necked down area with a torch causing the quartz walls to collapse due to the pressure differential between the atmospheric surroundings and the evacuated interior.

The samples were annealed by placing the sealed ampoules in a furnace maintained at the desired annealing temperature for the required time period. Following the anneal the samples were quenched to room temperature by immersing the ampoules in a distilled water bath. Two furnaces were available for annealing samples. The first was actually an oven capable of a maximum temperature of 900°C and it was used primarily for short anneals of two hours or less at relatively low temperatures, below 600°C. The second furnace was a ceramic tube type useable to achieve temperatures up to 1200°C and possessing a flat zone of 12 inches where the temperature was maintained to within ±1°C of the desired value. This furnace was used primarily to bake unimplanted samples at temperatures of 900°C or higher for periods up to 240 hours.

To induce an atmosphere of a normally solid substance such as zinc, several pellets of UHP zinc metal obtained from the Eagle-Picher Company were simply added to the ampoule along with the sample before the ampoule had been necked down. One then followed the procedure described previously to flush and seal the ampoule. Subsequent annealing by placing the sealed ampoule in a furnace resulted in vaporization of the zinc metal to produce a partial pressure of zinc atoms. Assuming that all the metallic zinc is vaporized, and assuming further that the ideal gas law is valid for this case, the pressure of Zn atoms is given by (Reference 147)

$$p = \frac{nRT}{V} \tag{19}$$

where

p is the pressure in atmospheres

n is the number of moles

T is the absolute temperature

V is the volume in liters

R is the universal gas constant equal to .08206 liter-atm/g-mole-°K.

For an average ampoule with two Zn pellets, at 900°C this results in a Zn pressure of approximately 8 atmospheres.

It was found that an atmosphere of a normally gaseous element such as oxygen could be provided by first initiating the procedure for flushing and sealing the ampoule, except that prior to heating the neck of the ampoule to seal it, the valve to the diffusion pump was closed. The valve normally used to introduce UHP argon for flushing was then opened to admit the desired gas, the flow of which was controlled by a needle valve so that a pressure of 15 inches of water could be attained. This was still a vacuum suitable for sealing the ampoule, while it provided a sufficient amount of gas to produce a pressure of one atmosphere or greater for annealing temperatures above 600°K (assuming that the ideal gas law holds).

d. Sputtering

Sputtering was used in two different phases of sample preparation. It was employed to deposit gold and platinum for electrical contacts and to deposit SiO_2 for protecting implanted layers during annealing. A simple d.c. sputtering system was fabricated, using a small bell jar and a 5 kV supply to provide a capability for depositing metals for electrical contacts.

The deposition of SiO_2 was performed using the RF sputtering of a quartz target. This was done at the Air Force Avionics Laboratory (AFAL) using an RF sputtering system built by the Mathis Company. It was found that sputtering for 50 minutes in an atmosphere of 10×10^{-3} torr of UHP argon with an effective d.c. bias of 1 kV produced a SiO_2 film which was 2500 Å thick. The thickness of the film was measured using a Sloan Dektak located at the AFAL.

e. Implant Conditions

The purpose of this section is to set forth the variety of implantations and substrate conditions used during the investigation. Table 2 provides a complete listing of the implanted ZnO samples available. Naturally, it was not possible to study all the implanted samples in great detail using the three methods employed for this study, however, most types of implants were given at least a cursory examination to see if any startling changes had taken place. Results of more thorough

TABLE 2

IMPLANT CONDITIONS

Ion	Temp	Substrate Type: UN-baked	Vac-baked	Zn-baked	O_2-baked	Beam Energy (keV)	Dose
N	RT	X				150	$10^{11,12,13,14,15}$
P	RT	X				300	$10^{13,14,15,16}$
Ne	RT	X				300	10^{14}
Na	RT	X				100	10^{14}
						200	10^{14}
						300	10^{14}
Na Ne (Multiple energy implant)	RT	X	X	X		275	1×10^{13} 1×10^{16}
						125	6×10^{12} 1×10^{15}
						50	3×10^{12} 1×10^{15}
Li (Multiple energy implant)	RT	X	X	X	X	175	1×10^{13} 1×10^{16}
						80	7.5×10^{12} 7.5×10^{15}
						30	4.5×10^{12} 4.5×10^{15}
Li	475°C		X			275	10^{15}
						400	10^{15}
Na Ne	475°C		X			750	10^{15}
N	475°C		X			875	10^{15}
P	475°C		X			1000	10^{15}

investigations obtained from selected samples are presented and discussed in Section IV.

Since an attempt was being made to produce type conversion in ZnO which, as mentioned previously, is normally n-type, attention was centered on the implantation of elements from Group I (Li and Na) and Group V (N and P) of the periodic table. Implants of Ne were also made since it is very close to Na in atomic mass. However, it was felt that it would produce similar radiation damage effects yet being an inert ion it would produce no centers due to chemical doping. A number of different doses were used because the literature revealed that electrical measurements provided more information when higher doses had been employed; however, the heavy dose implants drastically quenched the luminescence. This indicated a need for lower doses in order to better study the luminescent properties of the implanted centers.

Earlier work on implanted II-IV compounds had indicated an annealing step occurred between 300 and 500°C. This was found to be the case in ZnO as well (Reference 142). Hence, most of the samples were annealed at 450°C for a period of approximately two hours. Some samples were annealed at 900°C since this was the temperature at which the unimplanted samples were normally baked, and there appeared to be a significant step at this temperature as well. In most cases SiO_2 was used to protect the implanted layer during the anneal, as other workers had found this to be necessary for the achievement of consistent results.

2. CATHODOLUMINESCENT SYSTEM

A schematic of the system used to perform the cathodoluminescent measurements is shown in Figure 14. The major portions of the system are: the sample environment, which consists of the dewar, sampleholder, and vacuum system; the excitation source, which consists of the electron gun, gun supply, and high voltage supply; and the signal processing section, which consists of the spectrometer, detector, amplifier, and recorder. Each of these will be described more fully in the succeeding paragraphs.

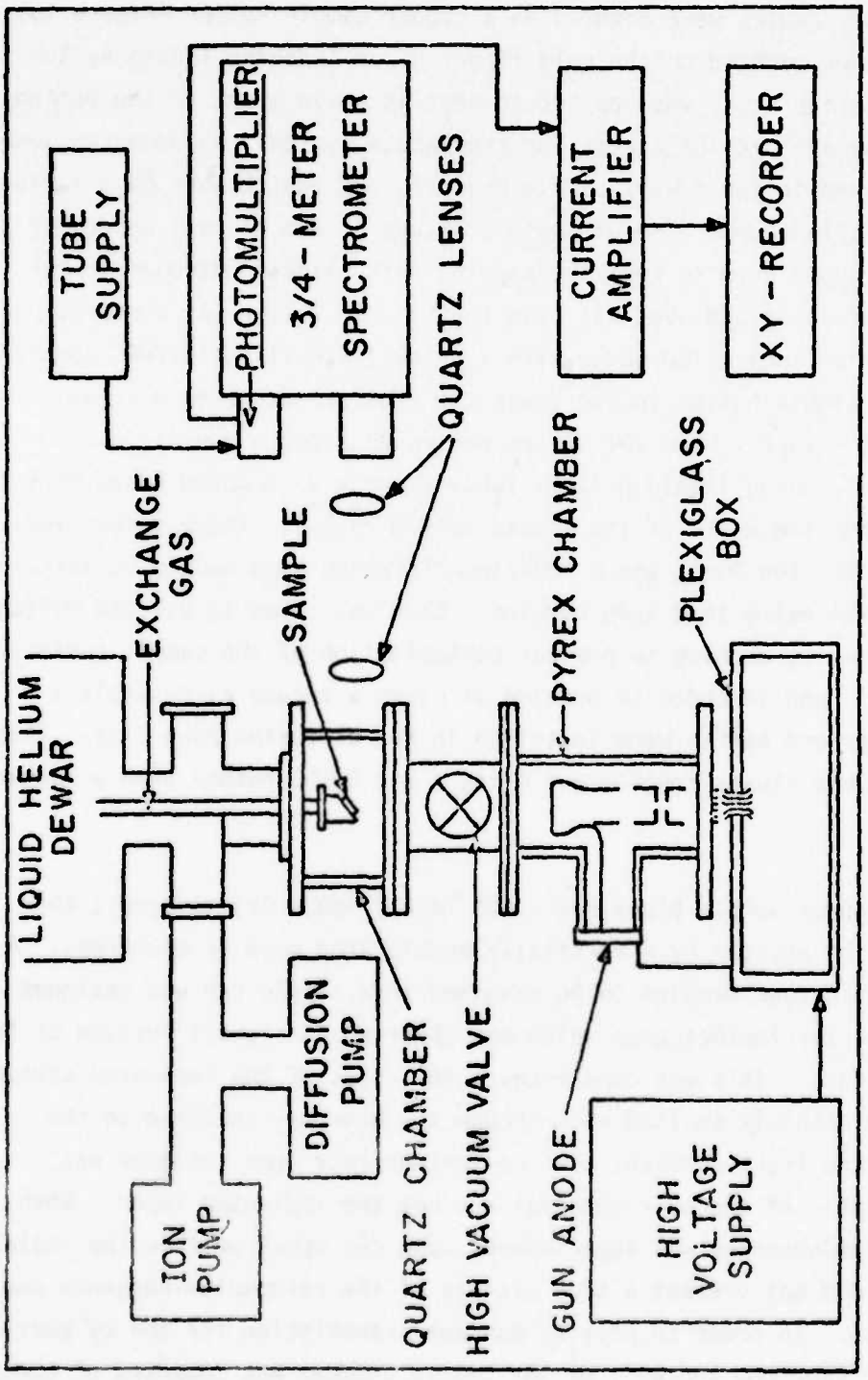

Figure 14. Cathodoluminescence System

a. Sample Environment

The samples were mounted on a copper sample holder (Figure 15) which was then mounted on the cold finger of an Andonian liquid helium dewar. A Varian cross was adapted so that it would mount to the bottom of the dewar and provide access for the vacuum system. A common vacuum was maintained in the dewar, sample chamber, and gun chamber by a Varian 50 L/sec Vac Ion Pump. The ultimate pressure obtainable was dependent upon the cryogen used to cool the sample. With liquid nitrogen in the dewar the pressure achieved was less than 1×10^{-6} torr (as measured using a Varian ionization gauge with a Granville Phillips 02/006 control), while with liquid helium in the dewar the pressure achieved was less than 1×10^{-7} torr. When the system warmed up after a run at low temperatures, using liquid helium, large amounts of trapped gases were released from the walls of the liquid helium vessel. These gases overloaded the Vac Ion Pump, and a 100L/sec diffusion pump had to be installed to handle the extra load upon warming. Care was taken to use the diffusion pump only during warming to prevent contamination of the sample surfaces by pump oil, and in order to provide as clean a vacuum as possible a zeolite trap and baffle were installed in the diffusion pump line. Also, the system was always roughed out using a Vac Sorb, rather than a mechanical pump.

The copper sample block had a 45° face (Figure 15) to permit the samples to be excited by a vertically accelerated beam of electrons. A mask allowing four samples to be examined in a single run was designed to restrict the luminescence which was observed to a small portion of the sample surface. This was done because the edges of the implanted crystals often were strongly excited even though the beam was centered on the middle of the front surface, and the luminescence from the edge was characteristic of the bulk material and not the implanted layer. When the bulk luminescence was superimposed upon the spectrum from the implanted layer, it did not present a true picture of the cathodoluminescence due to the implant. In order to provide maximum transmission for the UV portion of the ZnO spectrum the wall of the sample chamber was composed of quartz.

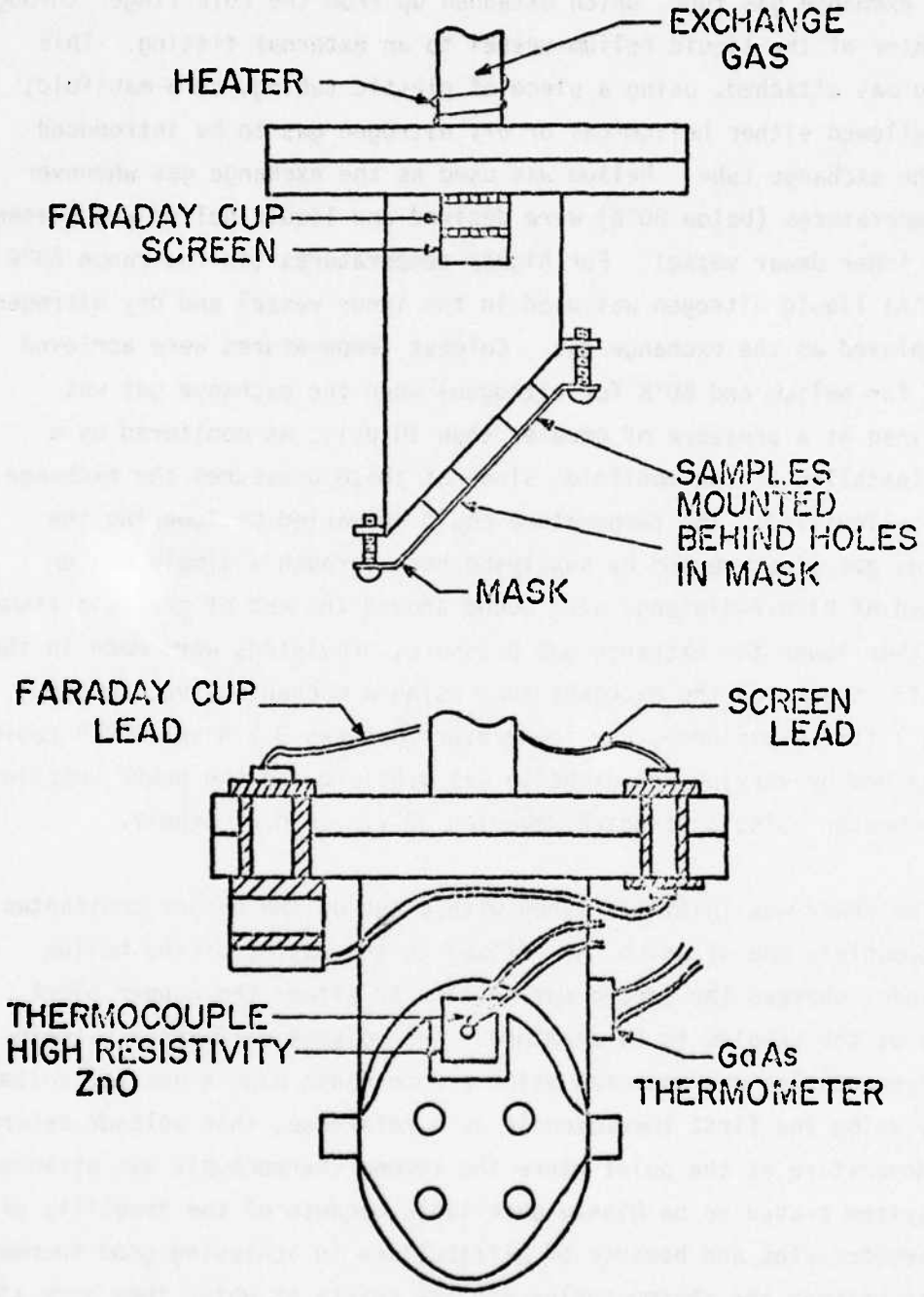

Figure 15. Cathodoluminescence Sample Holder

The temperature of the sample block was controlled by the gas pressure in the exchange gas tube, which extended up from the cold finger through the center of the liquid helium vessel to an external fitting. This fitting was attached, using a piece of plastic tubing, to a manifold; which allowed either helium gas or dry nitrogen gas to be introduced into the exchange tube. Helium was used as the exchange gas whenever low temperatures (below 80°K) were desired and liquid helium was present in the inner dewar vessel. For higher temperatures (in the range 80°K to 300°K) liquid nitrogen was used in the inner vessel and dry nitrogen was employed as the exchange gas. Coldest temperatures were achieved (8.5°K for helium and 80°K for nitrogen) when the exchange gas was maintained at a pressure of greater than 10 psi., as monitored by a gauge installed at the manifold, since at these pressures the exchange gas was liquified. The temperature could be varied by lowering the exchange gas pressure and by supplying heat through a simple heater composed of high resistance wire wound around the end of the cold finger. To further lower the exchange gas pressure, provisions were made in the manifold to pump on the exchange tube using a mechanical vacuum pump. With a little experience, any temperature between 8.5°K and 300°K could be attained by varying the exchange gas pressure and the power supplied to the heater using a standard Hyperion 30 V, .6A d.c. supply.

The dewar was initially wired with a set of two copper-constantan thermocouples, one of which was affixed to the bottom of the helium reservoir, whereas the second was mounted to either the copper block or one of the samples to be examined. The voltage difference between the thermocouples was measured using a John Fluke 8300 Å digital voltmeter; and by using the first thermocouple as a reference, this voltage determined the temperature at the point where the second thermocouple was attached. This system proved to be highly unreliable because of the fragility of the thermocouples and because of difficulties in achieving good thermal contact between the thermocouples and the points at which they were attached without shorting them together electrically, thus providing no voltage output. This problem was circumvented by installing a GaAs thermometer in the copper sample block. The GaAs thermometer proved to be extremely

reliable and provided consistent readings throughout the duration of the experimental program. In addition, a new set of thermocouples was made from heavier gauge wires. Using indium solder, the reference junction was soldered directly to the bottom of the helium reservoir; and the measurement junction was soldered to a piece of ZnO which had been made electrically insulating by baking it in oxygen. This piece of ZnO was then affixed to the copper block using indium-gallium amalgam. During the initial low temperature runs made using this configuration the GaAs thermometer always read 8.5°K with liquid helium in the reservoir and an exchange gas pressure of 15-25 psi , while the thermocouple reading was consistently in the range 9-10°K. Later, the thermocouple again failed; however, since the GaAs reading remained the same it was assumed that the sample temperature remained within a few °K of that obtained for the copper block using the GaAs thermocouple.

b. Excitation Source

The excitation source consisted of a Superior Electronics 5AZP4 electron gun whose leads were mechanically fastened to the leads of a standard Varian, 8 pin, 2 1/4-inch feedthrough flange. This was then inserted into a pyrex tee which was securely clamped between two aluminum flanges by six plexiglass rods located circumferentially about the outside of the tee. An O-ring groove in the bottom flange mated with the gun feedthrough, while O-rings were located at the top and bottom of the tee to create vacuum seals between the tee and the flanges. This whole assembly was mounted to the bottom of the sample chamber with a high vacuum valve in between so that the gun chamber could be filled with dry nitrogen gas and closed off from the rest of the system while the samples were changed, during which time a small current was run through the filament of the gun. This procedure prevented poisoning of the oxide-coated cathode by water vapor while the samples were changed.

When the gun was in operation the upper flange, as well as the sample holder, was maintained at ground potential, and the lower flange and the filament were floated at a negative high potential equivalent to the desired beam voltage. Since the cathode was maintained at a

potential only slightly more positive than that of the filament, the electrons emitted from the cathode were accelerated through a potential difference essentially equivalent to the voltage setting on the high voltage power supply, which was a Universal Voltronics BAC 50-16. A capacitor rated at .01 μf and capable of withstanding 69 kV was hooked in parallel between the high voltage lead and the ground to serve as a filter and this configuration was found to provide good beam stability at all voltages used.

The 5AZP4 gun has two grids and an anode which provide for focusing of the beam. The first grid is maintained at a voltage slightly negative with respect to the cathode while the second grid is maintained at a voltage which is positive with respect to the cathode and has a magnitude equal to about 1% of the total beam voltage. A potential of approximately 30% of the beam voltage and positive with respect to the cathode must be applied to the anode. For this reason the anode contact was made through the side of the pyrex tee using an aluminum rod with a flexible feeler of titanium sheet welded to it. The other end of the rod was threaded and screwed into a tapped hole in an aluminum cap, which was in turn affixed to the side part of the pyrex tee using RTV. The anode lead was then secured to the outside of the cap with a machine screw. This prevented any breakdown problems which might have occurred had the anode lead been connected by employing the same feedthrough as that used for the grid, cathode, and filament leads.

The bias voltages for the grids, the cathode, and the anode were provided by a string of resistors, switchable taps, and potentiometers enclosed in a plexiglass box (Figure 16) and hooked from the negative high voltage to the ground. Mechanical connection from adjusting knobs to the pots and switches was made via plexiglass rods. Using this arrangement, the beam could be readily focused to a spot on the order of 3 mm in diameter for beam voltages in the range 1-25 kV. The position of the spot was determined by steering it with a small permanent magnet, and it could easily be moved to whichever of the four samples was to be investigated.

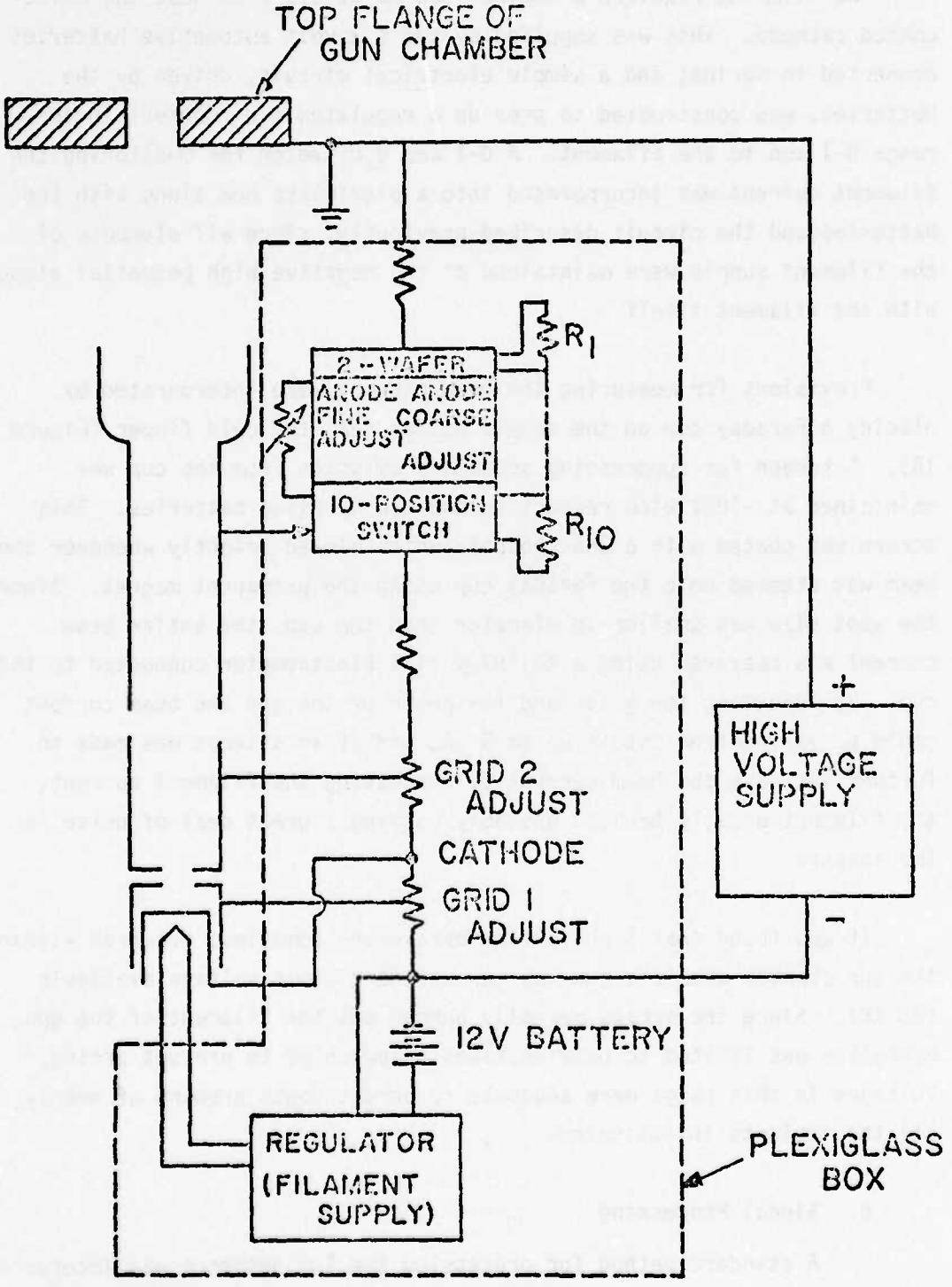

Figure 16. Gun Bias System

The filament required a nominal 600 ma at 6.3 V to heat the oxide-coated cathode. This was supplied by two six-volt automotive batteries connected in series; and a simple electrical circuit, driven by the batteries, was constructed to provide a regulated d.c. current in the range 0-1 amp to the filament. A 0-1 amp d.c. meter for monitoring the filament current was incorporated into a plexiglass box along with the batteries and the circuit described previously, since all elements of the filament supply were maintained at the negative high potential along with the filament itself.

Provisions for measuring the beam current were incorporated by placing a Faraday cup on the sample holder near the cold finger (Figure 15). A screen for suppressing secondary emission from the cup was maintained at -180V with respect to the cup by using batteries. This screen was coated with a ZnS phosphor which glowed brightly whenever the beam was steered onto the Faraday cup using the permanent magnet. Since the spot size was smaller in diameter than the cup, the entire beam current was measured using a Keithley 610A Electrometer connected to the cup. By adjusting the grids and the anode of the gun the beam current could be varied from cutoff up to 5 μA, and if an attempt was made to further increase the beam current by increasing the filament current, the filament usually behaved unstably causing a great deal of noise in the spectra.

It was found that high voltage breakdowns sometimes occurred within the gun chamber when the gun was run at the highest voltage available (30 kV). Since the arcing normally burned out the filament of the gun, operation was limited to beam voltages below 25 kV to prevent arcing. Voltages in this range were adequate to permit depth probing of nearly all the implants investigated.

c. Signal Processing

A standard method for processing the luminescence was incorporated into the system. The emission from the sample was focused onto the input slits of a Spex 3/4-Meter Czerny-Turner spectrometer using two spherical

quartz lenses, which provided maximum transmission for the ultraviolet portion of the ZnO emission spectrum. An ultimate resolution of .1Å is achievable using this instrument with its narrowest slits (10 μ). Two different photomultiplier detectors were used depending upon the wavelength region of interest. An RCA 1P2I tube was used when the ultraviolet portion of the spectrum was examined closely, because it had more sensitivity (120 A/Lum) in this region than the RCA C31025C (5 A/Lum) experimental photo-cathode tube that was used to examine the broad visible emissions which extended far out into the red region of the spectrum, almost to 9000 Å.

The output of the detector was amplified using a Keithley 417 amplifier with a remote preamplifier head located as closely as possible to the detector to minimize cable loss and noise. The current amplifier was used to drive the Y-channel of a Houston 3000 Omnigraphic recorder, while the X-channel was swept with a particular time base. Use of this time base in conjunction with the various sweeping speeds available on the spectrometer allowed a wide variety of wavelength ranges to be scanned (from 30Å up to 6000Å) over the length of the X-axis. Plots produced in this manner represented luminescent intensity vs. wavelength. These plots could be calibrated by running similar scans incorporating the standard wavelength lines available from mercury or neon lamps.

3. PHOTOLUMINESCENCE SYSTEM

A photoluminescence system suitable for performing time-resolved spectroscopy on ZnO was established using a nitrogen laser. The operating characteristics of the Avco-Everett laser used for this system are shown in Table 4. The capabilities to vary the intensity of the exciting light as well as vary the sample temperature from 4.2°K were also included. These capabilities were incorporated to provide for a thorough investigation of the luminescence mechanisms (Section II.5.a) responsible for emission from ion implanted ZnO. Measurements of this nature provide maximum information about the centers responsible for the luminescence.

TABLE 3

OPERATING PARAMETERS OF THE NITROGEN LASER

Output Wavelength	3371 Å
Output Bandwidth	1 Å
Peak Output Power	100 kW
Effective Pulse Width	10 nsec
Repetition Rate	5-500 pps
Average Power	.5 Watts
Beam Dimensions	.32 cm x 5.1 cm

Some problems were encountered in establishing this system. The first stemmed from the fact that the absorption coefficient for the laser wavelength in ZnO is very great. This meant that the penetration of the exciting light was very shallow, and most of the electron hole pairs were created near the surface of the sample. As revealed from the cathodoluminescent probing this region of the crystal sustains a high degree of radiation damage during the implant and probably contains a high concentration of nonradiative centers. Hence, the photoluminescence in this region is severely quenched, and because of this a complete investigation is made more difficult. Secondly, the extremely short duration of the laser pulse requires a sophisticated system of electronics to achieve optimum detection of the luminescent signal.

The configuration of the system, the details of the sample holder, and the associated electronics required for temperature control and signal processing are shown in Figure 17. Each of these will be discussed briefly in the paragraphs that follow.

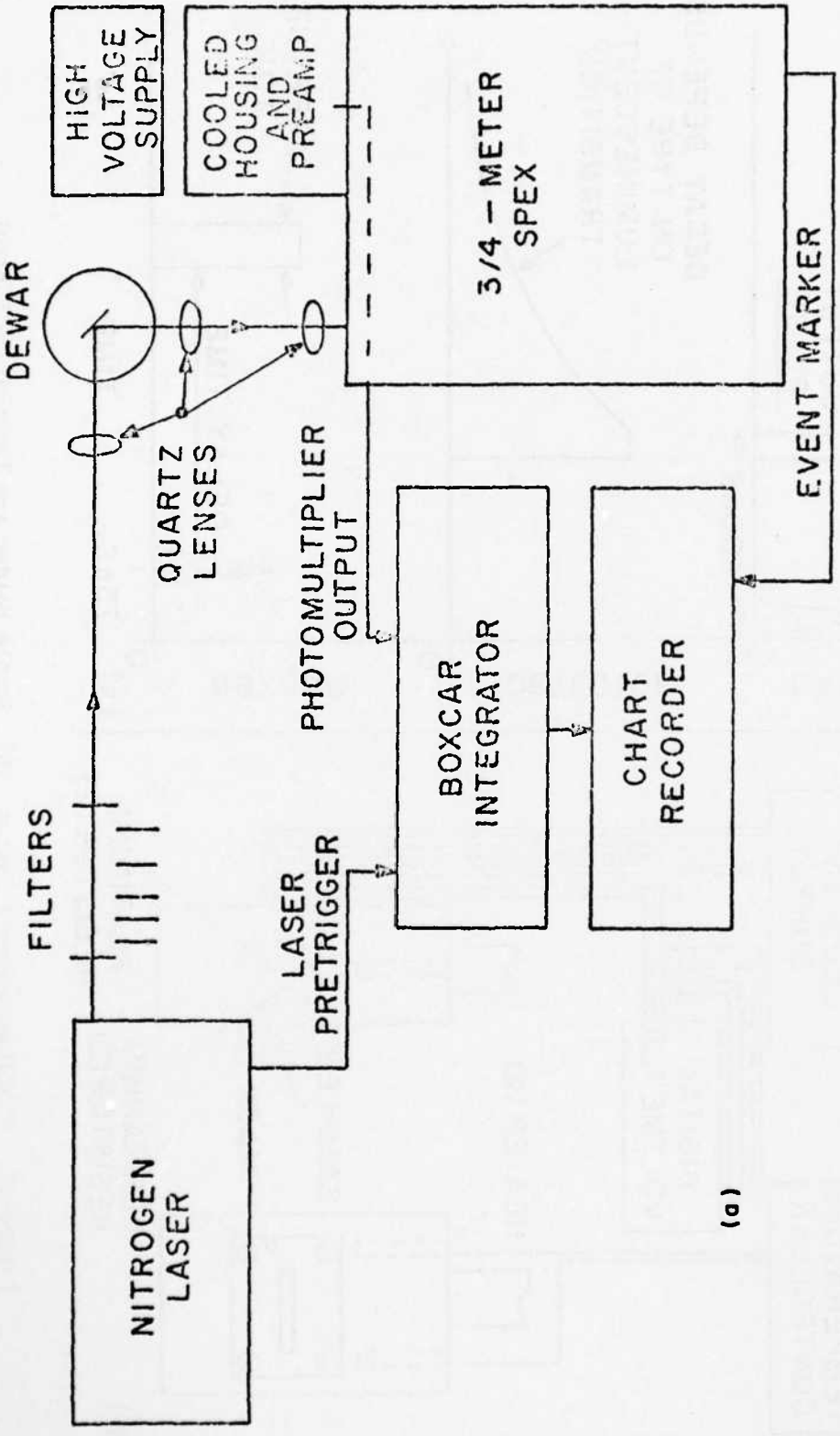

Figure 17. Photoluminescence System (a) Configuration

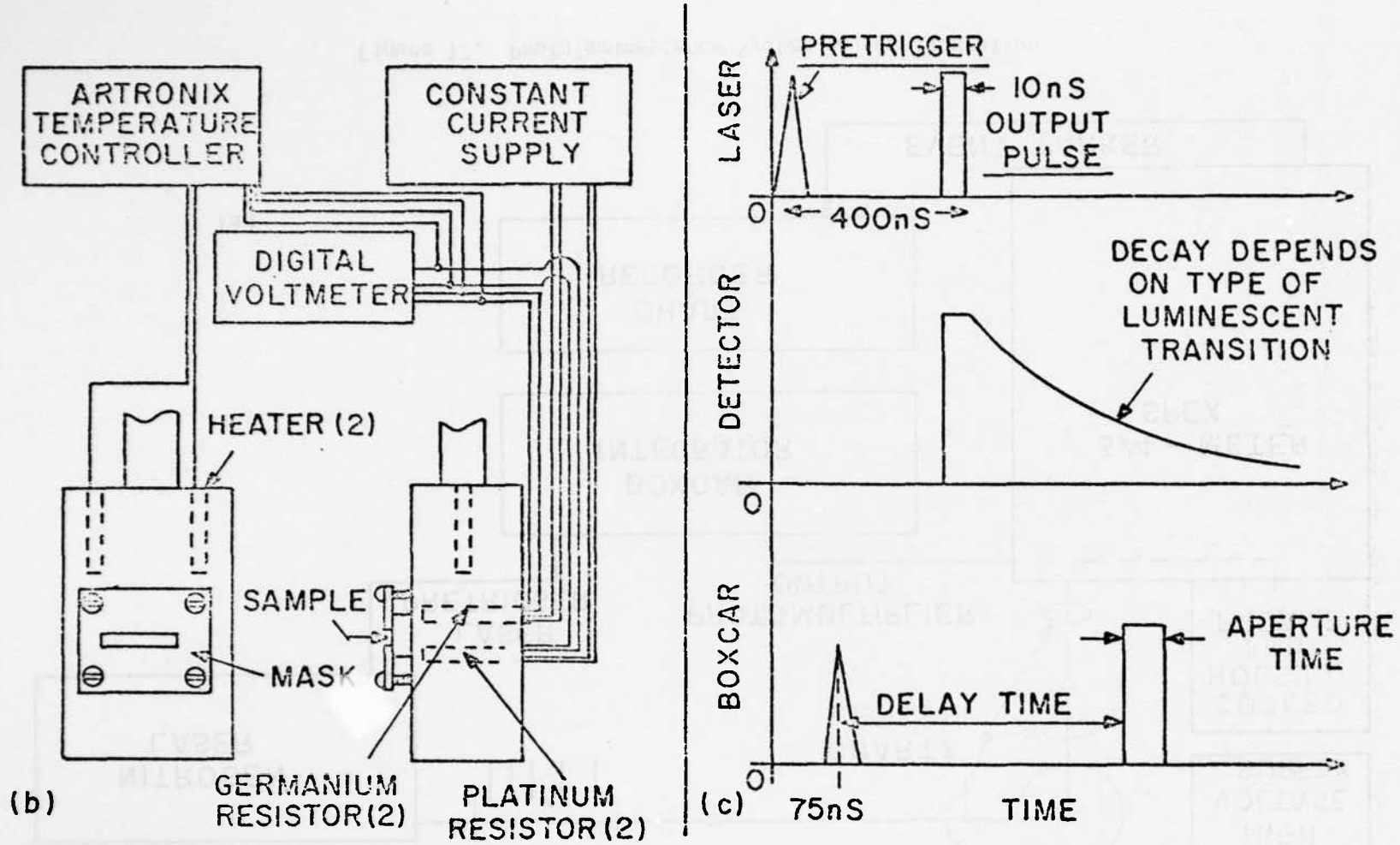

Figure 17. Photoluminescence System (b) Sample Holder and Temperature Control
(c) Signal Processing for Time Resolved Spectra

a. Configuration of Photoluminescence System

This is a standard configuration for obtaining photoluminescent spectra. All dewar windows and lenses were quartz to permit maximum transmisssion of the exciting laser light as well as the ultraviolet portion of the ZnO luminescence. In order to direct the laser light onto the sample, cylindrical lenses were used because of the rectangular shape of the beam. An optimum focus produced a 10 mm X 1 mm horizontal slit of exciting light on the sample.

The 3371 Å interference filter and the neutral density filters were positioned so that they could be rotated into position as desired. Using the neutral density filters singly or in various combinations the intensity of excitation could be varied over ten orders of magnitude. Since the laser produced a number of strong lines in addition to the lasing line, the interference filter was used at all times.

b. Sample Holder and Temperature Control

The sample holder consisted of a large copper block mounted on the end of a long rod which was in turn attached to a rotatable head that contained the feedthroughs for the necessary wires to monitor and control temperature. A copper mask with a horizontal slit to admit the laser beam was placed in front of the sample to suppress light emitted from the unimplanted portions of the sample as discussed previously. Two germanium and two platinum resistors were used to monitor the temperature. One set of germanium and platinum resistors was used to provide a temperature readout at the low (below 40°K) and high (above 40°K) regions, respectively. The other set was used by the Artronix controller to monitor the temperature of the block. This controller had an internal power supply and controlled the amount of voltage supplied to two platinum heaters which were mounted in the copper block.

Cooling of the sample was provided by liquid helium maintained within the inner reservoir of a standard Janis dewar. This inner vessel was connected to the sample chamber by means of a thin stainless steel capillary.

Before the liquid helium entered the sample chamber it had to pass through a copper frit. An external valve controlled the flow of helium while a heater in the frit controlled the vaporization rate. With the frit heater off, the sample could be immersed in a liquid helium bath, however, it was found that this lowered the intensity of the luminescent signal significantly because of scattering of the light by bubbles in the rapidly boiling liquid helium. For this reason most spectra were obtained at approximately 5°K.

c. Signal Electronics

The pulses of light emitted by the samples were processed by a Spex 3/4-Meter spectrometer as described earlier. Detection was accomplished by an RCA 7265 photomultiplier tube in a cooled housing. This produced at any one wavelength a string of pulses whose amplitude was proportional to the intensity of the light emitted by the crystal. These pulses were amplified by a wide-band preamplifier designed and built in conjunction with the University of Dayton Research Institute.

A pretrigger from the laser was used to trigger a PAR Model 160 Boxcar Integrator. With the use of the boxcar two modes of operation were possible for investigation of the recombination kinetics. In one mode the spectrometer was set at a fixed wavelength and the luminescent intensity was recorded as a function of the decay time. In the second mode the decay time was fixed and the spectrometer was scanned to provide a normal spectrum at a given time after excitation of the luminescence.

d. van der Pauw System

The most positive means of determining type conversion in a semiconducting substrate is through a Hall Effect measurement. Such a measurement determines the density and sign of the majority carriers (i.e. whether holes or electrons), as well as the mobility of the majority carriers and the resistivity of the substrate. For very pure samples or for those which are highly compensated the resistance of the sample is high ($>10^7$ ohms), and guarding is required to provide impedance isolation between the sample and the instrumentation and to reduce the leakage currents, thereby decreasing the time constant of the measuring apparatus (Reference 119).

For the case of an implanted sample where it is necessary to measure the electrical properties of a very thin layer it is desirable to employ the van der Pauw method for transport measurements, and the system used to perform the measurements is shown schematically in Figure 18. Being guarded, it is useful for samples having resistances as high as 10^{12} (Reference 119). Each of the sections of the rotary switch corresponds to one of the functions: V_1, V_2, ammeter, ammeter relay, battery, and battery relay; while the six positions correspond to (a) - (f) of Figure 13. The system is shown as it would be for (a) or Figure 13.

The sample to be measured was contacted by sputtering platinum or gold before soldering or by soldering directly using In/Hg amalgam and pure In solder. Three-mil gold wires soldered to the contacts were connected to the appropriate leads for making the measurements, which were mechanically fastened on the cold finger of a liquid helium dewar. The sample was tightly clamped to a BeO holder using spring clips and the holder was in turn securely fastened to the copper cold finger of the dewar. This provided good electrical insulation while assuring maximum thermal conduction. Sample temperature was monitored by a platinum resistor in the copper block and the temperature was controlled by a Thermac unit which controlled the flow of current to a heater which was also mounted in the copper block. This system had been calibrated so that a desired temperature between 20°K and 400°K could be obtained by a simple dial setting. Liquid helium was the required cryogen for temperatures below 80°K, whereas liquid nitrogen was used for the higher temperatures.

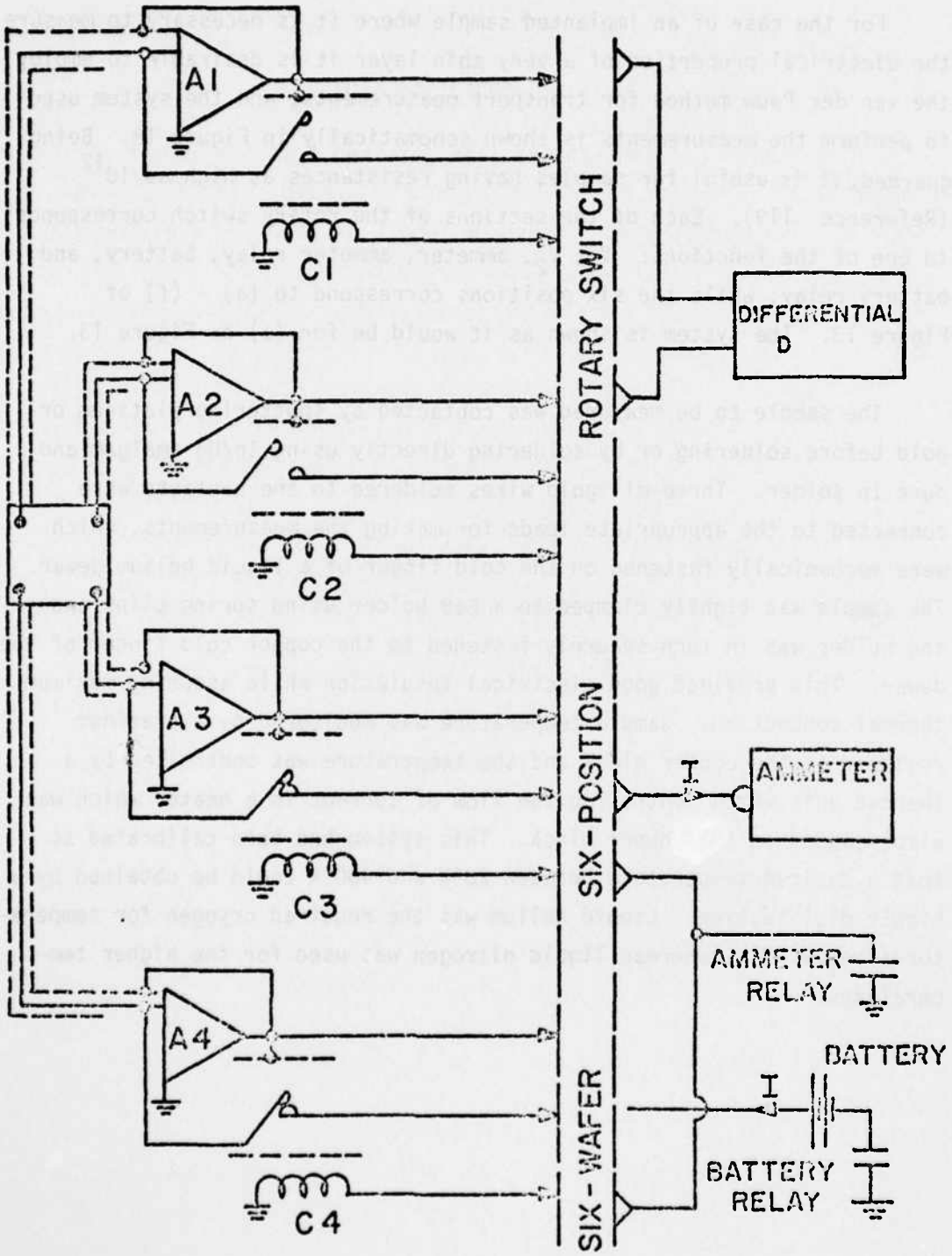

Figure 18. van der Pauw System

SECTION IV

RESULTS AND DISCUSSION

This section provides the results obtained from the investigation of ion implanted layers of Li, Na, N, P, and Ne in ZnO substrates. The intent of the accompanying discussion (which is based on the theory and results provided in Section II) is a presentation of the physical processes responsible for the observed properties. Emphasis has been placed on the depth-resolved cathodoluminescence study since it was the primary method of investigation. A description of the physical appearance of the implanted layers precedes the discussion of the cathodoluminescence data, which is in turn followed by the presentation and analysis of the data obtained from the van der Pauw and photoluminescence experiments. A summary of the key results is provided in the final section.

1. PHYSICAL APPEARANCE OF IMPLANTED LAYERS

Samples of ZnO which were implanted at room temperature exhibited a discoloration near the implanted surface. This discoloration appeared as a light tan for low dose implants ($10^{11}/cm^2$) and ranged to a dark brown for high dose implants ($10^{16}/cm^2$), the amount of discoloration increased as the dose was increased. As mentioned previously, the creation of an amorphous layer in ion implanted Si is accompanied by the formation of a discolored layer with a milky-white hue. However, it is doubtful that this is the case in ZnO because there is little evidence that an amorphous layer is formed in II-VI compounds. In addition, a similar discoloration produced by electron bombardment has been observed in ZnO and used to monitor the creation of radiation damage, as described earlier. Thus, it is more likely that the discoloration is due to the creation of native defects such as oxygen vacancies (F centers). The discoloration was removed and the crystals regained their clear, colorless, pre-implantation appearance after an anneal for two hours at 450°C. Hot implants, performed while the substrate was maintained at 475°C, revealed no evidence of discoloration for doses as high as $10^{15}/cm^2$.

2. CATHODOLUMINESCENCE RESULTS

As described in Section III the samples used for this investigation were prepared from large single crystals of hydrothermally grown ZnO, which contained relatively high concentrations of Li. The luminescent properties of this material were virtually unknown, as all of the previous luminescence studies of ZnO had been made using powders or single crystals grown from the vapor phase with the exception of a lasing study by Nicoll which was performed on samples similar to those available for this study. This necessitated a preliminary investigation of unheated, unimplanted samples.

a. Cathodoluminescence of Virgin Crystals

Figure 19 is the cathodoluminescent spectrum of an unimplanted, unbaked ZnO sample, which had been polished and etched according to the procedures described in Section III. In Figure 20 (a) and (b) the luminescence near the band edge is represented on successively expanded wavelength scales. The spectra shown in Figures 19 and 20 are very similar to those obtained previously from vapor grown crystals, however there are some significant differences. The observed luminescence from the samples at 10°K has a greenish-yellow appearance, and the broad band peaks at approximately 5265 Å. None of the structure of the green band attributed to Cu by Dingle (Reference 105) is observed in the as-grown samples typified by Figure 19. Reynolds, et al. (Reference 76) were able to observe ten prominent, sharp emission lines in the region between 3676 Å and 3697 Å at 1.2°K; and these lines were shown to be the result of bound exciton transitions. In this study at 10°K a total of five lines were observed, as shown in Figure 20(b); and using the notation of Reynolds, et al. these lines may be correlated as depicted in Table 4. Such a correlation is not definite, however, due to temperature shifts in the emission lines. In addition, the lines observed at 10°K with a 3/4-meter instrument may be super-positions of several lines, which could only be resolved at 1.2°K with a two-meter instrument. The I_9 line observed previously as a predominant sharp line near 3693 Å by Reynolds et al. is clearly not observed in the samples typified by the spectra shown in Figure 20(b). This line was attributed to an exciton

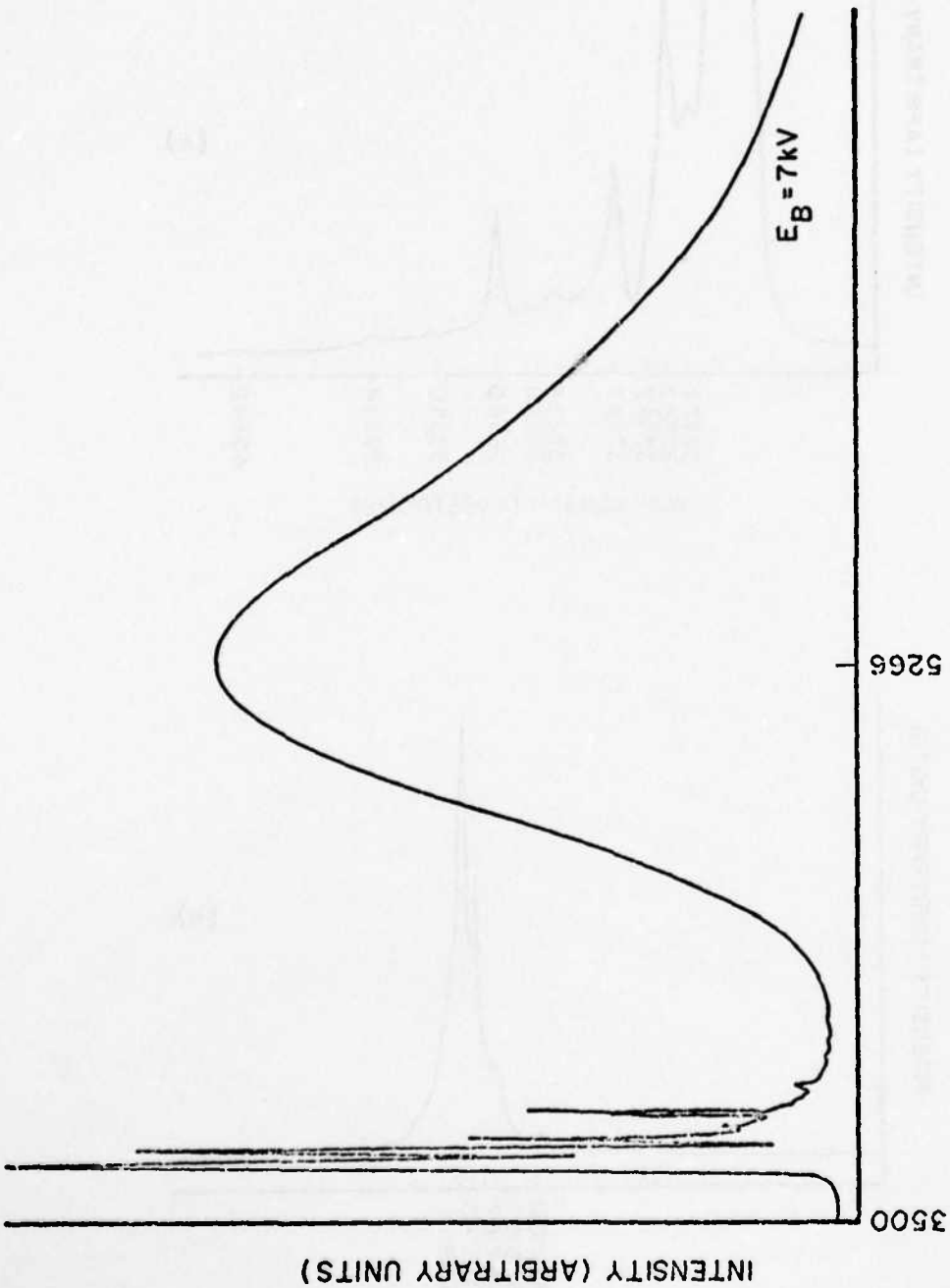

Figure 19. Cathodoluminescence of an Unbaked, Unimplanted Sample

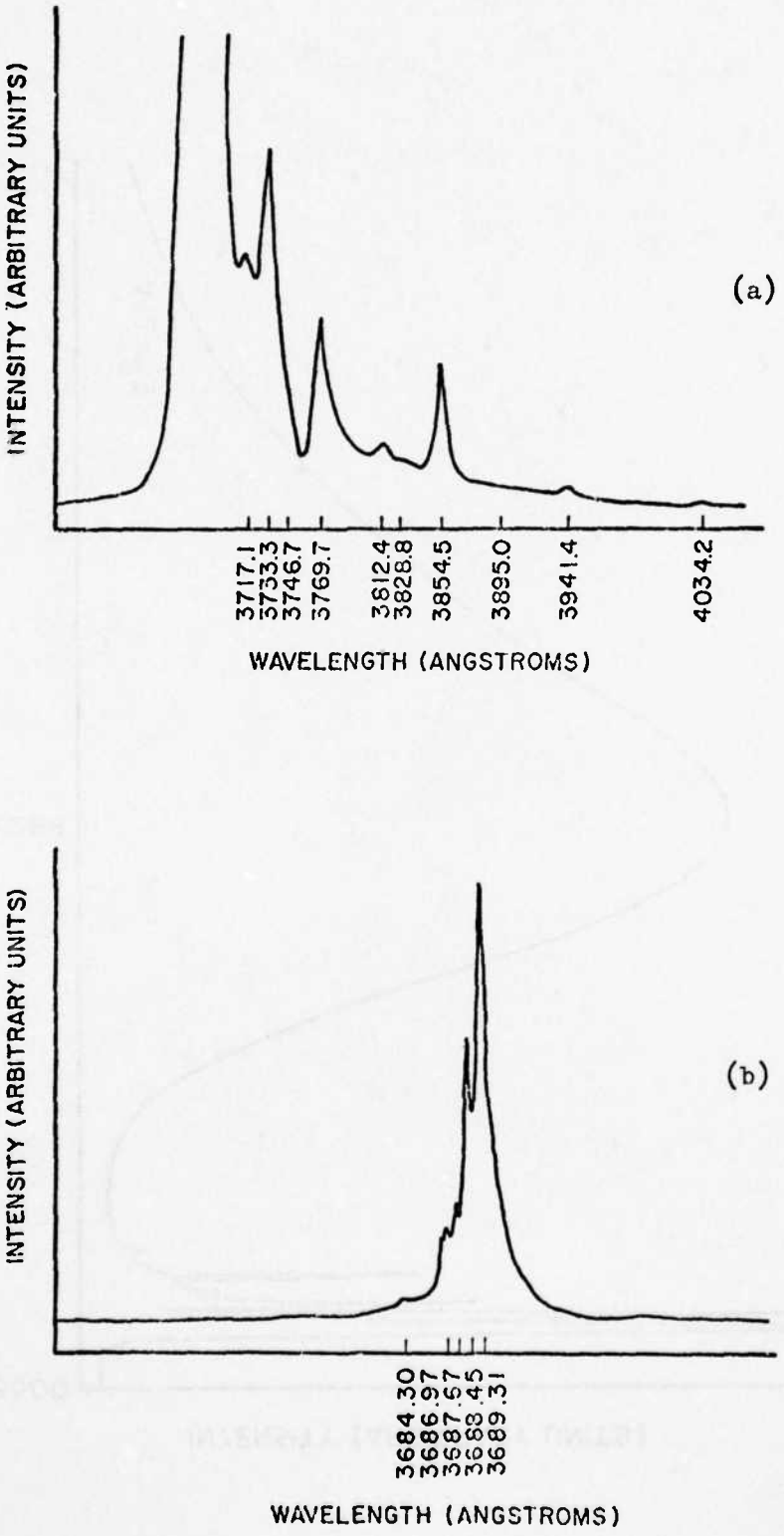

Figure 20. Cathodoluminescence of an Unbaked, Unimplanted Sample

TABLE 4

COMPARISON OF BOUND EXCITON LINES
IN UNIMPLANTED UNANNEALED ZnO

This Work	Reference 91	Nomenclature
	3676.32	I_1
	3680.63	I_2
	3681.59	I_3
3684.30 ?		
3686.97	3687.12	I_4
3687.67	3687.54	I_5
3688.45	3688.40	I_6
	3689.03	I_7
3689.31	3689.26	I_8
	3692.24	I_9
	3696.50	I_{10}

bound to a neutral donor by Reynolds et al. and was also observed by Filinski and Skettrup (Reference 93). Apparently, the donor center responsible for this line is not present in very high concentrations in the crystals used for this study. The phonon-coupled transitions, as described previously, are clearly visible in Figure 20(a). Table 5 is a listing of the wavelengths of the emission lines of Figure 20(a) and the transition energies corresponding to these lines. The energy of the longitudinal optical (LO) phonon in ZnO was given as .0725 eV by Filinski and Skettrup (Reference 93), but Reynolds, et al. (Reference 97) were able to measure two values of .0721 eV and .0707 eV for the Γ_5 and Γ_1 LO phonons, respectively. In the spectrum of Figure 20(a) the repeatability of measurement is approximately ±1.0 Å so that extremely accurate correlation of LO phonon energies was not possible, and two peaks differing in energy by approximately .071 - .073 eV were considered to be phonon replicas.

TABLE 5

UV BANDS OF UNIMPLANTED UNANNEALED ZnO

Wavelength (Å)	Energy (eV)	Transition Type
3687.53	3.3621	Composite of Bound Excitons
3717.11	3.3353	Unassigned
3733.33	3.3208	Excited Donor Transition*
3746.68	3.3090	Free Exciton - 1LO
3769.69	3.2888	Bound Excitons - 1LO
3812.41	3.2519	Excited Donor - 1LO*
3828.84	3.2380	Free Exciton - 1LO
3854.52	3.2164	Bound Excitons - 2LO
3894.98	3.1830	Excited Donor - 2LO*
3941.40	3.1455	Bound Excitons - 3LO

*Energy difference is .0689 eV for this series

Several features of the spectrum in Figure 20(a) require further discussion. The shoulder at 3746.68 Å had been identified as the first LO phonon replica of the free exciton transition based on the results of Weiher and Tate (Reference 92). These workers found that the 3747 Å peak dominated their spectra, which were obtained at 77°K in "pure" crystals; and they argued that a peak at 3677 Å corresponded to the no-phonon line. Based on the LO phonon energy, however, one would expect the no-phonon line to occur close to 3667 Å. No such peak is observed in the spectra shown in Figure 20(a) however, it is possible that this peak is obscured by the large contribution due to the excitons bound to impurity centers. It is not uncommon, as discussed in Section II, for the free exciton transition to be evidenced primarily by its phonon replicas.

A previously unreported peak was observed at 3717 Å in the virgin crystals, and a similar peak was observed in the region 3717 Å - 3720 Å for many of the crystals examined as part of this study. There appeared to be no correlation between this peak and any of the implants or heat treatments performed during the course of the investigation. Because of the apparent lack of correlation between the appearance of this peak

and its position with respect to the various conditions of sample preparation and excitation, it is not possible to ascribe it to any particular luminescence mechanism.

A study by Reynolds and Collins (Reference 95) has provided evidence that the peak at 3733.33 Å is the result of a two-electron transition, which arises when an exciton bound to a neutral donor recombines and simultaneously imparts energy to the electron residing on the donor. Their crystals were dominated by the I_6 line, and the two-electron emission line occurred at 3732.35 eV. As displayed in Figure 20(a) the 3733.33 Å peak appears to have two phonon replicas at 3812.41 Å and 3894.98 Å, however, the spacing between these lines is only .0689 eV which is considerably less than the LO phonon energy. The assignment of these lines near 3812 Å and 3895 Å as phonon replicas must therefore be considered as tentative. The spectra shown in Figures 19 and 20 showed no changes due to variations in beam energy or beam current, and spectra were readily obtained with a beam energy as low as 3 keV which produced most of the electron-hole pairs within a few hundred angstroms of the crystal surface. This indicated that the surface was relatively free from damage after being polished and etched, otherwise one would expect damage centers to quench the luminescence and change its character.

The luminescence obtained from the same sample shown in Figures 19 and 20, as the sample temperature was raised in steps to 150°K, is displayed in Figures 21 and 22. The bound exciton lines become thermally broadened and shift toward longer wavelengths as the temperature increases, as would be expected (References 148, 149, 150, 151), since the half-width (peak width at half maximum) for a bound exciton transition is approximately kT, and the peak position shifts in a manner similar to the bandgap. Also, as expected, the intensity of the bound exciton luminescence is rapidly quenched as the temperature is increased due to dissociation of the exciton complexes (see Section II). The relative growth of the free exciton emission similar to that observed in CdS (Reference 148) is illustrated in Figure 22(a), however, in this case the sample is dominated

AD-A045 649 AIR FORCE MATERIALS LAB WRIGHT-PATTERSON AFB OHIO F/G 20/3
LUMINESCENCE AND HALL EFFECT OF ION IMPLANTED LAYERS IN ZNO.(U)
OCT 76 B J PIERCE

UNCLASSIFIED AFML-TR-75-161 NL

2 OF 2
AD A045649

END
DATE FILMED
11-77
DDC

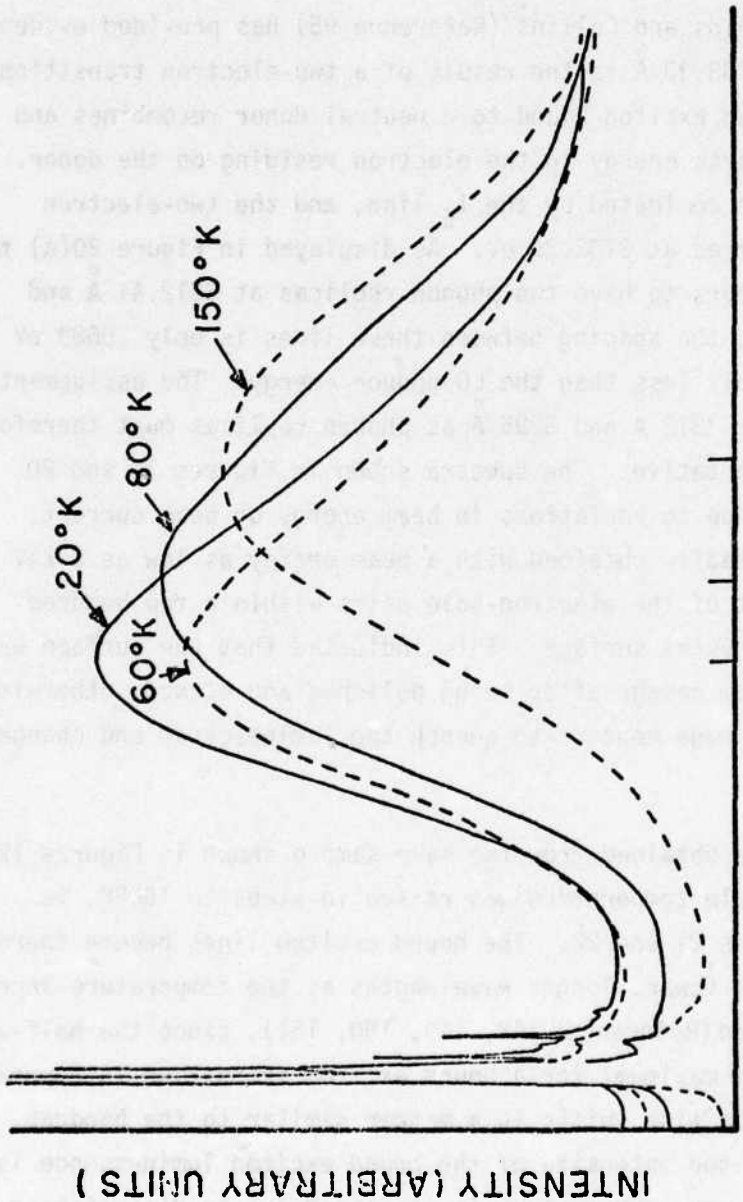

Figure 21. Cathodoluminescence of Unimplanted, Unbaked Sample (Variable Temperature)

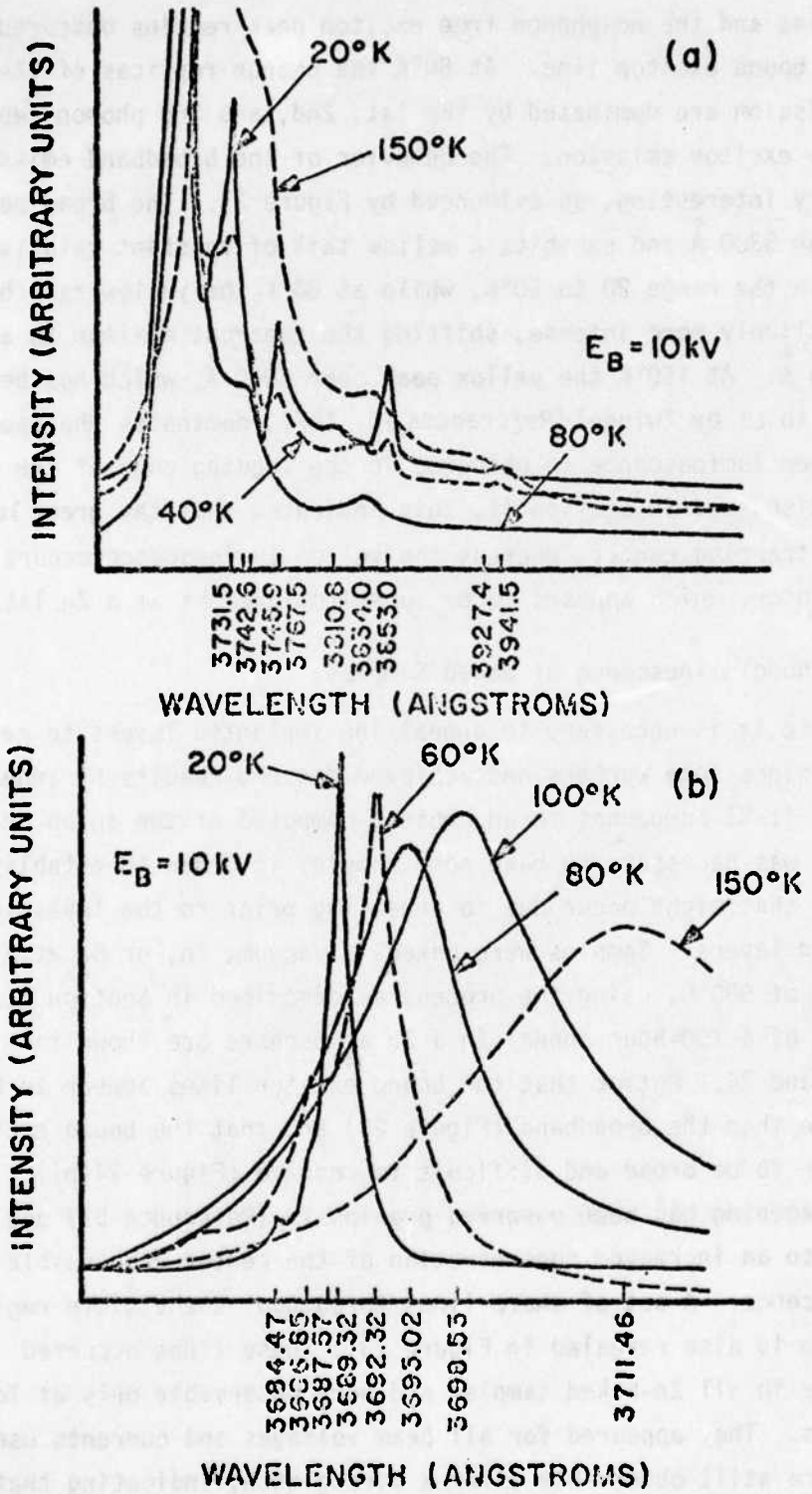

Figure 22. Variable Temperature Cathodoluminescence of an Unbaked, Unimplanted Sample (a) UV Bands (b) Bound Exciton Lines

by impurities and the no-phonon free exciton peak remains obscured by the strong bound exciton line. At 80°K the phonon replicas of the bound exciton emission are dominated by the 1st, 2nd, and 3rd phonon replicas of the free exciton emission. The behavior of the broadband emission is also very interesting, as evidenced by Figure 21. The broad peak remains near 5300 Å and exhibits a yellow tail of constant relative intensity in the range 20 to 60°K, while at 80°K the yellow tail has become relatively more intense, shifting the apparent maximum to approximately 5700 Å. At 150°K the yellow peak near 6000 Å, which has been attributed to Li by Zwingel (References 18, 107), dominates the spectrum; and the green luminescence is obscured in the leading edge of the yellow peak. As discussed in Section II, this indicates that the green luminescence involves a trapping center, whereas the yellow luminescence occurs at a recombination center, which appears to be substitutional Li at a Zn lattice site.

b. Cathodoluminescence of Baked Samples

Since it is necessary to anneal ion implanted layers to remove damage and since some workers had achieved desired results by annealing implants of II-VI compounds in an ambient composed of the anion or cation species; it was necessary to bake some samples in order to establish any changes that might occur due to annealing prior to the investigation of implanted layers. Samples were baked in vacuum, Zn, or O_2 at a temperature of 900°C, using the procedures described in Section III. The results of a 100-hour anneal in a Zn atmosphere are shown in Figures 23 and 24. Notice that the bound exciton lines appear to be much more intense than the broadband (Figure 23) and that the bound exciton lines appear to be broad and difficult to resolve (Figure 24(b)). A similar broadening has been observed previously (Reference 52) and was attributed to an increased concentration of the center responsible for the luminescence. A set of sharp lines throughout the visible region of the spectrum is also revealed in Figure 23. These lines occurred consistently in all Zn-baked samples and were observable only at low temperatures. They appeared for all beam voltages and currents used, and they were still observable after a strong etch, indicating that a surface phenomenon was not responsible for the luminescence. Although

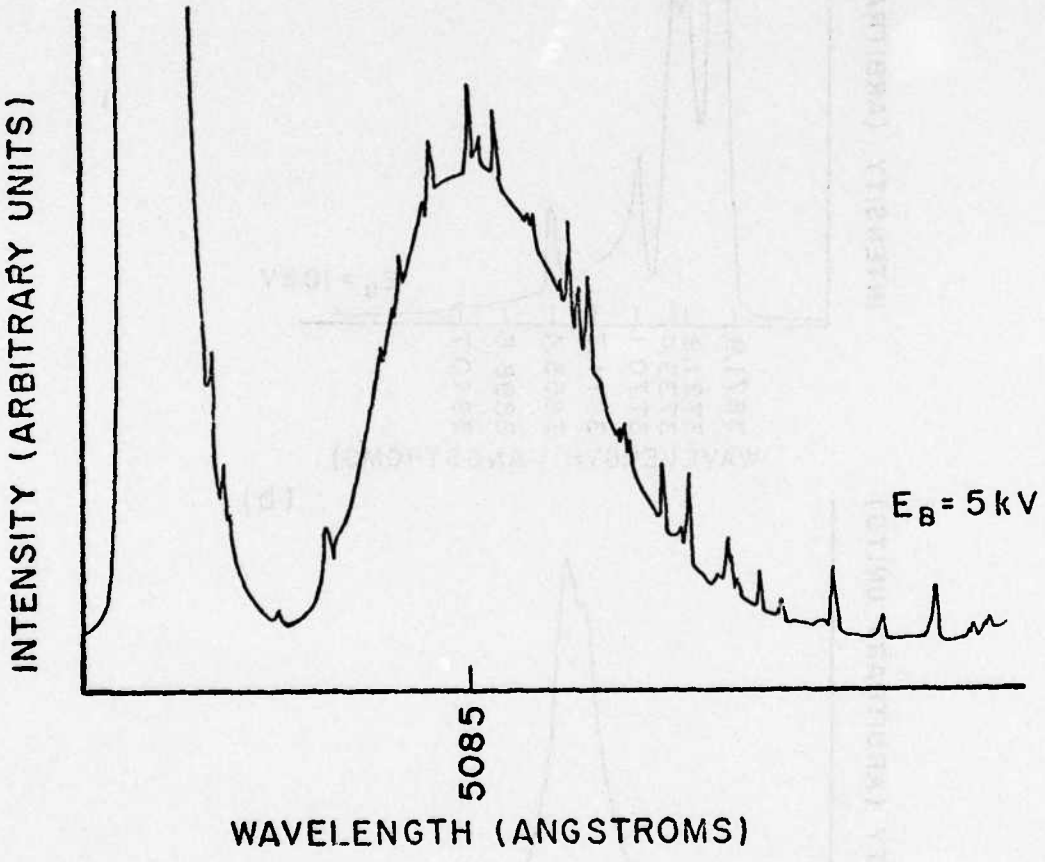

Figure 23. Cathodoluminescence of a Zn-Baked Sample

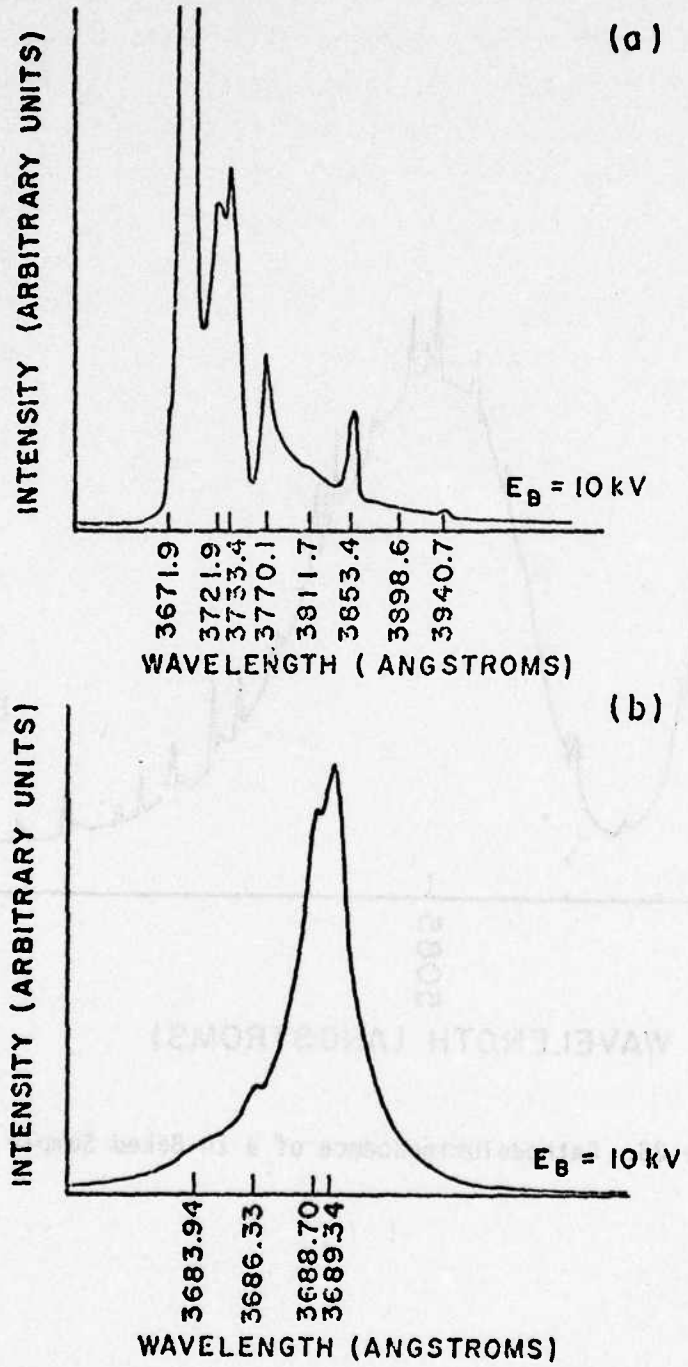

Figure 24. Cathodoluminescence of a Zn-Baked Sample (a) UV Bands and (b) Bound Exciton Lines

these lines were of interest, a lengthy investigation of their origin was beyond the scope of this work. For this reason a detailed study of the lines was not performed, however, it is possible that such lines could result from interatomic transitions occurring at an impurity whose atomic orbitals have been perturbed by the crystalline field of the ZnO lattice (Reference 54). Also, it should be noticed that the broadband shifts toward higher energy, appearing at approximately 5085 Å, as a result of the baking treatment, and a comparison of the broadbands in various baked samples is displayed in Figure 25. The structure of the UV bands (Figure 24(a)) is similar to that obtained for the unbaked sample except that a peak near 3672 Å appears on the shoulder of the dominant exciton emission, and an unexplained peak occurs at 3722 Å in the same region as the 3717 Å peak seen in the unbaked sample. As the sample temperature is increased the bound exciton lines and the UV bands behave in a fashion similar to that described in the previous section; however, the broadband emission, unlike that in the unbaked samples, exhibits no significant changes for temperatures as high as 150°C.

The spectra obtained from a sample baked in vacuum for a period of 100 hours at 900°C are presented in Figures 26 and 27. A peak appears near 4100 Å at very low beam energy and this peak appears to shift rapidly toward higher energy as the beam voltage is increased, until it becomes obscured by the bound exciton emission (Figure 26). This peak is apparently produced by centers near the surface of the sample. A peak near 4000 Å was also observed by Vehse, et al. (Reference 19) who found that it was produced by baking in Zn or H_2 and that it was suppressed by electron bombardment. Since this peak did not appear to be correlated with the implantation of a particular ion and since it did not appear in all vacuum-baked samples a detailed investigation was not made. Notice also that the green peak appears to shift toward higher energy with increasing beam energy, and that this is apparently correlated with a decrease in the yellow tail. In addition, a few of the sharp lines observed in the Zn-baked samples appear in this vacuum-baked sample. As shown in Figure 27(b), the I_6 line dominates the I_8 line after a vacuum bake, and the I_9 line (Reference 76), which was absent in the previous spectra (Figures 20(b), 24(b)), appears in the spectrum for

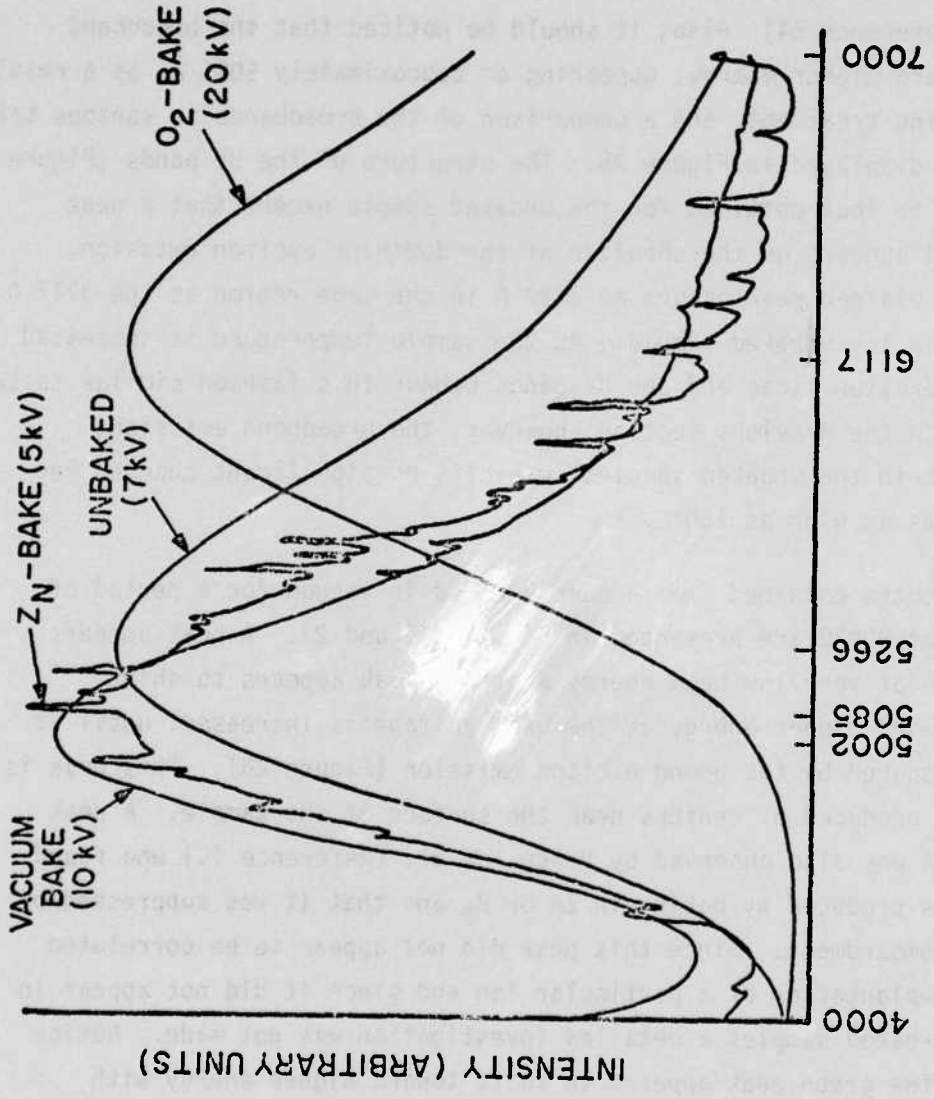

Figure 25. Comparison of Cathodoluminescence in Baked Samples

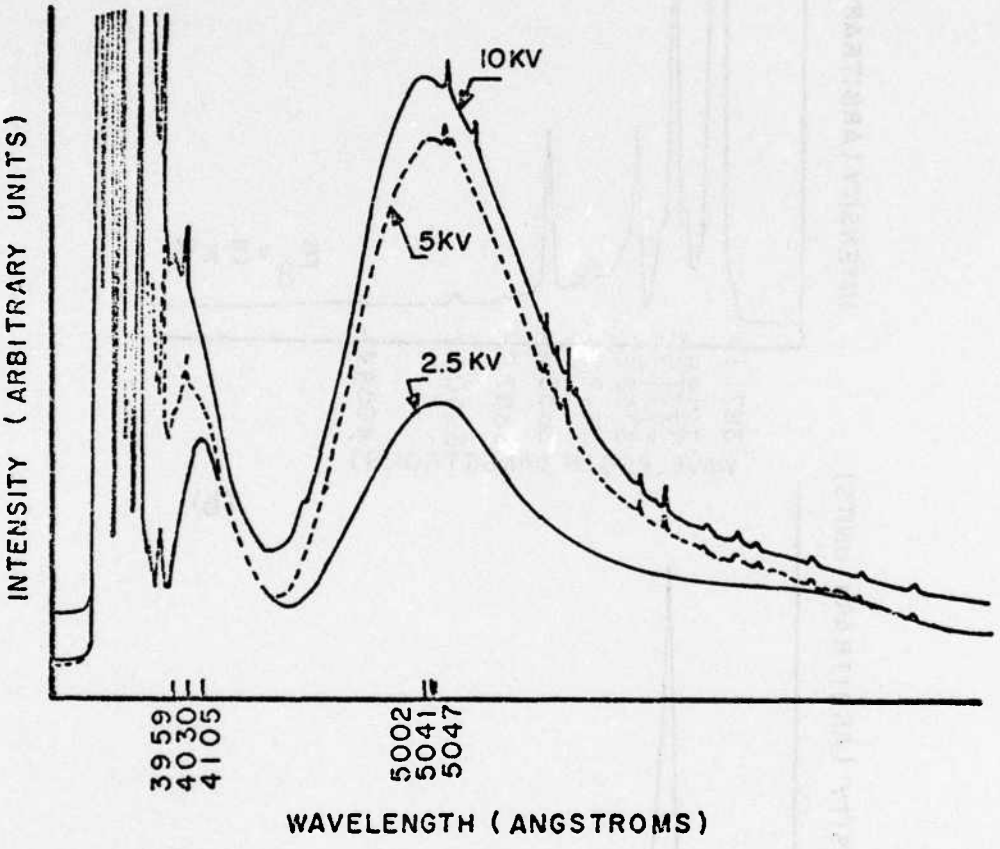

Figure 26. Cathodoluminescence of a Vacuum-Baked Sample

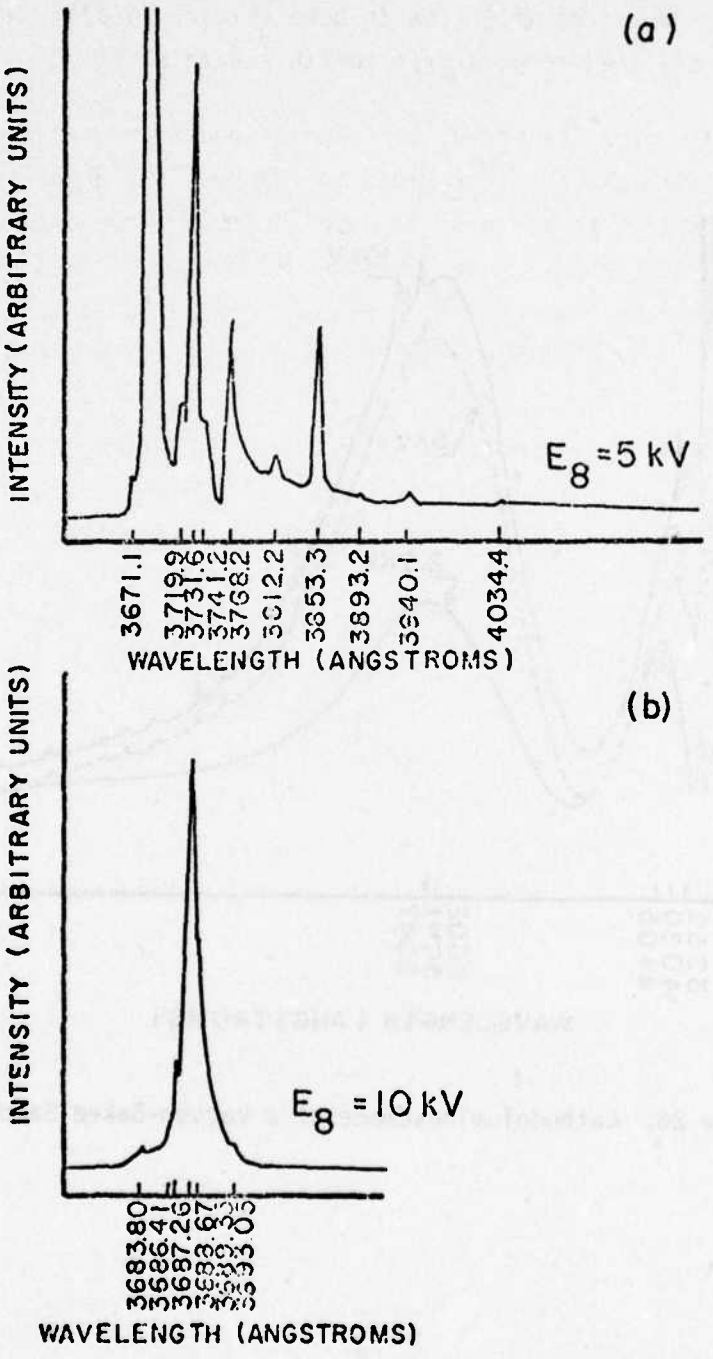

Figure 27. Cathodoluminescence of a Vacuum-Baked Sample (a) UV Bands and (b) Bound Exciton Lines

the first time. The UV bands displayed in Figure 27(a) are very much the same as those observed after the Zn bake (Figure 24(a)). No spectra were recorded at elevated temperatures for this sample.

A comparison of the broadband emission peaks induced by baking in the various atmospheres is provided in Figure 25, and the spectrum of the unbaked sample is included to complete the picture. The intensity of the O_2-baked sample was greatly reduced, and the UV emission was much less than that obtained for the broadband. Because of this lack of intensity it was not possible to obtain highly resolved spectra near the band edge for the O_2-baked sample. Both the Zn and vacuum bake produce a shift of luminescence which favors the green band, whereas the O_2 bake induces a dramatic shift to the yellow region. One possible explanation for this is that the O_2 bake results in the substitution of Li impurity ions at Zn lattice sites, which leads to an increase in the yellow band attributed to substitutional Li, as mentioned earlier. On the other hand, the Zn bake forces the Li ions off the Zn lattice sites thereby suppressing the yellow band (a similar mechanism has been proposed for Li - doped CdS) (Reference 115). Notice that the yellow tail is nearly absent in the luminescence of the Zn-baked crystal (Figures 23, 25). Since Li is a rapid diffuser in ZnO at relatively low temperatures (Reference 120), it is not surprising that the vacuum-baked crystal also shows an apparent decrease in the concentration of Li acceptors evidenced by a shift toward the green and a decrease in the yellow tail (Figures 25, 26). It appears, based on the previous explanation, that the as-grown crystal contains an intermediate concentration of Li acceptors, and this is not unreasonable if one considers the growth temperature (Reference 145).

c. Cathodoluminescence of Unimplanted Annealed Samples

As discussed in Section III, most of the implants were protected by a layer of SiO_2 prior to annealing. In order to determine whether or not the SiO_2 affected the luminescence of the samples, several unimplanted samples were coated with SiO_2 and subjected to a two-hour anneal at temperatures equivalent to those used for annealing the implanted samples.

The results of this annealing study are shown in Figure 28, and it is revealed in (a) that the act of sputtering the SiO_2 induces a slight change in the luminescence. There are several possible explanations for the observed shift toward higher energy (shorter wavelength) with increased beam voltage. It is possible that the surface of the crystal was affected by the sputtering process which may have heated the sample to a temperature as high as 200°C, in which case the shift observed in Figure 28(a) arises from probing through the surface layer. A second possibility is that the luminescence peak is the result of a bound-bound transition, and that the shift is due to the increased excitation intensity, as described previously in Section II. The shift might also be explained on the basis that the recombination centers associated with the yellow band become saturated under conditions of high intensity excitation, whereas the trapping centers giving rise to the green emission are not saturated. In this case more of the transitions occur through the trapping centers increasing the intensity of the green luminescence and causing an apparent shift of the broad peak toward shorter wavelengths.

The result of baking at 475°C for two hours, which produces a dramatic shift of the luminescence to the yellow portion of the spectrum (similar to the 900°C bake in an oxygen ambient) is shown in Figure 28(b). This shift raises some question as to the effects of the SiO_2 layer, however, a similar change (Figure 28(c)) occurs in a sample baked in vacuum at 475°C for two hours in the absence of SiO_2. The broadbands in both Figures 28(b) and (c) exhibit a shift toward the green as the beam voltage is increased, and the same possible explanations provided above may be considered. Since the sample whose spectra are displayed in Figure 28(c) was strongly etched, it would seem to rule out the mechanism of probing a surface layer induced by the heating during deposition of the SiO_2. As shown in Figure 28(d), a similar intensity shift may be induced with a fixed beam voltage by varying the beam current.

The results of a two-hour anneal at 600°C are displayed in Figure 28(e), while the spectra of a sample annealed at 900°C are shown in Figure 28(f). The structure which appears on the high energy (short wavelength) edge of the spectra in Figure 28(e) and the sturcture of the spectra obtained

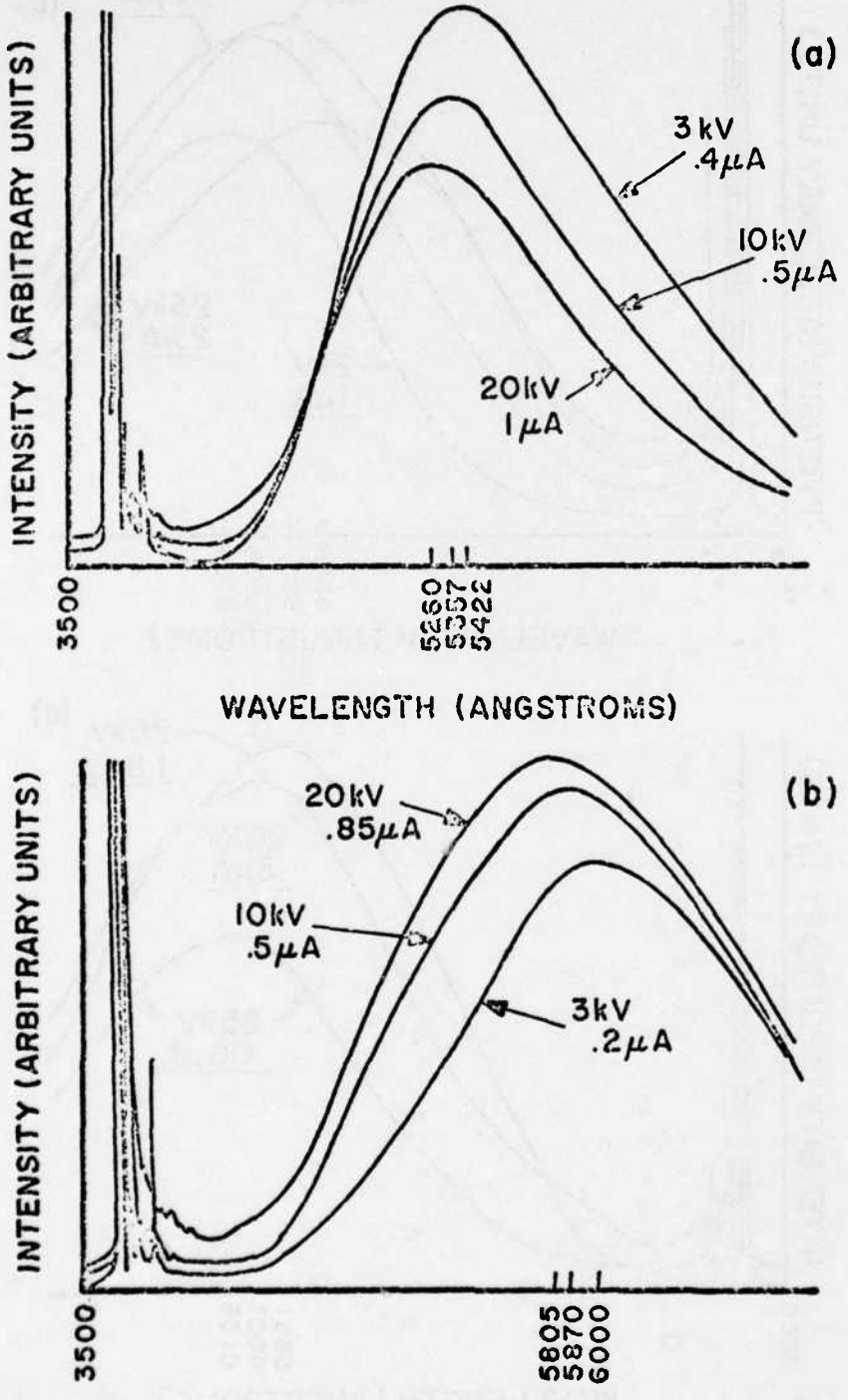

Figure 28. Annealed, Unbaked, Unimplanted Samples
(a) Unannealed (b) 475°C Two Hours with SiO_2

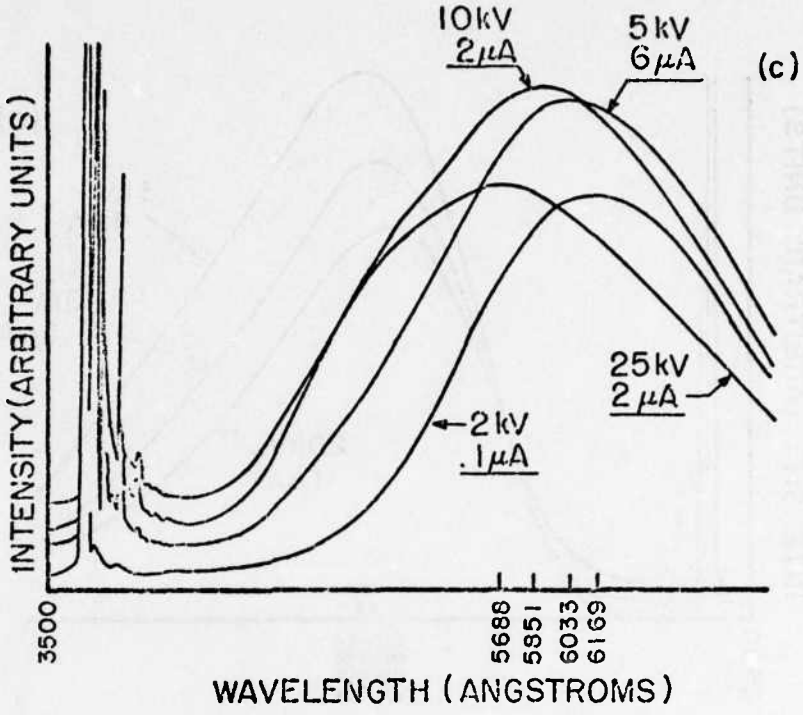

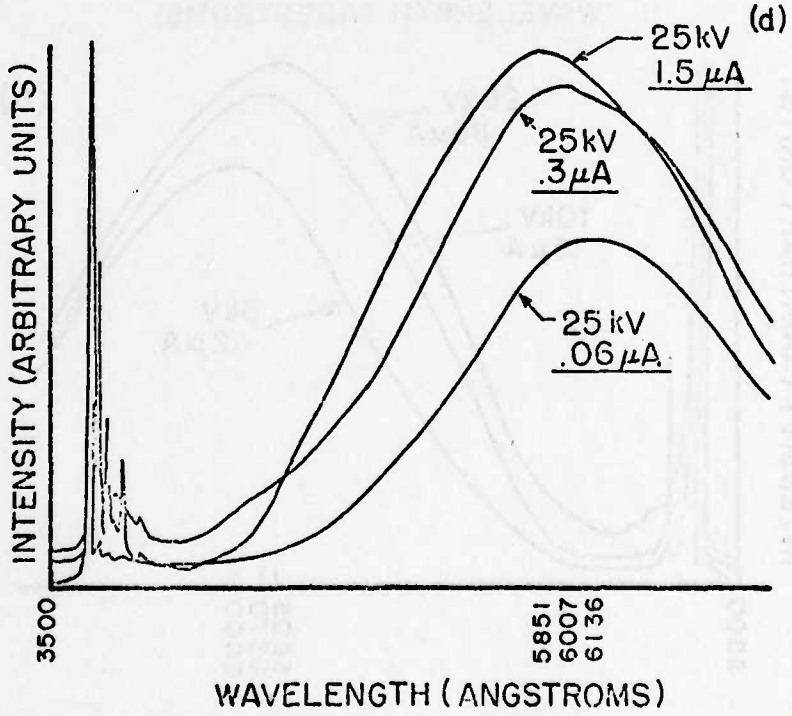

Figure 28. Annealed, Unbaked, Unimplanted Samples
(c) 475°C Two Hours No SiO_2 (d) 475°C Two Hours with SiO_2

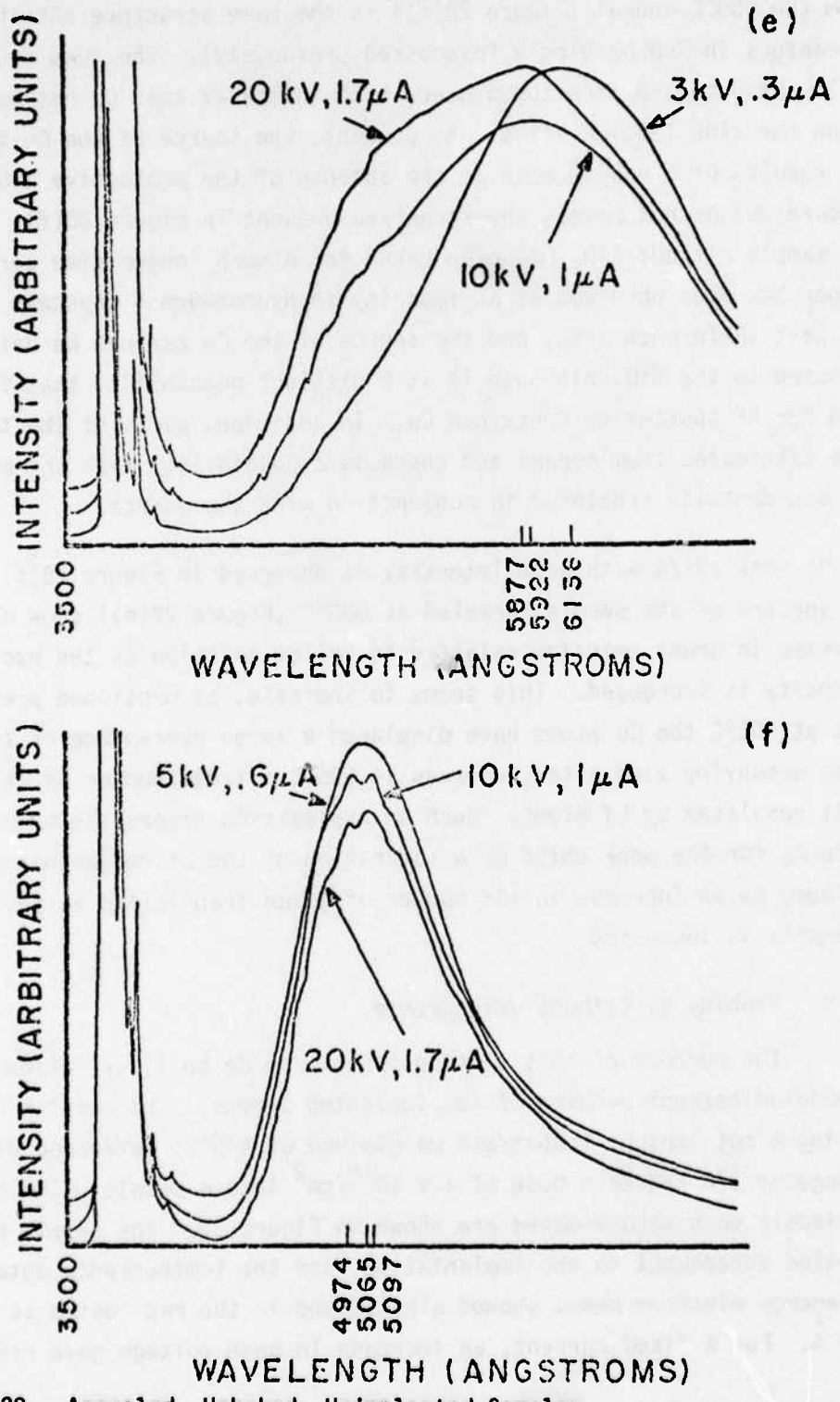

Figure 28. Annealed, Unbaked, Unimplanted Samples
(e) 600°C Two Hours with SiO_2 (f) 900°C Two Hours with SiO_2

from the 900°C anneal (Figure 28(f)) is the same structure attributed to Cu centers in ZnO by Dingle (discussed previously). The jump from the yellow band to the structured green band indicates that Cu has replaced the Li on the zinc lattice sites. At present, the source of the Cu is uncertain. The results of a vacuum bake in the absence of the protective SiO_2 layer (Figure 26) do not reveal the structure present in Figure 28(f), however, the sample without SiO_2 has been baked for a much longer time period. Copper has been observed as an impurity in hydrothermal crystals of ZnO in the past (Reference 146), and the source of the Cu can not be definitely attributed to the SiO_2 although it is a distinct possibility that the quartz target used for RF sputtering contained Cu. In addition, parts of the target holder were fabricated from copper and there is a possibility that the metallic copper was accidentally sputtered in conjunction with the quartz.

No peak shift with beam intensity is observed in Figure 28(f), while the spectra of the sample annealed at 600°C (Figure 28(e)) show a large increase in green emission relative to yellow emission as the excitation intensity is increased. This seems to indicate, as mentioned previously that at 900°C the Cu atoms have displaced a large percentage of the Li atoms occupying zinc sites, whereas at 600°C a large number of Zn sites are still populated by Li atoms. Such an explanation favors the model which accounts for the peak shift by a saturation of the Li recombination centers followed by an increase in the number of green transitions as the excitation intensity is increased.

d. Probing by Cathodoluminescence

The purpose of this section is to provide an illustration of the cathodoluminescent probing of ion implanted layers. The results obtained from probing a hot implant (substrate maintained at 475°C) performed with a beam voltage of 275 keV to a dose of $1 \times 10^{15}/cm^2$ into a sample which had previously been vacuum-baked are shown in Figure 29. The sample had not been annealed subsequent to the implantation, and the luminescence obtained with low energy electron beams showed a broadband in the red region at about 6500 Å. For a fixed current, an increase in beam voltage gave rise to a

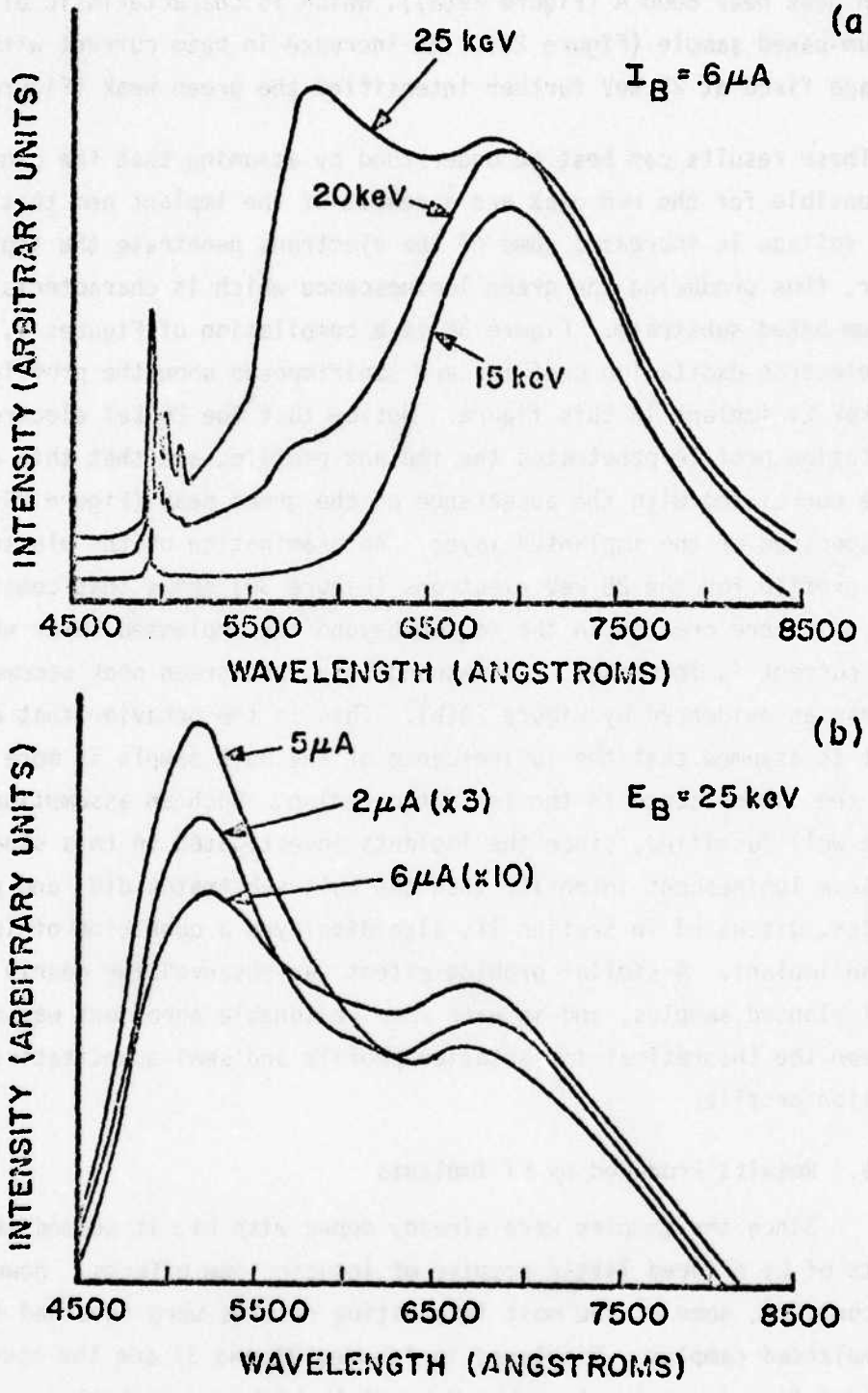

Figure 29. Probing of a 275 keV Li Implant

green peak near 5000 Å (Figure 29(a)), which is characteristic of a vacuum-baked sample (Figure 26). An increase in beam current with the voltage fixed at 25 keV further intensified the green peak (Figure 29(b)).

These results can best be understood by assuming that the centers responsible for the red peak are a result of the implant and that as the beam voltage is increased some of the electrons penetrate the implanted layer, thus producing the green luminescence which is characteristic of the vacuum-baked substrate. Figure 30 is a compilation of Figures 9, 10, and 4. The electron excitation profiles are superimposed upon the profile of the 275 keV Li implant in this figure. Notice that the 20 keV electron excitation profile penetrates the implant profile, and that this appears to be correlated with the appearance of the green peak (Figure 29(a)) in the spectrum of the implanted layer. An examination of the electron-hole pair profile for the 25 keV electrons (Figure 30) shows that considerably more pairs are created in the region beyond the implanted layer when the beam current is increased. Correspondingly, the green peak becomes more intense as evidenced by Figure 29(b). This is the behavior that one expects, if it is assumed that the luminescence of the bulk sample is more efficient than the luminescence in the implanted region. Such an assumption seems to be well justified, since the implants investigated in this study always had less luminescent intensity than the bulk substrates did; and previous studies, discussed in Section II, also displayed a quenching of luminescence by the implant. A similar probing effect was observed for nearly all of the implanted samples, and in each case reasonable agreement was observed between the theoretical implantation profile and semi-quantitative pair creation profile.

e. Results Produced by Li Implants

Since the samples were already doped with Li, it seemed that implants of Li offered little promise of inducing new effects. However, to the contrary, some of the most interesting results were obtained from Li-implanted samples. Displayed in Figures 31 and 32 are the spectra obtained from a previously unbaked crystal which was implanted successively at energy steps of 175, 80, and 30 keV using respective doses of Li ions

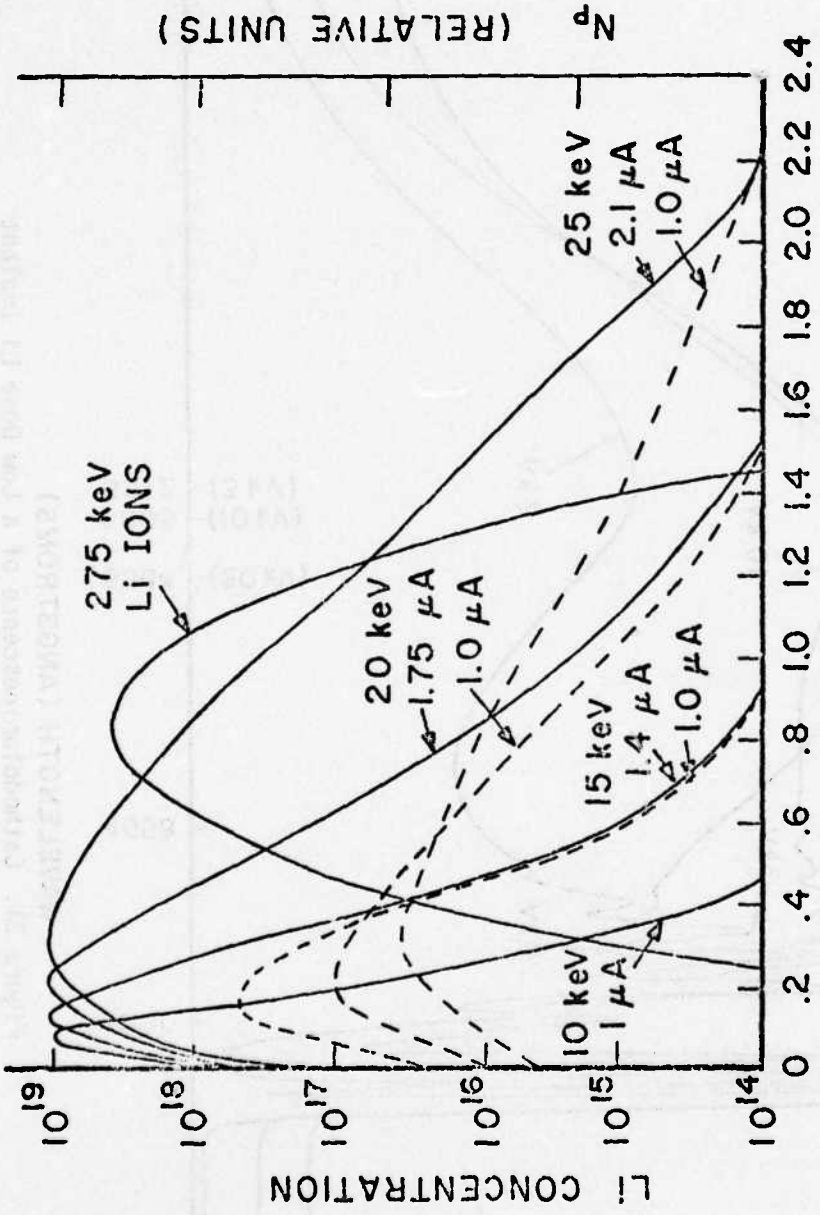

Figure 30. Compilation of Electron Profiles with 275 keV Li Profile

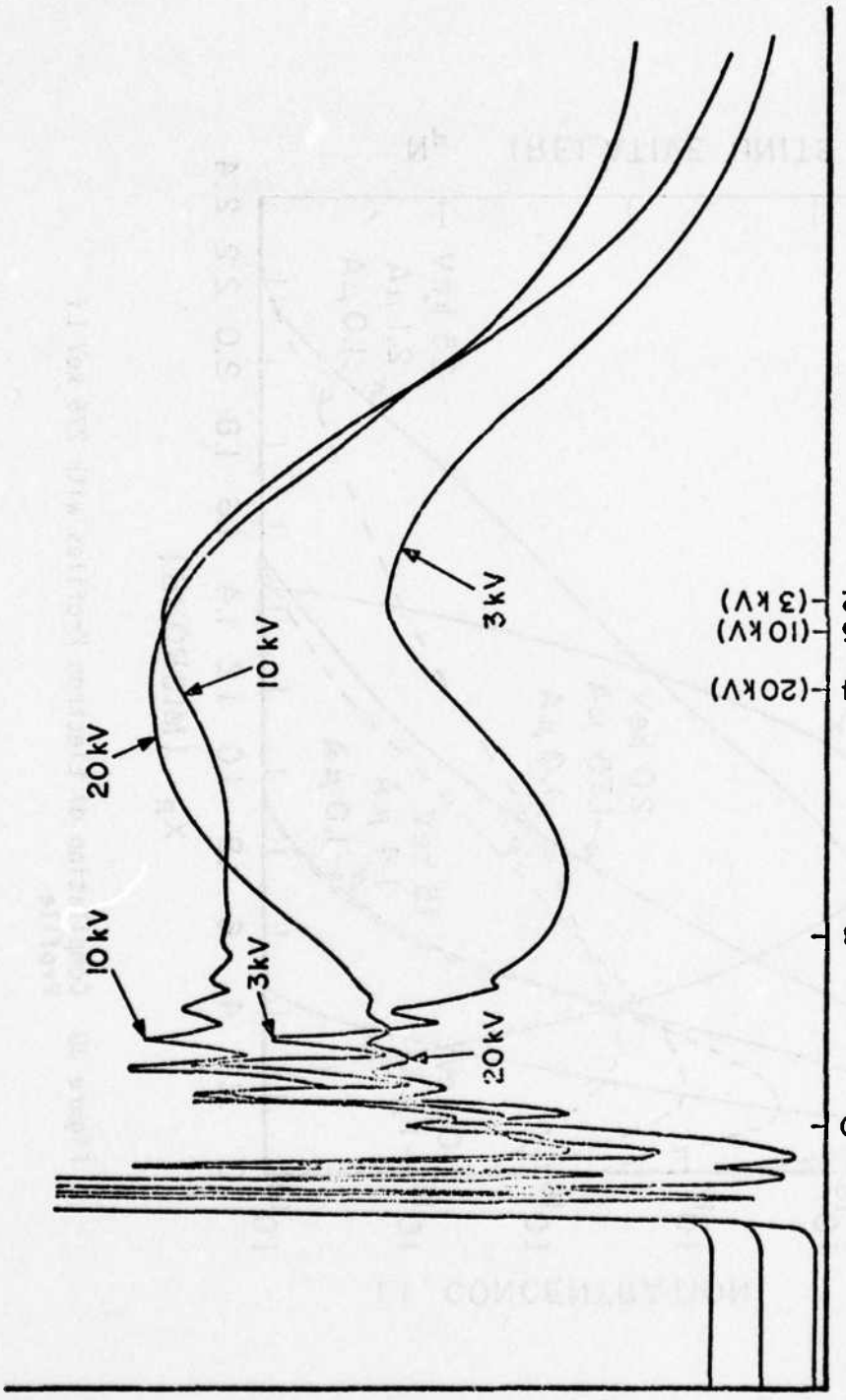

Figure 31. Cathodoluminescence of a Low Dose Li Implant After a 475°C Anneal for Two Hours

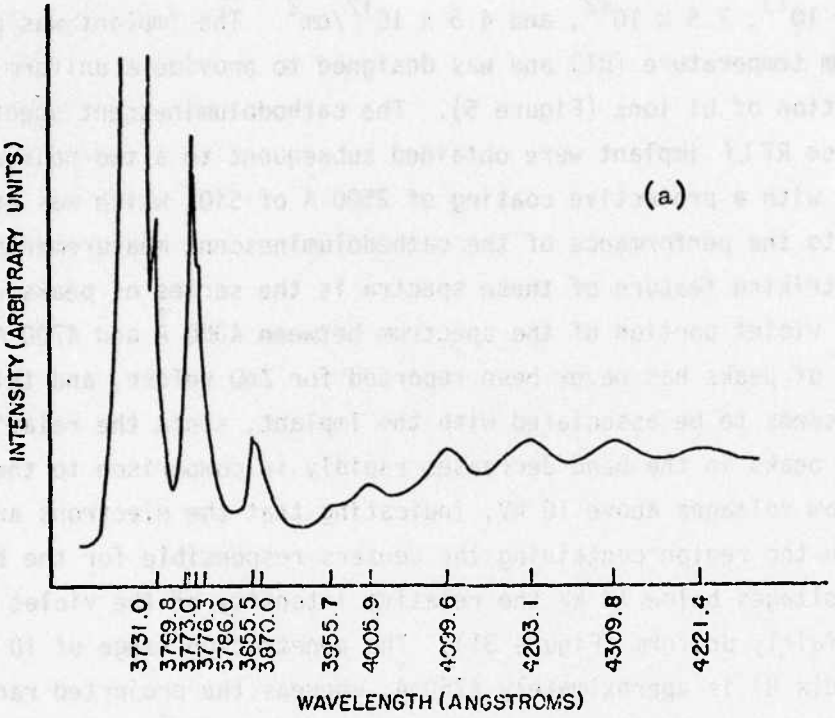

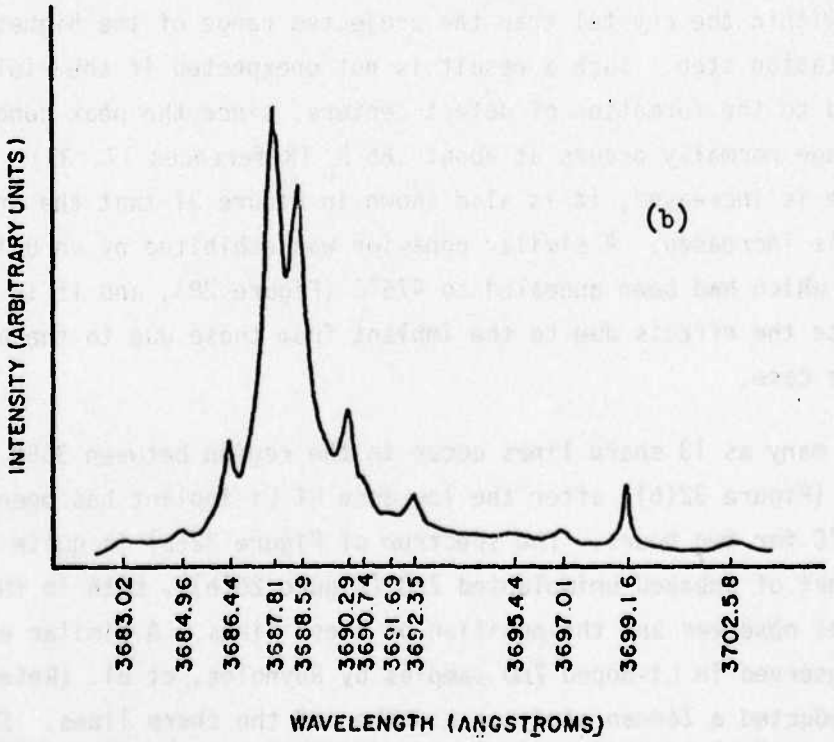

Figure 32. Cathodoluminescence of a Low Dose Li Implant
(a) UV Bands and Violet Bands and
(b) Bound Exciton Lines

of 1×10^{13}, 7.5×10^{12}, and $4.5 \times 10^{12}/cm^2$. The implant was performed at room temperature (RT) and was designed to provide a uniform low concentration of Li ions (Figure 5). The cathodoluminescent spectra of this low dose RT Li implant were obtained subsequent to a two-hour anneal at 475°C, with a protective coating of 2500 Å of SiO_2 which was etched off prior to the performance of the cathodoluminescent measurements. The most striking feature of these spectra is the series of peaks which appear in the violet portion of the spectrum between 4000 Å and 4700 Å. Such a series of peaks has never been reported for ZnO before, and this band of peaks seems to be associated with the implant, since the relative intensity of the peaks in the band decreases rapidly in comparison to the broadband for beam voltages above 10 kV, indicating that the electrons are probing through the region containing the centers responsible for the band. For beam voltages below 10 kV the relative intensity of the violet band is seen to be fairly uniform (Figure 31). The penetration range of 10 kV electrons (Appendix B) is approximately 4250 Å, whereas the projected range of the 175 keV Li ions is (Appendix A) approximately 5800 Å. This indicates that the centers which give rise to the violet band are located at a lesser depth within the crystal than the projected range of the highest energy implantation step. Such a result is not unexpected if the violet band is related to the formation of defect centers, since the peak concentration of damage normally occurs at about .66 R_p (References 17, 37). As the beam voltage is increased, it is also shown in Figure 31 that the green luminescence is increased. A similar behavior was exhibited by an unimplanted sample which had been annealed to 475°C (Figure 28), and it is difficult to separate the effects due to the implant from those due to the annealing in this case.

As many as 13 sharp lines occur in the region between 3680 Å and 3705 Å (Figure 32(b)) after the low dose RT Li implant has been annealed at 475°C for two hours. The spectrum of Figure 32(b) is quite different from that of unbaked unimplanted ZnO (Figure 20(b)), both in the number of lines observed and the position of these lines. A similar effect has been observed in Li-doped ZnO samples by Reynolds, et al. (Reference 152), who conducted a Zeeman study on a number of the sharp lines. Some of the

lines shown in Figure 32(b) appear to be coincident with strong lines attributed to Li doping by Reynolds, et al. (Reference 152); however, it must be pointed out that the spectra of Reference 152 were recorded at approximately 1°K using a two-meter instrument. It is possible that the spectrum of Figure 32(b) consists of a superposition of unresolved sharp lines, since it was recorded at 10°K with a 3/4-meter instrument. Reynolds, et al. attributed the sharp lines in Li-doped ZnO samples to the formation of exciton complexes in which the exciton is bound to an associated donor (acceptor pair created by molecular-like binding between a neutral donor and a charged acceptor). The existence of such a complex had been proposed by Halsted (Reference 49), and the Zeeman data obtained from Li-doped ZnO supported the model. The lines occurred at lower wavelengths than those observed for excitons bound to neutral donors, because the binding energy of the exciton is lowered by the presence of the acceptor center. It is natural to expect preferential pairing to occur in ZnO since it exhibits a high degree of ionic bonding, which tends to create more near neighbor associated pairs than would be expected for a random distribution of donors and acceptors. A similar effect has been observed in CdS by Litton and Reynolds (Reference 153).

The detailed structure of the violet band is shown in Figure 32(a) along with the ultraviolet series. The violet peaks are broader than the exciton peaks and appear to be LO phonon-coupled, with the no-phonon line at approximately 4005 Å. This series of phonon-coupled peaks is very similar in nature to the so-called "edge-emission" in CdS, being located within a few tenths of an eV from the fundamental edge. A series of broad, LO phonon-coupled peaks much like those described above has previously been observed in all of the wide bandgap II-VI compounds (References 59, 154, 155, 156), but it has never been reported for ZnO. In both CdS and ZnSe the edge emission has been shown to be the result of donor-acceptor pair recombinations (References 59, 157), and the acceptor centers responsible for the pair emission in CdS have been attributed to substitutional Li and Na at Cd sites (References 60, 113, 114, 115).

If the violet band in ZnO arises as a result of donor-acceptor pair recombination then this marks the first time that evidence of a shallow acceptor has been observed in ZnO. Assuming that the 4005 Å line is the long wavelength limit of the pairs and assuming a donor energy of .05 eV, based on the electrical results of Lander (described previously) one obtains from Equation 13 with $r \rightarrow \infty$, a value for the acceptor ionization energy of E_A = .198 eV. Since the violet band appears to some degree in all implanted samples, it is natural to assume that the acceptor center responsible for the pair emission is a native defect (e.g., Zn vacancies or O interstitials). However, since Li is present in all the crystals it is possible that the acceptor center is substitutional Li (with the Li being introduced on Zn sites by the creation of Zn vacancies during the implantation process and the subsequent occupation of these sites by Li during annealing). Although the latter mechanism is possible it does not seem very likely unless the analysis of Schirmer and Zwingel (Reference 81) (which attributes a .8 eV acceptor center to substitutional Li) is incorrect. The violet band has also been found to be very intense in samples implanted with Ne (Figure 33) at RT using 300 keV ions to a dose of $1 \times 10^{14}/cm^2$. Such an implant should produce only damage centers. Using the value of E-Nuclear from Appendix A for 300 keV Ne in ZnO and substituting in Equation 7 gives a value of approximately 724 Zn or O displacements per Ne ion (using the displacement energy, E_d = 57 eV, determined by Meese and Locker). Since the projected range for 300 keV Ne ions is approximately 3300 Å (Figure 3), then a relatively large concentration of defects may be induced within the implanted layer. On the one hand, this supports the argument that the violet band is induced by defect centers, yet, on the other hand it does not rule out the mechanism of Zn vacancy creation followed by occupation of Zn sites by Li. At the present, however, this is all highly speculative for it remains first to be proven that the violet band is a result of donor-acceptor pair recombination, similar to the edge emission in ZnSe and CdS.

Another interesting result shown in Figure 32(a) is the appearance of sharp structure near 3700 Å. The sharp peak at 3773 Å overshadows the normally observed (Figure 20(a)) first LO phonon replica of the bound

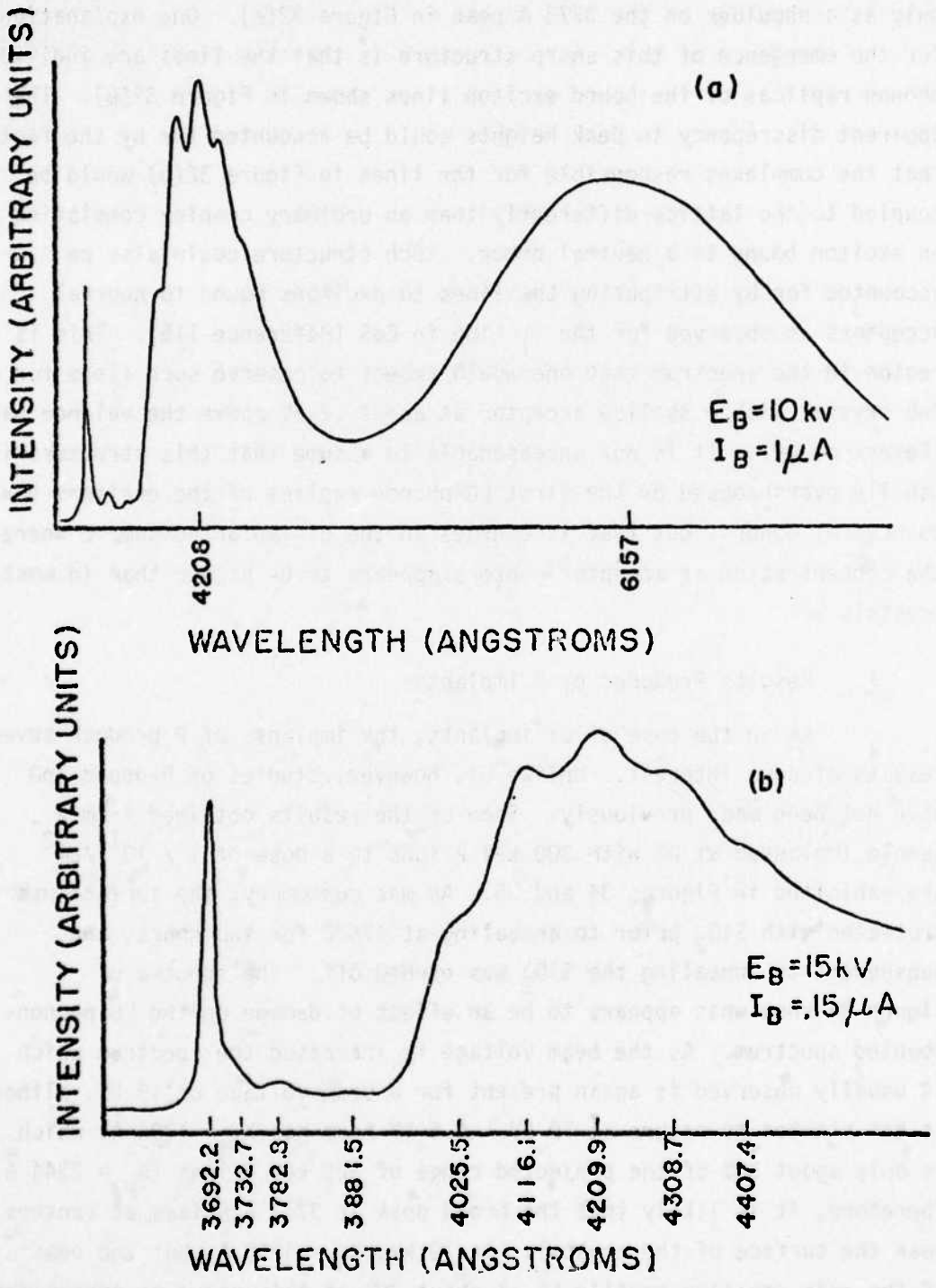

Figure 33. Cathodoluminescence of a Ne Implant
(a) Entire Spectrum (b) Violet and Ultraviolet Bands

exciton lines, which usually occurs at 3769.7 Å. This peak is observed only as a shoulder on the 3773 Å peak in Figure 32(a). One explanation for the emergence of this sharp structure is that the lines are individual phonon replicas of the bound exciton lines shown in Figure 32(b). The apparent discrepancy in peak heights could be accounted for by the fact that the complexes responsible for the lines in Figure 32(b) would be coupled to the lattice differently than an ordinary complex consisting of an exciton bound to a neutral donor. Such structure could also be accounted for by attributing the lines to excitons bound to neutral acceptors as observed for the I_1 line in CdS (Reference 115). This is the region in the spectrum that one would expect to observe such lines for a ZnO crystal with a shallow acceptor at about .2 eV above the valence band (Reference 49). It is not unreasonable to assume that this structure is usually overshadowed by the first LO phonon replica of the excitons bound to neutral donors, but that it emerges in the Li-implanted sample where the concentration of acceptor centers appears to be higher than in most crystals.

f. Results Produced by P Implants

As in the case of Li implants, the implants of P produce several results of some interest. Unlike Li, however, studies of P-doped ZnO have not been made previously. Some of the results obtained from a sample implanted at RT with 300 keV P ions to a dose of $1 \times 10^{14}/cm^2$ are exhibited in Figures 34 and 35. As was customary, the surface was protected with SiO_2 prior to annealing at 475°C for two hours, and subsequent to annealing the SiO_2 was etched off. The spectra of Figure 34 show what appears to be an effect of damage on the LO phonon-coupled spectrum. As the beam voltage is increased the spectrum which is usually observed is again present for a beam voltage of 15 kV, although it has started to return at 10 kV. A 5 kV beam has X_R = 1200 Å, which is only about 50% of the projected range of 300 keV P ions (R_p = 2344 Å). Therefore, it is likely that the broad peak at 3773 Å arises at centers near the surface of the crystal. At 10 kV, X_R = 4250 Å, but the peak of the pair creation profile is at about 20% of this value or approximately 800 Å, so that the argument that the effect is one arising near the

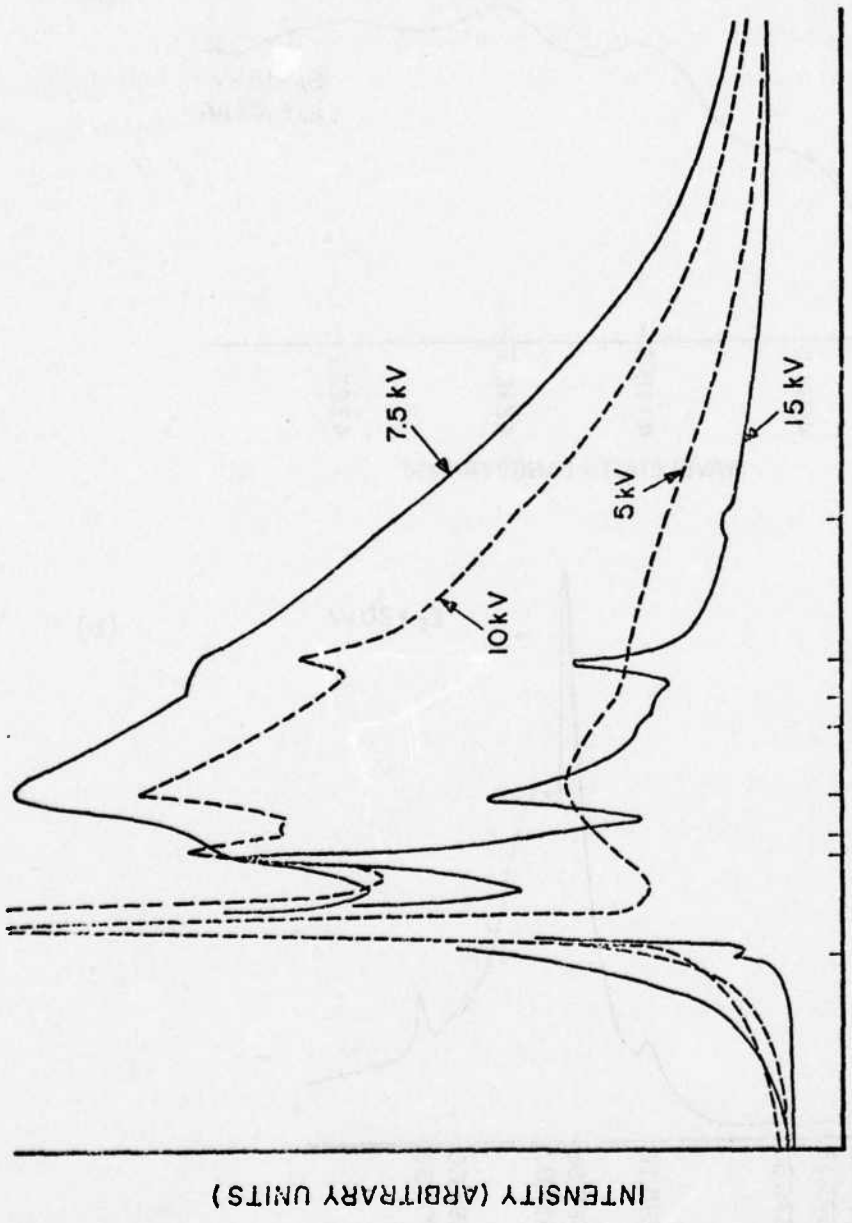

Figure 34. Cathodoluminescence of P Implant - UV Bands

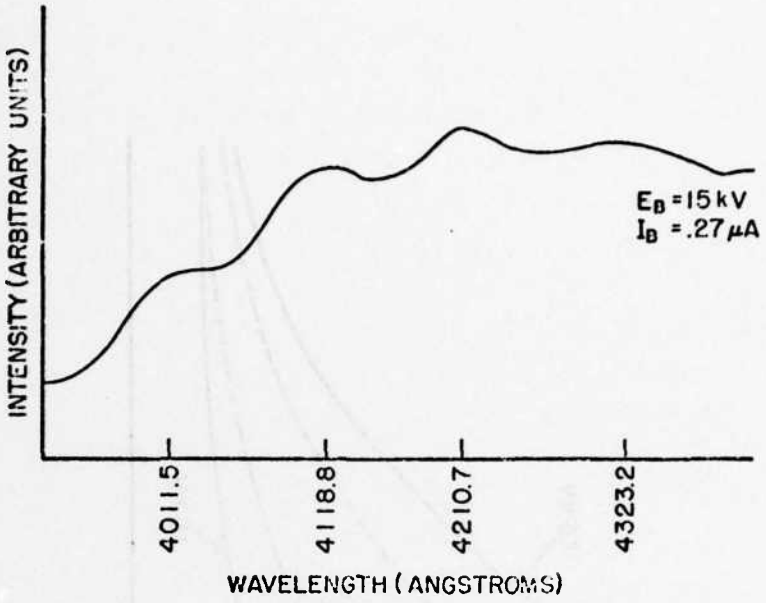

(a)

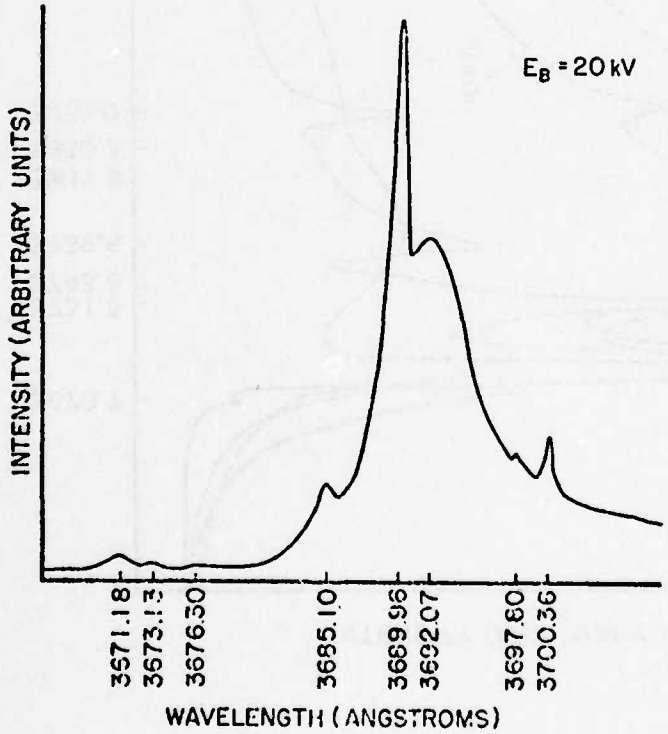

(b)

Figure 35. Cathodoluminescence of P Implants
(a) Violet Band (b) Bound Exciton Lines

surface of the sample is still valid. It is possible that strains and distortions produced in the lattice by gross damage due to the implant cause an alteration of the normal modes which leads to the type of spectra shown in Figure 34. A similar distortion is observed in Figure 33(b) for the Ne implant, and the effect has also been observed in a RT N implant.

The violet band produced by the P implant is depicted in Figure 35(a). In this case the band is very weak in intensity compared to the bound exciton and broadband visible emissions, so weak in fact that it does not even appear on the same scale as that used for Figure 34. Notice that the series of peaks composing the violet band is shifted approximately 6 Å toward longer wavelength in comparison to the series shown in Figure 32(a). A comparison of the wavelengths of the violet peaks in samples implanted with Li or P is provided in Table 6. A possible explanation for the shift may be expressed in light of the results depicted in Figure 35(b), which shows a new band located at 3692 Å that has apparently been produced by the P implant. Recalling that the peak of the pair production profile is approximately 20% of X_R, then the peak for 20 keV electrons is at approximately 3000 Å; which is near the peak of the profile of P ions. At present, the exact nature of the luminescent peak at 3692 Å has yet to be resolved, but suppose that it is the result of a bound exciton transition. It is doubtful that the exciton is bound to a simple substitutional P atom

TABLE 6

COMPARISON OF VIOLET EMISSION BANDS

Li Implant	P Implant
4005.9	4011.5
4099.6	4118.8
4203.1	4210.7
4309.8	4323.2
4421.4	

because P at an O site should behave as an acceptor and the peak at 3692 Å corresponds to a center having too low an ionization energy for an acceptor. Thus, it is reasonable to assume that P forms a donor complex in ZnO, and that the exciton is bound to the complex. A similar effect occurs in CdS and CdSe where substitutional P forms a deep acceptor, but complexes involving the P give rise to shallow acceptors (Reference 115) (based upon optical evidence). If the P complex is also one of the centers involved in the donor-acceptor pair emission (which has been postulated as the mechanism for the violet series) then the shift of the peaks toward longer wavelength may be attributed to the increased ionization energy exhibited by the P complex. In this case the P complex is most likely a shallow donor center, and the pair recombination occurs between this donor and the .2 eV acceptor level described earlier.

Similar effects are observed in samples which have been implanted at 475°C with 1 MeV P ions to a dose of $10^{15}/cm^2$. The peak at 3692 Å which has been postulated as arising from a P complex is displayed in Figure 36. This spectrum was obtained from a sample which had undergone a 900°C anneal for two hours subsequent to the hot implant. The surface of the sample had been protected by a layer of SiO_2 during the anneal. A shift of the violet band toward longer wavelength is observed in Figure 37, which is a comparison of hot impalnts of various ions. The spectra of Figure 37 were obtained from samples which had not undergone any annealing subsequent to being implanted.

g. Results of Hot Implants: The Red Peak

Ions of Li, Na, N, P, and Ne were implanted into substrates which were maintained at 475°C during the implant. A characteristic feature of these hot implants was the appearance of a broad peak in the red region of the spectrum near 6500 Å (Figure 38). This red peak was observed to result from all hot implants which had not been processed after the implantation had been completed. Since this peak appeared in all the samples implanted at 475°C, it is reasonable to associate this peak with the formation of damage centers. As was discussed in Section II, one expects less severe damage to arise in samples implanted at elevated

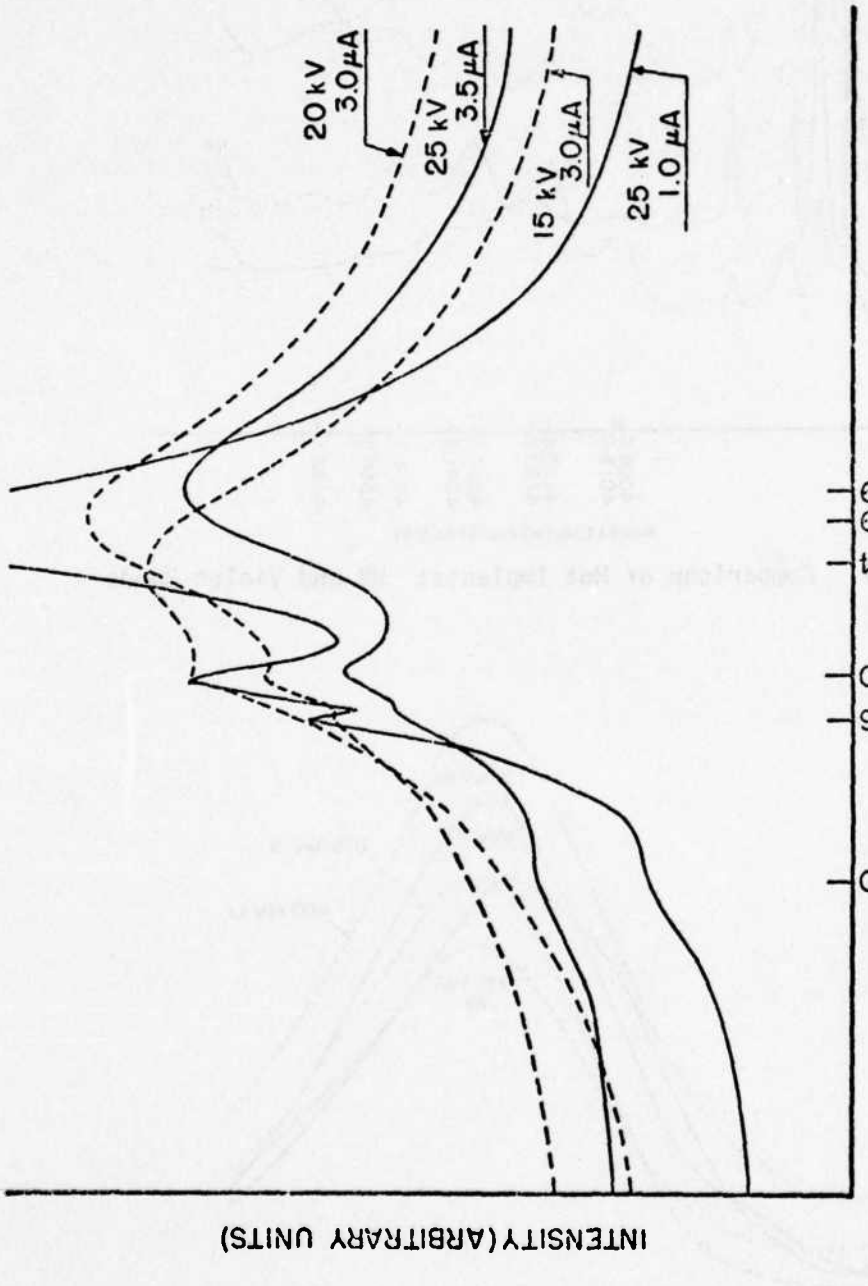

Figure 36. Cathodoluminescence of a Hot P Implant After a Two-Hour Anneal at 900°C

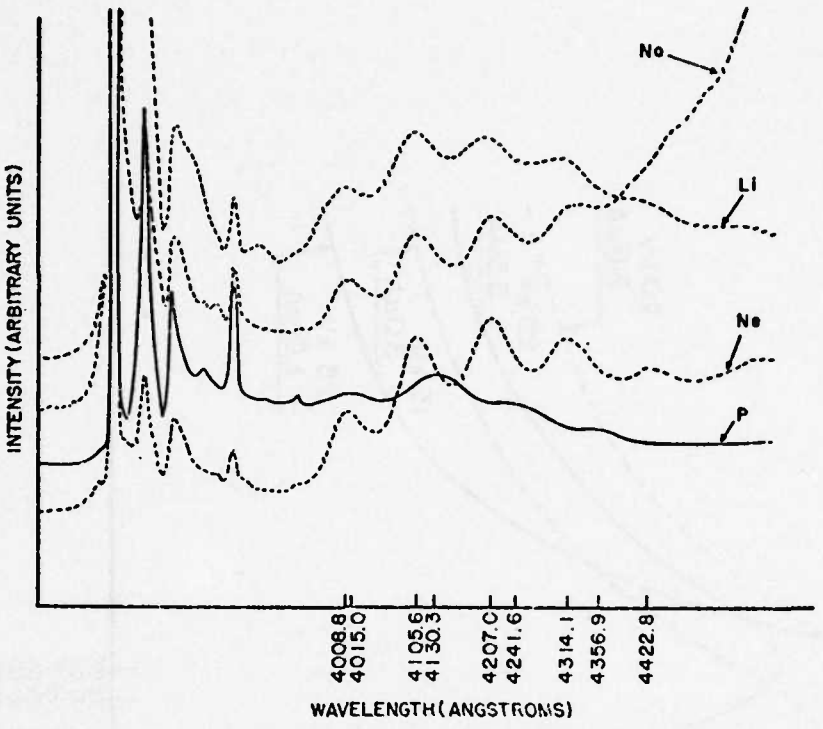

Figure 37. Comparison of Hot Implants: UV and Violet Bands

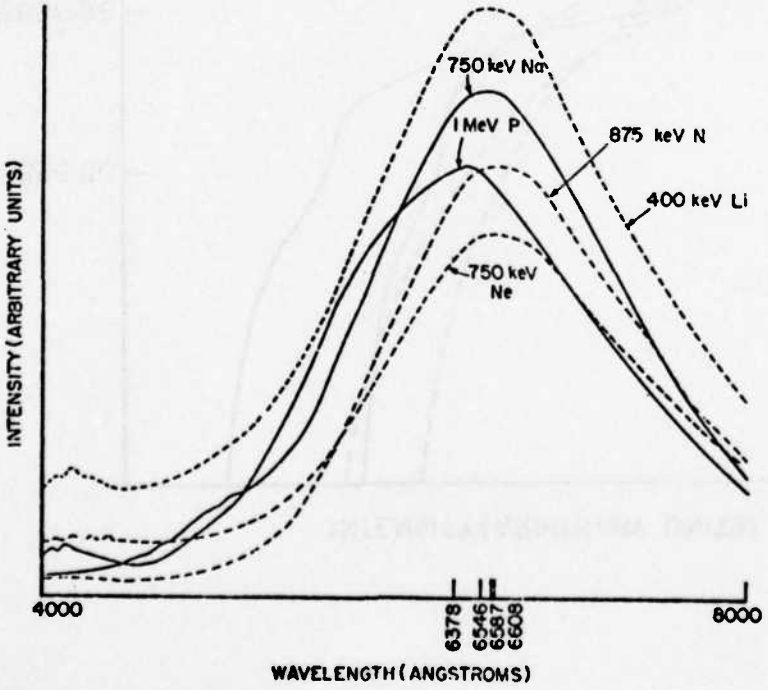

Figure 38. Comparison of Hot Implants in the Visible Portion of the Spectrum

temperatures. Therefore, it might be possible that the 6500 Å peak arises as a result of the formation of a simple defect. Another possibility is that the red peak is due to an aggregation of simple defects, which are mobile at the implantation temperature of 475°C and could reasonably be expected to form aggregates. However, if this is the case it would seem that the red peak should occur after annealing in other implanted samples besides those implanted at 475°C. After a hot implant is subsequently annealed at 900°C (while being protected by an SiO_2 layer) the 6500 Å peak is no longer present in the spectrum. In addition, the violet peaks shown in Figure 37 are deleted from the spectrum of a hot implant by annealing at 900°C, indicating that this band is also due to damage. The luminescence mechanism responsible for the red peak cannot be identified at this point. An identification of whether it is the result of a free-bound or bound-bound transition requires further study.

3. ELECTRICAL RESULTS

As mentioned previously (Section II), Hall effect measurements are extremely useful for determining the electrical properties of semiconductors. One may determine the type of majority carrier and its concentration as well as the resistivity of the material and the Hall mobility. In addition, if the temperature of the sample is varied during the measurement one may obtain values for the ionization energy of the predominant impurity centers. It is of great interest to compare the ionization energies of the electrically active centers with those obtained from centers which are optically active and give rise to luminescence as discussed in the preceding section.

Prior to investigating the electrical properties of implanted layers it was first necessary to conduct an evaluation of unimplanted ZnO. The results obtained from an unimplanted, unannealed sample are shown in Figures 39 and 40. This sample was cut, polished, and etched using the procedures described in Section III, and the Hall data were obtained using the van der Pauw technique and system. The sample is n-type, but it is quite strongly compensated having a room temperature resistivity, ρ, on the order of 100Ω-cm. The degree of compensation is also indicated

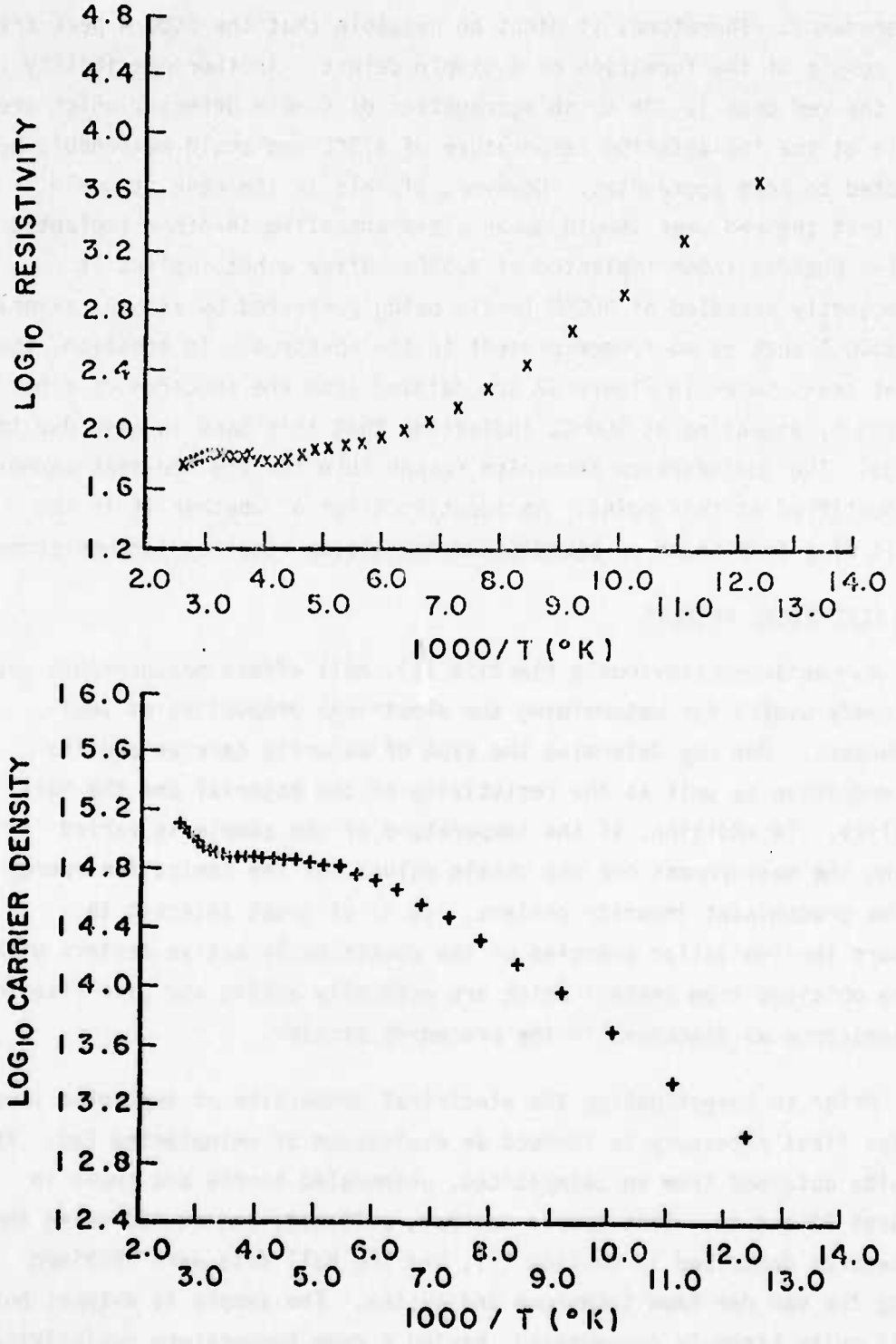

Figure 39. Resistivity and Carrier Concentration in an Unbaked, Unimplanted Sample

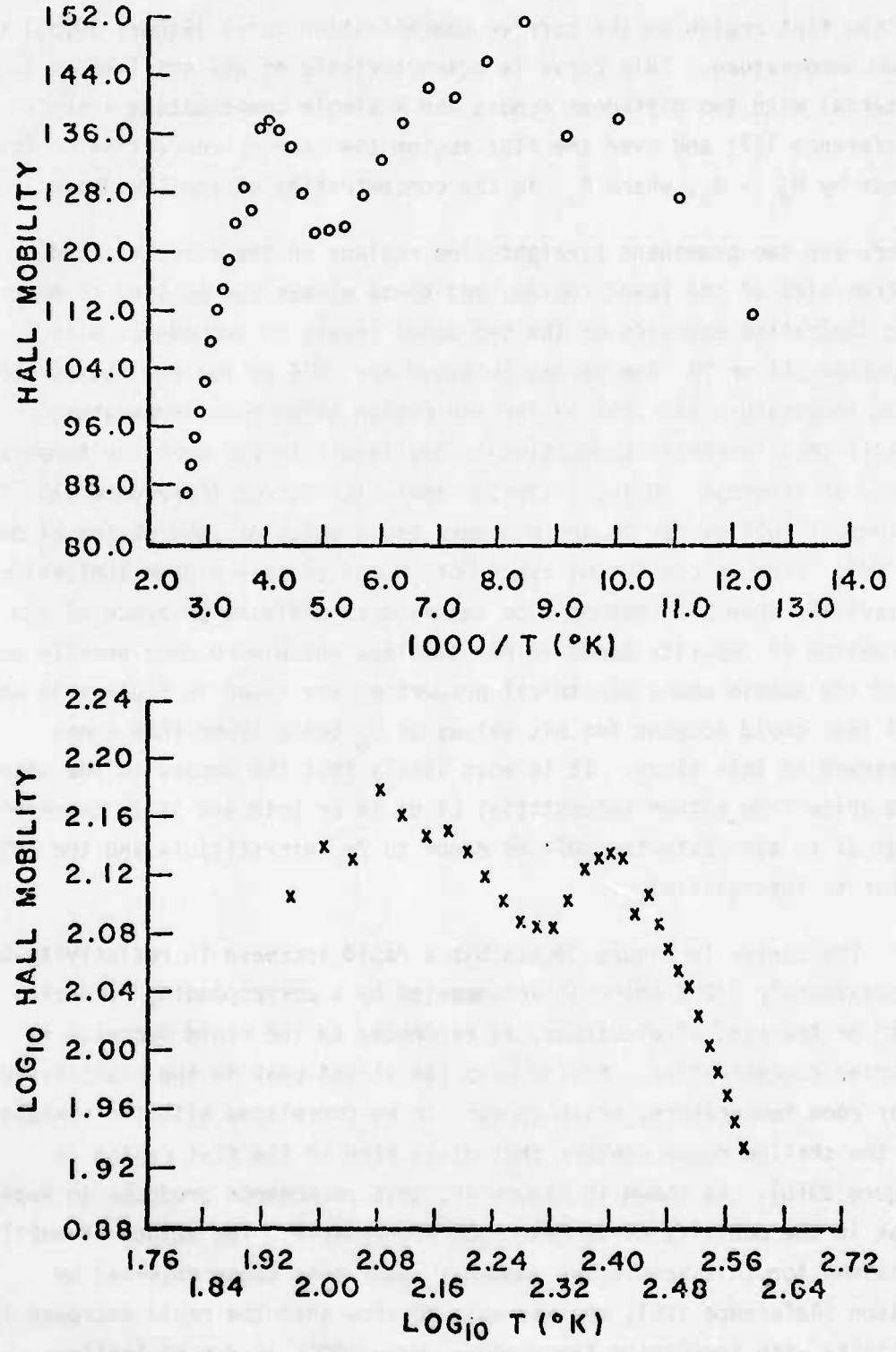

Figure 40. Hall Mobility of Unbaked, Unimplanted Sample

by the flat region on the carrier concentration curve (Figure 39(b)) near room temperature. This curve is characteristic of one obtained in a material with two different donors and a single compensating acceptor (Reference 127) and over the flat region the carrier concentration is given by $N_{d_1} - N_a$, where N_{d_1} is the concentration of shallow donors. There are two prominent straight-line regions on the curve located on either side of the level region, and these slopes can be used to determine the ionization energies of the two donor levels in accordance with Equations 17 or 18. The values obtained are .074 eV for the region above room temperature and .055 eV for the region below room temperature. Recall that intrinsic conduction is negligible in ZnO over the temperature range of interest. Using a similar analysis, Hutson (Reference 125) found values of .051 eV for Zn and H donors and a value of .044 eV for Li donors in ZnO. This is consistent since both H and Zn have higher ionization potentials than Li. Hutson also observed significant evidence of the formation of impurity bands in his samples, which were more heavily doped than the sample whose electrical properties are shown in Figures 39 and 40, and this could account for his values of E_d being lower than those observed in this study. It is most likely that the donors in the untreated ZnO arise from either interstitial Li or Zn or both and it is therefore logical to attribute the .074 eV donor to Zn interstitials and the .055 eV donor to interstitial Li.

The curves in Figure 39 exhibit a rapid increase in resistivity below approximately 170°K which is accompanied by a corresponding "freezing out" or trapping of electrons, as evidenced by the rapid decrease in carrier concentration. Notice also the slight peak in the resistivity near room temperature, which appears to be correlated with the exhaustion of the shallow donor centers that gives rise to the flat region in Figure 39(b). As shown in Figure 40, this phenomenon produces an apparent peak in the mobility curve near room temperature. The values of mobility obtained for this sample are somewhat lower than those observed by Hutson (Reference 125), who was able to show that the rapid decrease in mobility with increasing temperature above 200°K is due to lattice

scattering. Hutson's data also showed a much smaller contribution due to impurity scattering, which in this investigation apparently results in the decrease in mobility for temperatures below approximately 125°K.

a. Electrical Properties of Baked Samples

As in the case of cathodoluminescence, samples which had been baked in various atmospheres were examined using the van der Pauw technique. It was found that baking in vacuum or in O_2 drastically increased the resistivity of the ZnO samples, whereas baking in Zn lowered the resistivity dramatically. An O_2 bake produced resistivities at room temperature in excess of 10^{11} Ω-cm (making measurements impractical). Presumably, such an increase is due to compensation by Li accepter centers formed by substitutional Li at Zn sites. On the other hand, a vacuum bake gave rise to ZnO samples which had the properties shown in Figure 41. Although the resistivity (Figure 41(a)) of this material is not extremely high, the mobility was low (approximately 25 cm^2/volt-sec) and the measurement was very noisy resulting in large scatter in the data, which was not reproduced herein. Notice that measurements could not be obtained for temperatures below approximately 150°K (the reason for this was excessive noise). The usual analysis of the carrier concentration curve gives a single deep donor center with ionization energy = .144 eV, and these results from the vacuum bake are difficult to reconcile with a simple model. Apparently, impurity scattering is responsible for the loss of mobility, yet one would expect to reduce the amount of interstitial Zn and Li by such a heat treatment, indeed the ampoule is lined with a white substance after this heat treatment has been completed. One possible explanation would be the formation of a surface layer with a high concentration of Zn or Li caused by diffusion of the interstitial atoms out of the substrate; however, this is unlikely in this instance because the sample was strongly etched prior to performing the measurements.

The electrical properties obtained from a sample which had been baked in Zn for a period of 100 hours at 900°C are shown in Figures 42 and 43. In this case the room temperature resistivity has been lowered

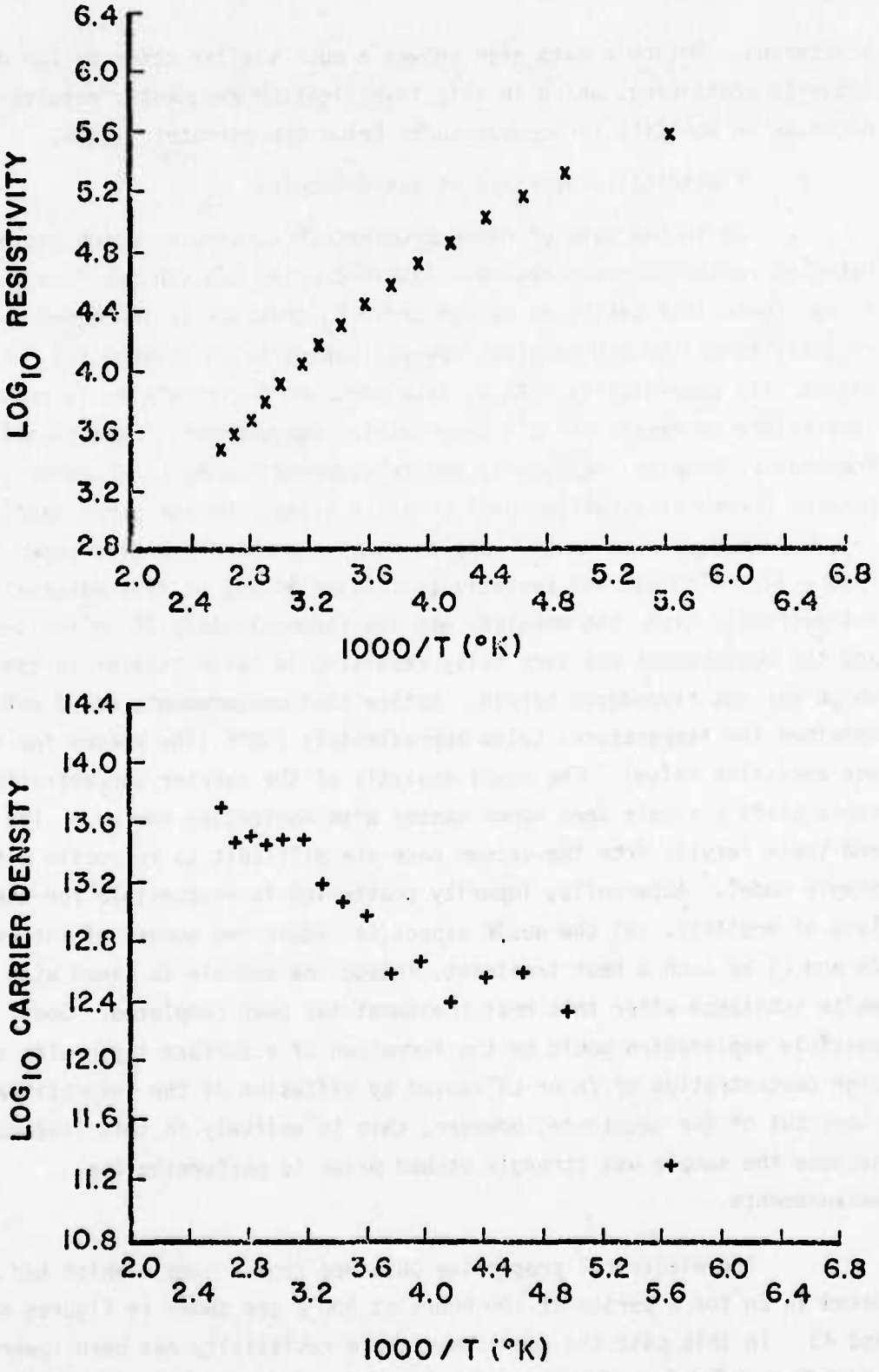

Figure 41. Resistivity and Carrier Concentration of a Vacuum-Baked Sample

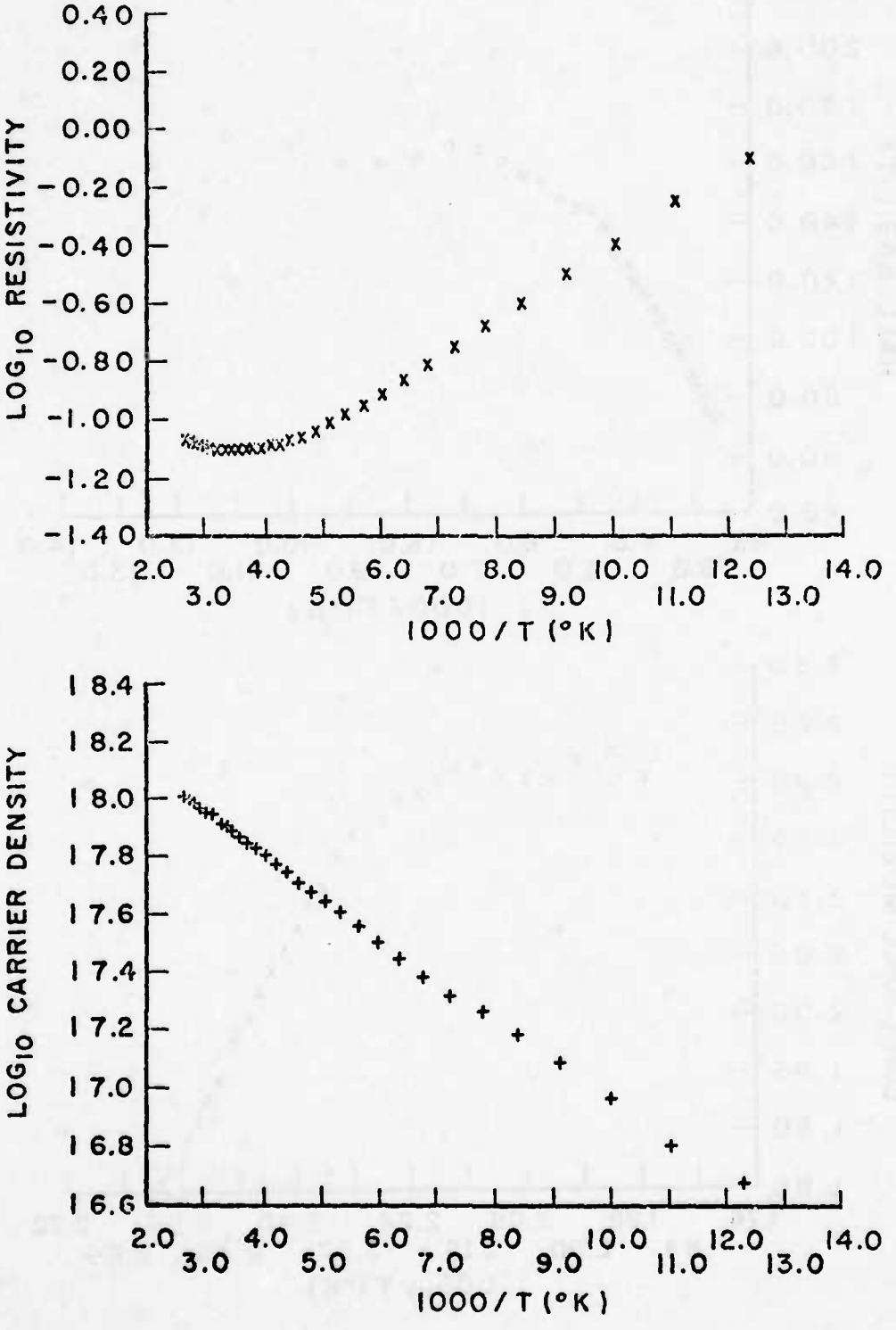

Figure 42. Resistivity and Carrier Concentration of a Zn-Baked Sample

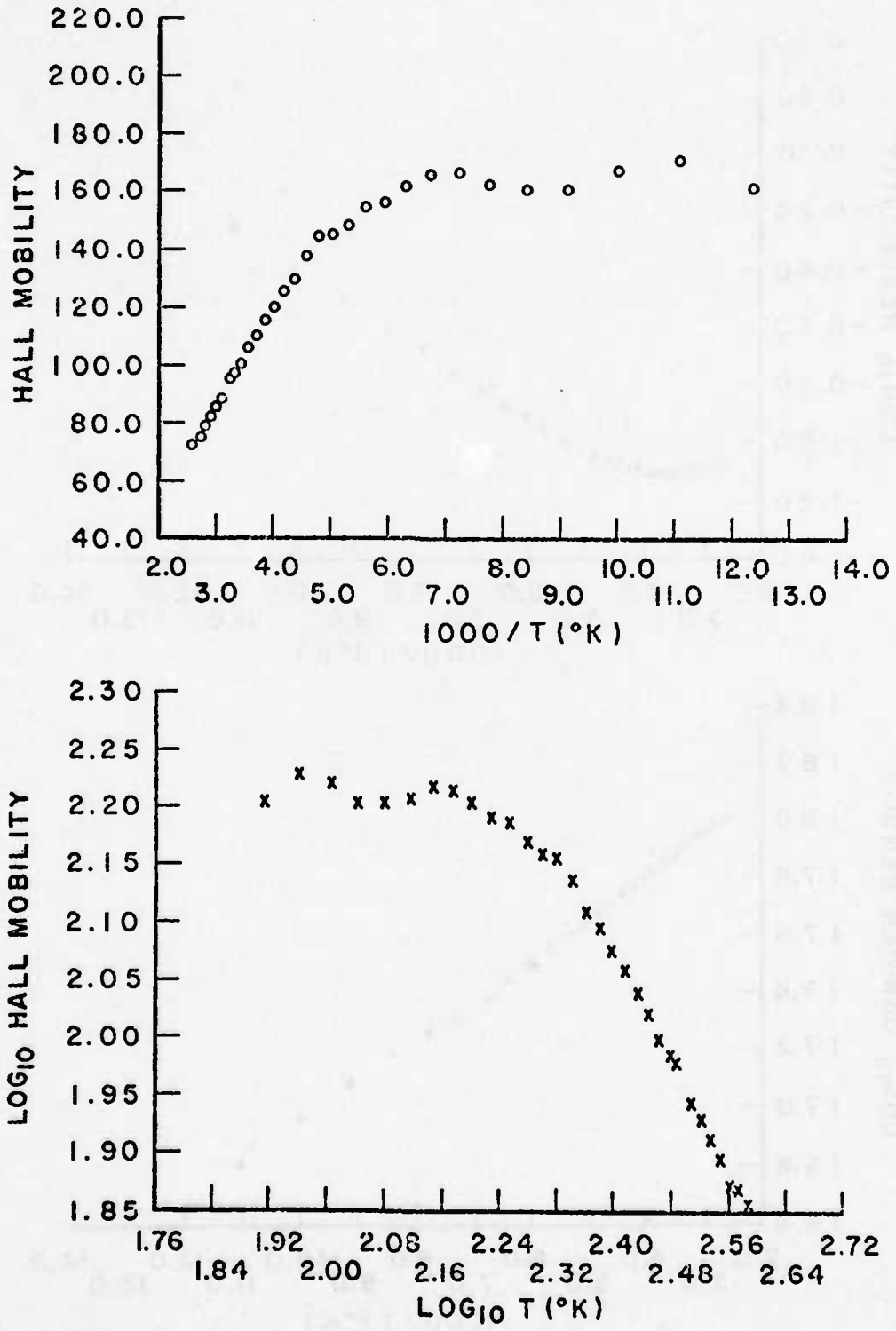

Figure 43. Hall Mobility of a Zn-Baked Sample

from the neighborhood of 100Ω- cm down to .1Ω- cm, and the concentration of donors has correspondingly grown larger. The curve in Figure 42(b) has the same basic shape as that shown in Figure 39(b) except that the flat (exhaustion) region, which indicates the degree of compensation, has been eliminated because of the increase in donor concentration. The two slopes of Figure 42(b) correspond to donors with ionization energy of .030 eV and .025 eV, and these are again attributed to interstitial Zn and Li respectively. The increase in the number of Li donors is believed to be due to removal of Li from Zn sites by the heat treatment in Zn, and the decrease in the ionization energies is attributed to the formation of impurity bands (Reference 117). As pointed out in the discussion of the unbaked sample, Hutson (Reference 125) also observed evidence for impurity banding in ZnO, and the concentrations present in the Zn-baked sample are sufficiently high to cause considerable banding to occur. The mobility curves shown in Figure 43 also have a shape similar to that shown in Figure 40. However, the apparent dip corresponding to the exhaustion region is missing from Figure 43, and impurity scattering appears to be less important at temperatures below 125°K.

b. Electrical Properties of Implanted Samples

The analysis of the electrical data from implanted layers is made more difficult by the uncertainty in the thickness, t, to be used in the van der Pauw formulas (Equations 14, 15, and 16). The data reported herein were obtained using the thickness of the sample which is certainly much larger than the thickness of the implanted layer. The equations show that in this case the values obtained for ρ will be too high, while those obtained for n will be too low. The mobility is unaffected by the value chosen for t. For the implants whose electrical properties are shown the layer is on the order of 1 μ whereas the sample thickness is approximately 1mm, which predicts that the values of ρ should be divided by 1000 and the values of n should be multiplied by 1000. However, this fails to account for diffusion during annealing, which could be quite considerable in the case of Li implants (Reference 124).

The data obtained from a hot Li implant (400 keV, 1 x $10^{15}/cm^2$, 475°C substrate temperature) after a 2-hour anneal at 475°C is shown in Figures 44 and 45. The decrease in mobility below approximately 200°K (Figure 45) is most likely due to an increase in impurity scattering. Since this implant was performed in a vacuum-baked substrate which was quite resistive (Figure 41) initially, then it is apparent from Figure 44(a) that the implant serves to lower the resistivity dramatically (bear in mind the thickness considerations discussed previously, which, if taken into account, provide even larger changes than those observed). Likewise, the concentration of donor centers is increased greatly by the implant. The usual analysis leads to the presence of two donor centers. The deeper center appearing above room temperature has an ionization energy of .179 eV, while the shallow center has an ionization energy of .030 eV. The shallow center is most likely interstitial Li ions or interstitial Zn ions or possibly both; since taking into consideration the thickness of the layer gives a higher concentration than that shown, which could then account for impurity banding. Both interstitial Li and Zn are likely to arise from the implant since Equation 7 predicts 165 displacements per Li ion in this case. The deeper donor probably is a result of the damage.

A sample identical to that described above was annealed at 900°C for two hours, and the results are shown in Figures 46 and 47. The mobility (Figure 47(a)) of this sample is considerably improved when compared to the 475°C sample (Figure 45(a)), and impurity scattering is greatly reduced presumably due to the annealing of the damage. As shown in Figure 46(a), the resistivity is very low and the sample is strongly n-type. The concentration of carriers is correspondingly increased (Figure 46(b)), and a single donor level at approximately .024 eV below the conduction band dominates. This is very similar to the level obtained in the Zn-baked sample for interstitial Li, and it is not unreasonable to attribute the center observed here to interstitial Li as well. The deeper donor appearing in the 475°C annealed sample, which had been attributed to damage centers, is apparently removed by the annealing process. If one considers the properties of the vacuum-baked substrate

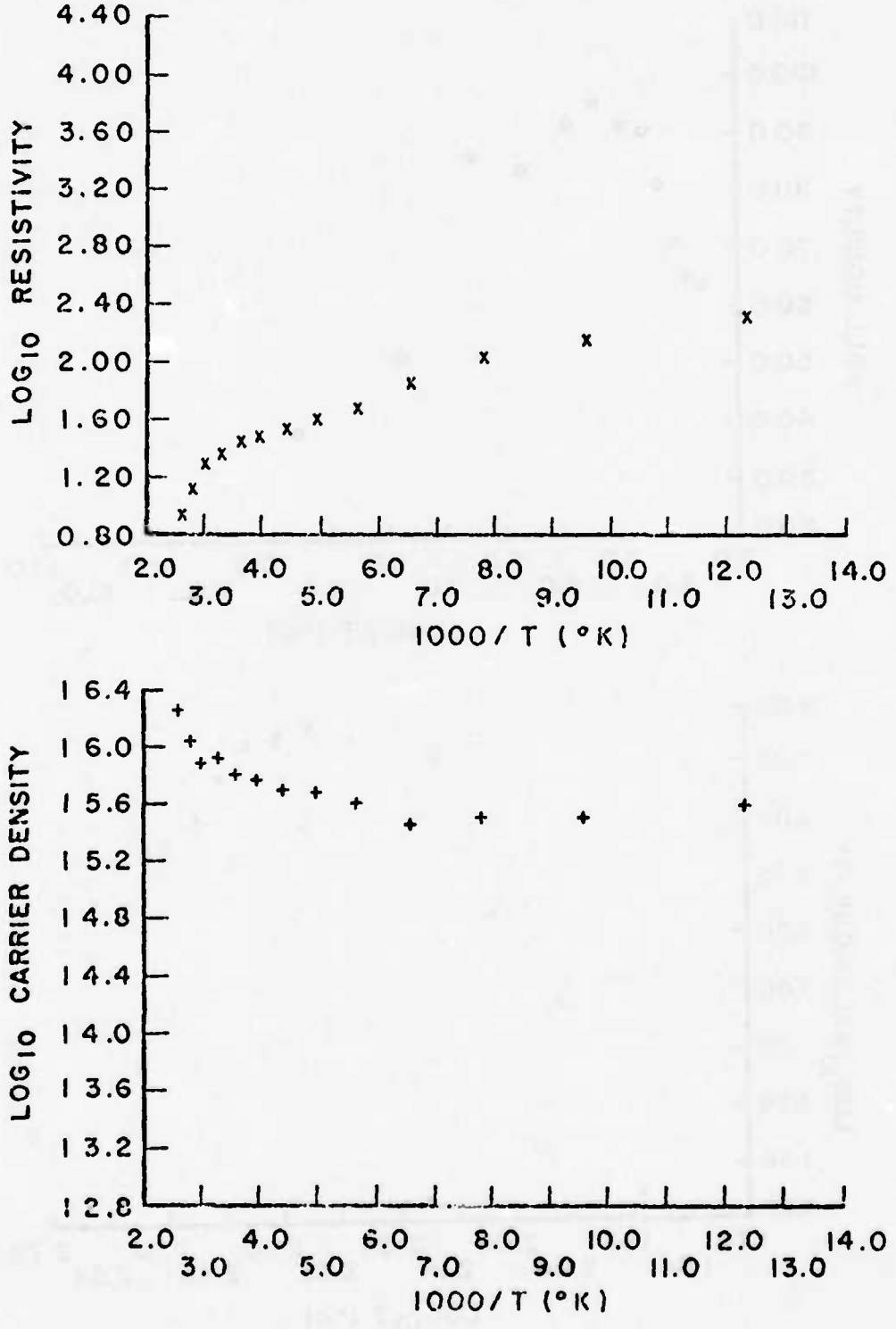

Figure 44. Resistivity and Carrier Concentration in a Hot Li Implant After a Two-Hour Anneal at 475°C

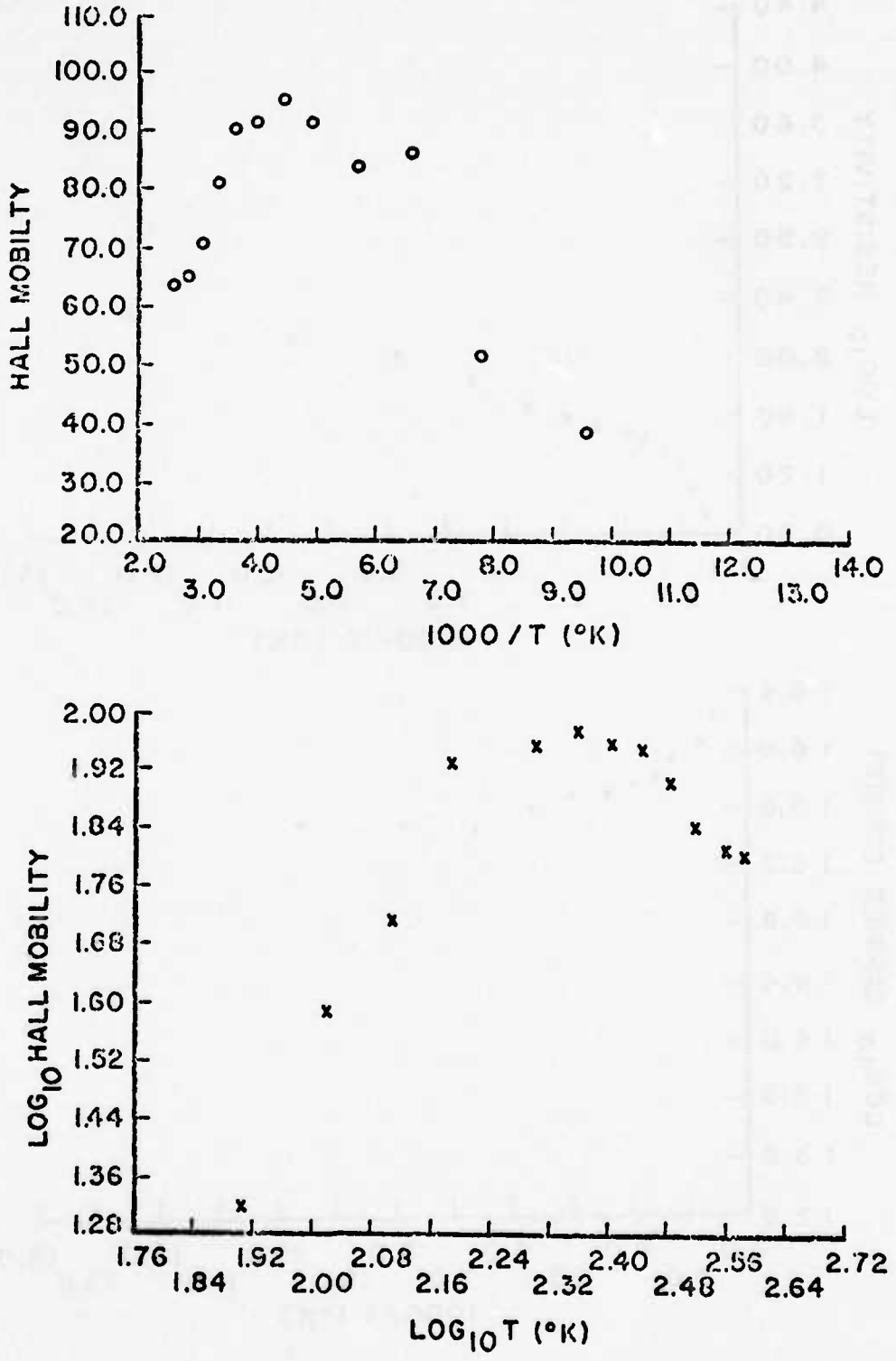

Figure 45. Hall Mobility in a Hot Li Implant After a Two-Hour Anneal at 475°C

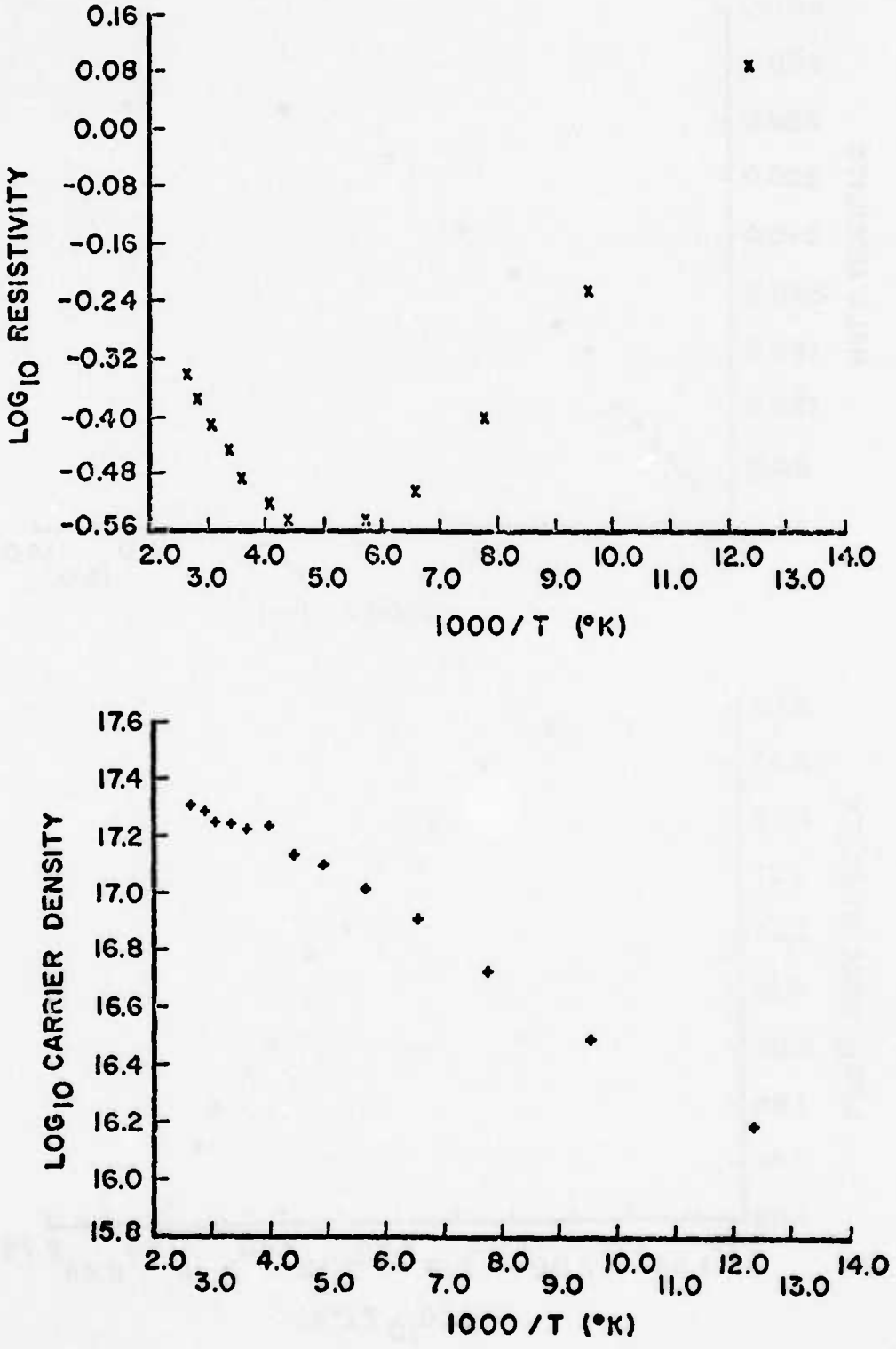

Figure 46. Resistivity and Carrier Concentration in a Hot Li Implant After a Two-Hour Anneal at 900°C

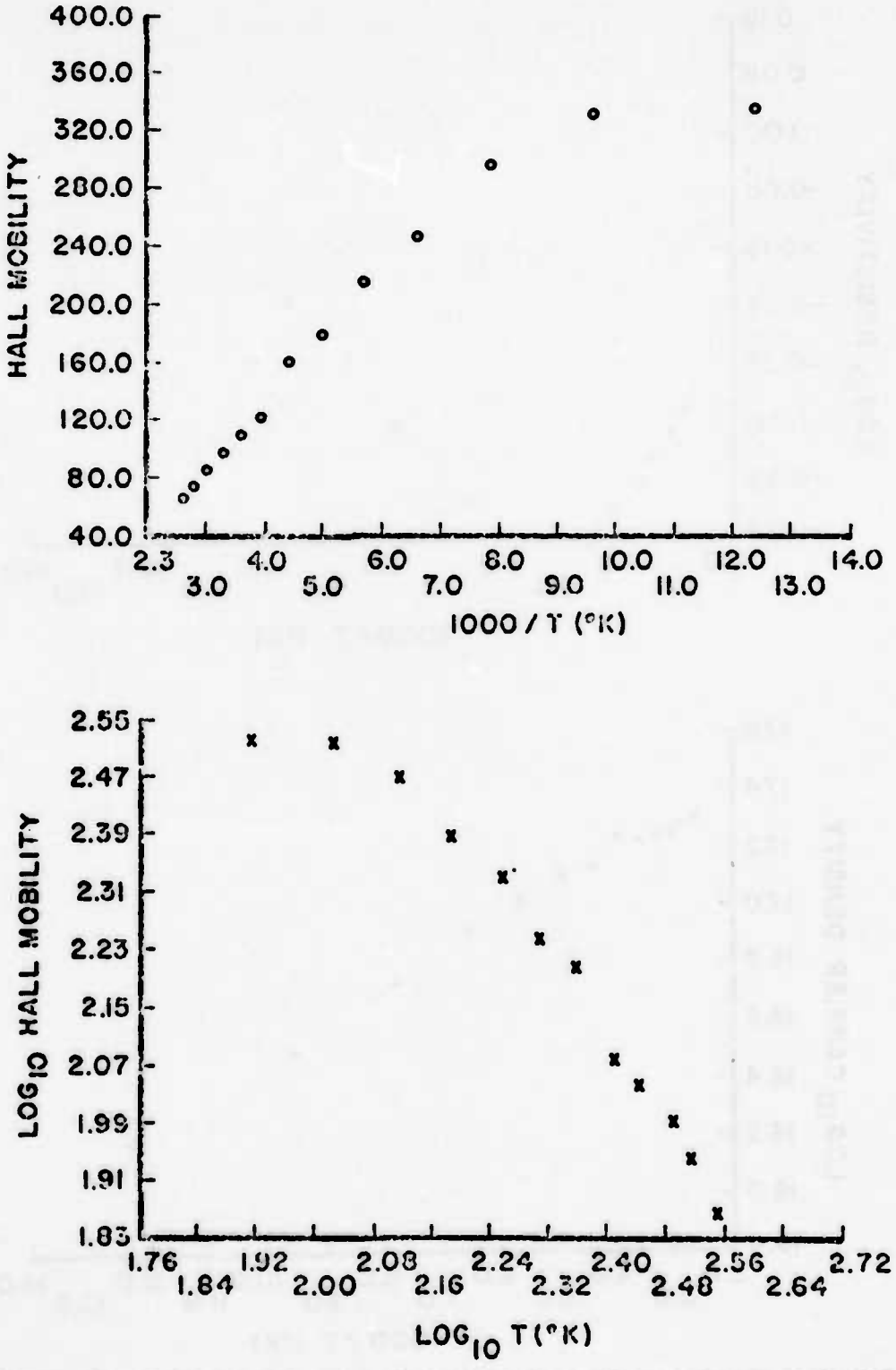

Figure 47. Hall Mobility in a Hot Li Implant After a Two-Hour Anneal at 900°C

(Figure 41) and bears in mind the thickness correction which has not been included in the data shown, then it is evident that remarkable changes in the electrical properties of the material have occurred as a result of the implant.

Data are also presented for a hot P implant (1 MeV, 1 x $10^{15}/cm^2$, 475°C substrate) in a previously vacuum-baked sample. The results obtained after an anneal for two hours at 475°C are shown in Figures 48 and 49, and the properties produced by a 900°C anneal are shown in Figures 50 and 51. Notice that the mobility is low and appears to be dominated by impurity scattering, even after the 900°C anneal (Figures 49 and 51). This is probably due to massive damage since Equation 7 gives 2100 displacements per ion in this case. The resistivity is relatively high in both samples (Figures 48 and 50), and the carrier concentration changes rapidly with temperature in the region near room temperature. A donor level of .034 eV is calculated for the sample annealed at 475°C, while a donor level of .080 eV is derived for the sample annealed at 900°C. The shallow level observed in the 475°C sample is probably associated with interstitial Zn, while the deeper level which appears subsequent to the 900°C anneal may arise as the result of formation of a complex involving the P atoms. Such a complex was postulated previously in the interpretation of the cathodoluminescence produced in an identical P implant, which had also been annealed at 900°C.

c. Photoluminescence Results

The photoluminescence system established as part of this investigation provided a means for examining the time decays of the various luminescence peaks. Such a capability was important because it was a useful adjunct to the steady state cathodoluminescence measurements. As mentioned in an earlier section, time-resolved spectra can produce a good deal of information concerning the nature of a luminescence transition.

The results of photoluminescence measurements were in general very similar to those obtained from cathodoluminescence. Due to the high absorption coefficient of ZnO for light at 3371 Å, however, it was not possible to probe the implanted layers. This resulted in a serious

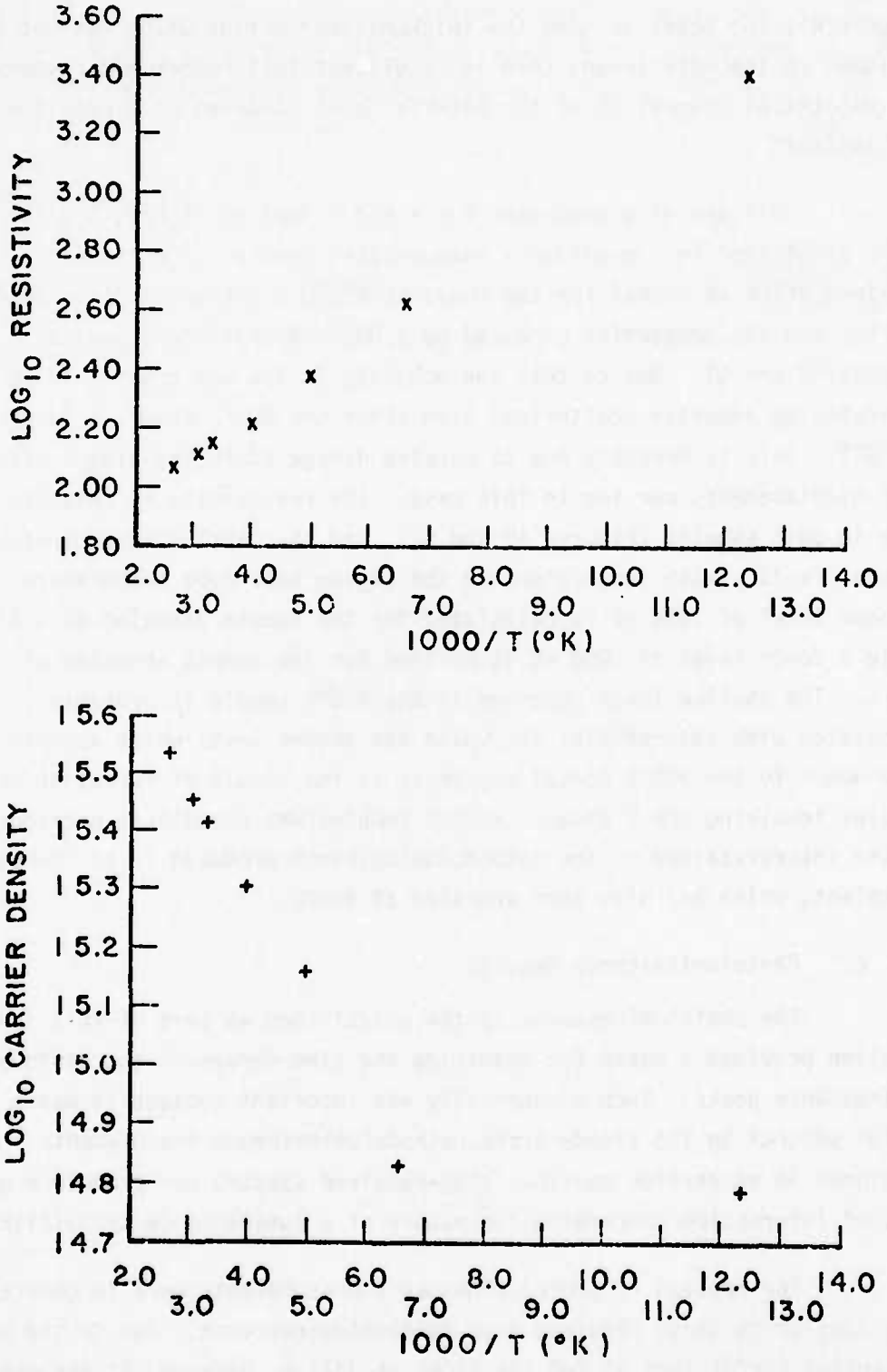

Figure 48. Resistivity and Carrier Concentration in a Hot P Implant After a Two-Hour Anneal at 475°C

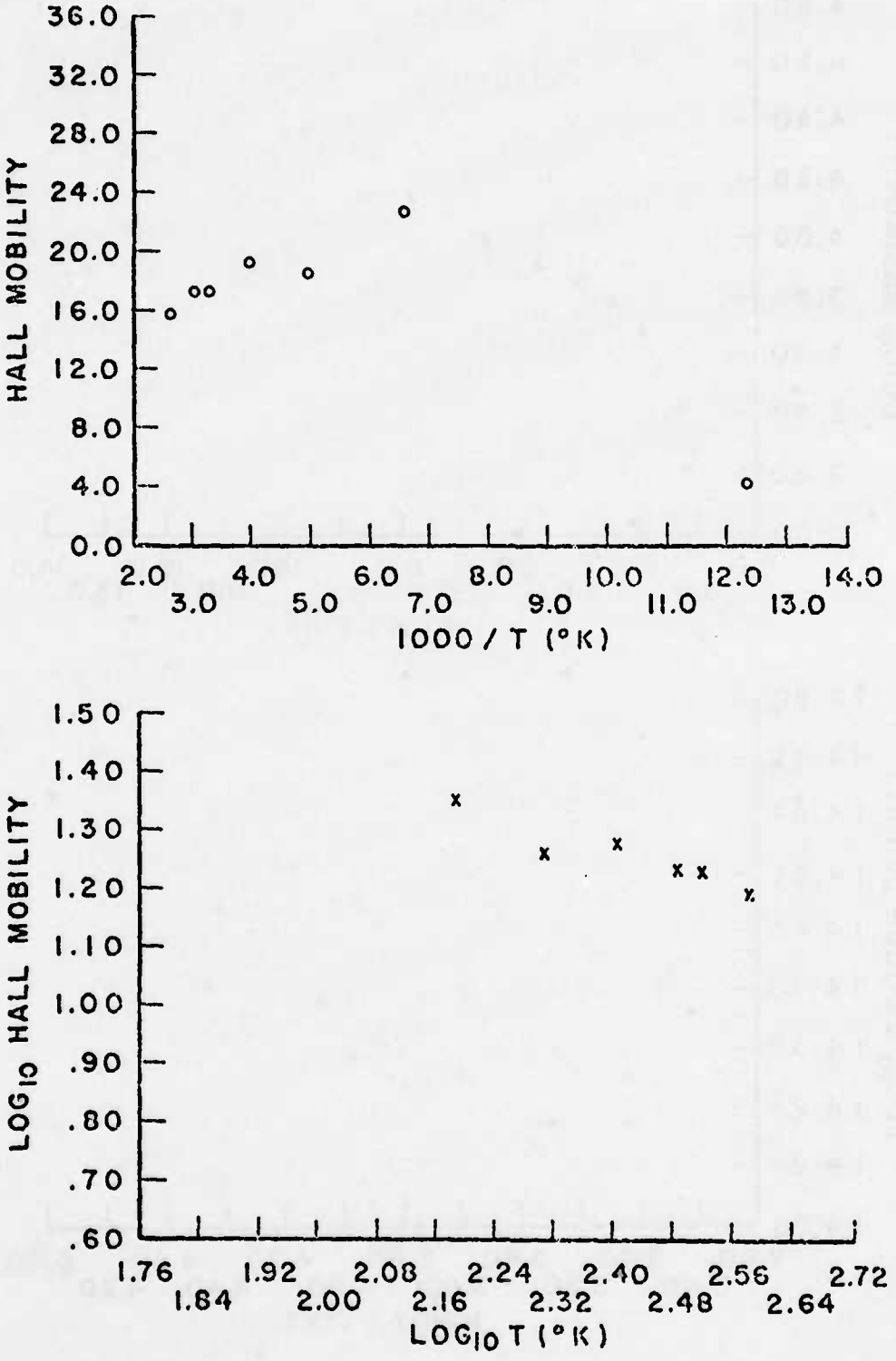

Figure 49. Hall Mobility in a Hot P Implant After a Two-Hour Anneal at 475°C

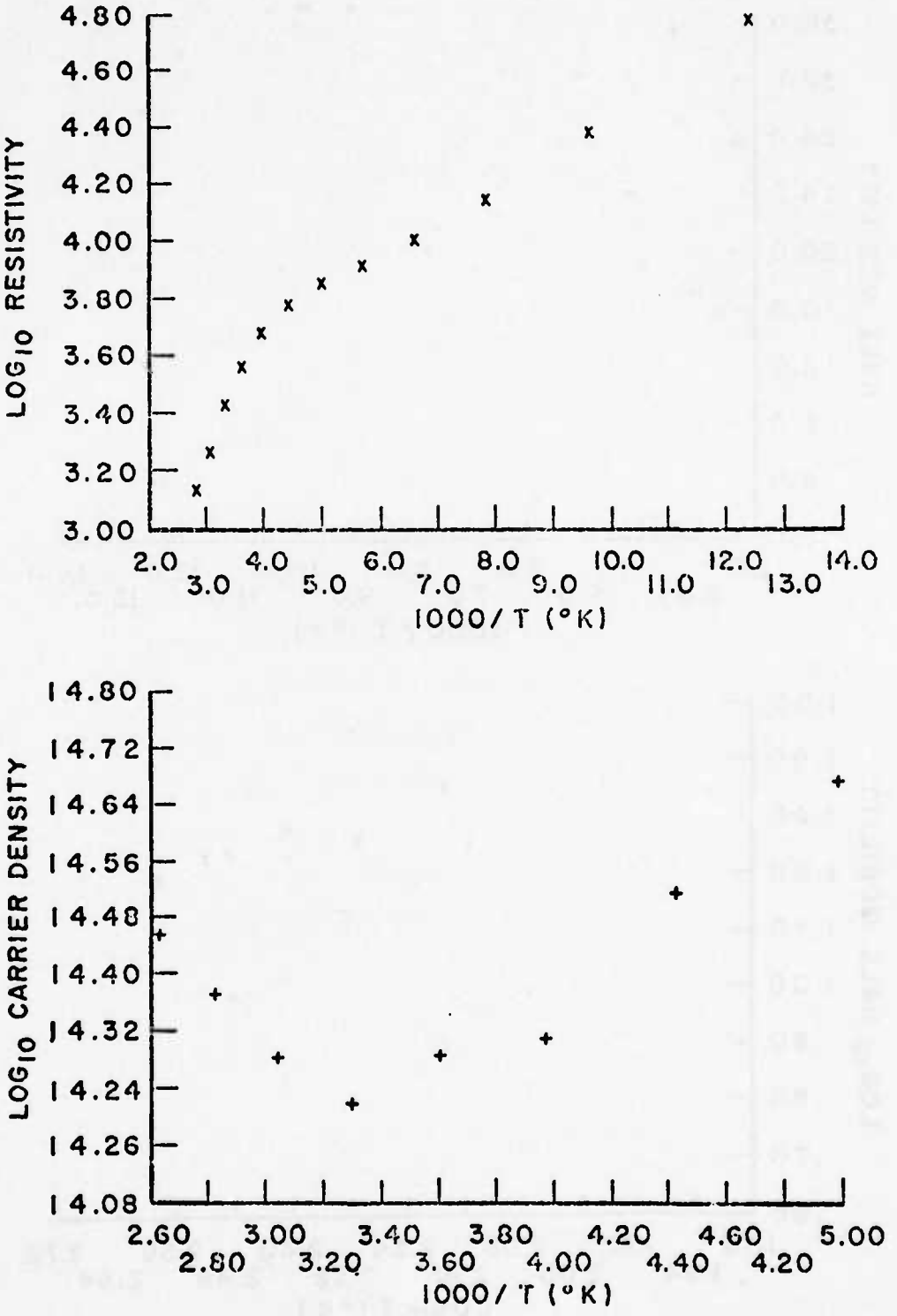

Figure 50. Resistivity and Carrier Concentration in a Hot P Implant After a Two-Hour Anneal at 900°C

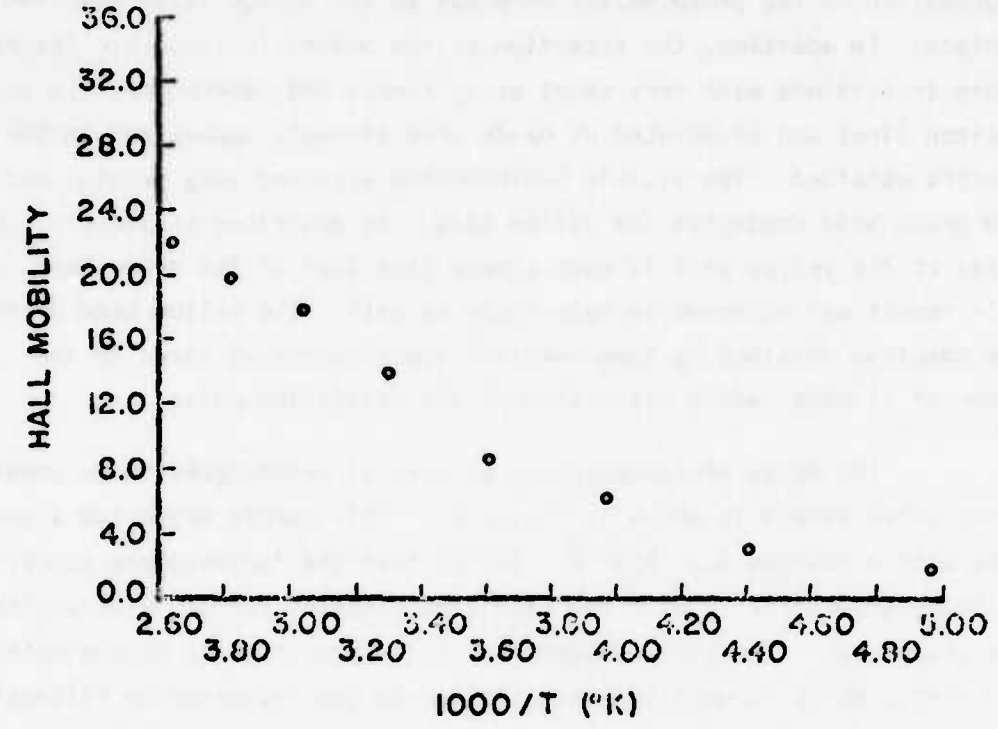

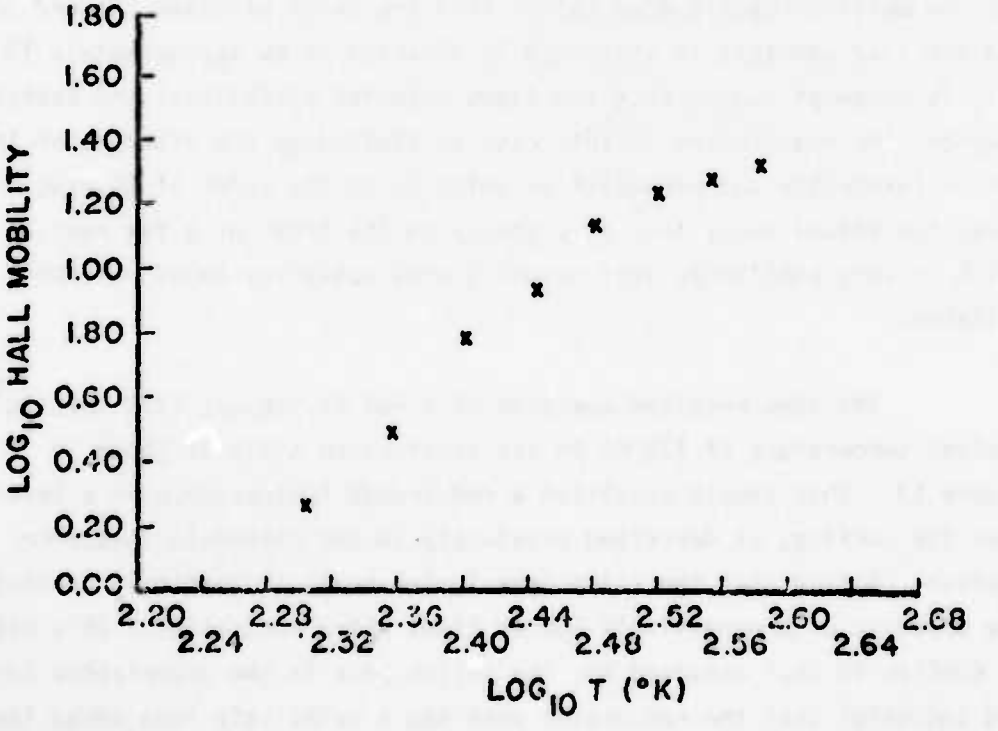

Figure 51. Hall Mobility in a Hot P Implant After a Two-Hour Anneal at 900°C

degradation of the photoluminescence due to the damage layer near the surface. In addition, the detection of the pulsed luminescence favored those transitions with very short decay times; and, therefore, the bound exciton lines and associated UV bands were strongly emphasized in the spectra obtained. The visible luminescence appeared very weakly, and the green band dominated the yellow band. As described previously, the decay of the yellow band is much slower than that of the green band, and this result was observed in this study as well. The yellow band dominated the spectrum obtained by time-resolved spectroscopy at times on the order of .1 msec. after extinction of the excitation pulse.

The decay of luminescence at several wavelengths in an unbaked, unimplanted sample is shown in Figure 52. This sample exhibited a green peak with a maximum near 5000 Å. Notice that the luminescence appears to decay exponentially with the same time constant for all wavelengths of the green peak. The time constant for this transition is approximately 100 nsec., which is qualitatively similar to that observed by Filinski and Skettrup (Reference 94). It is evident that the phonon-assisted bound exciton emission decays much faster than the green emission (Figure 52), and the time constant in this case is observed to be approximately 18 nsec. This is somewhat longer than the times observed by Filinski and Skettrup, however, the measurement in this case is limited by the risetime of the boxcar integrator and preamplifier which is on the order of 20 nsec. Thus, the actual decay time is probably on the order of a few nsec., which is very similar to that observed previously for bound exciton emission.

The time-resolved spectrum of a hot Li implant (275 keV, $10^{15}/cm^2$, implant temperature of 475°C) in its as-received state is shown in Figure 53. This sample exhibited a red-orange luminescence in a layer near the surface, as described previously in the cathodoluminescence section. Notice that the red-orange luminescence increasingly dominates the spectrum at progressively longer times after excitation. This behavior is similar to that observed for the yellow peak in the unimplanted sample and indicates that the red-orange peak has a relatively long decay time.

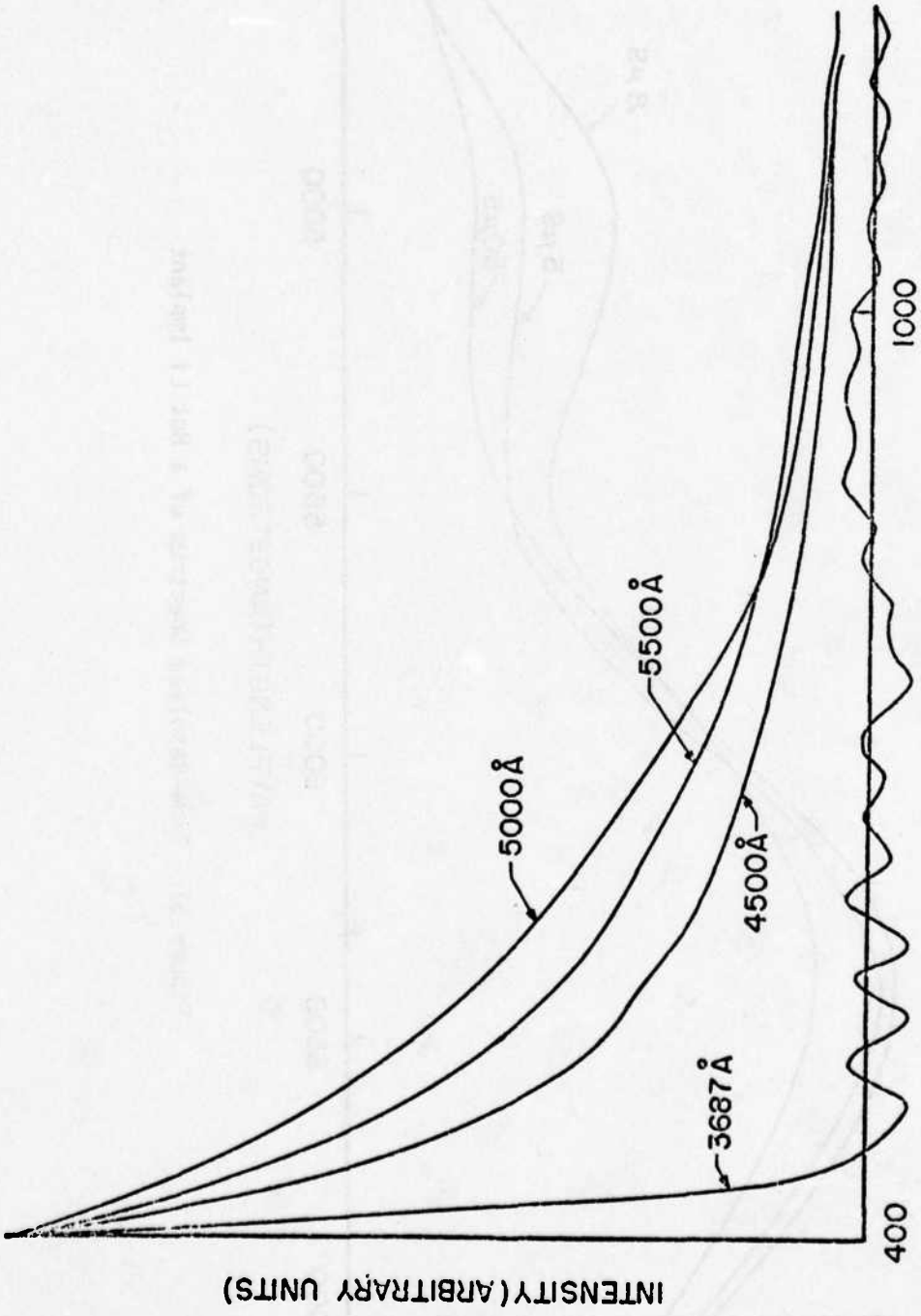

Figure 52. Decays of Photoluminescence at Various Wavelengths in an Unimplanted, Unannealed Sample

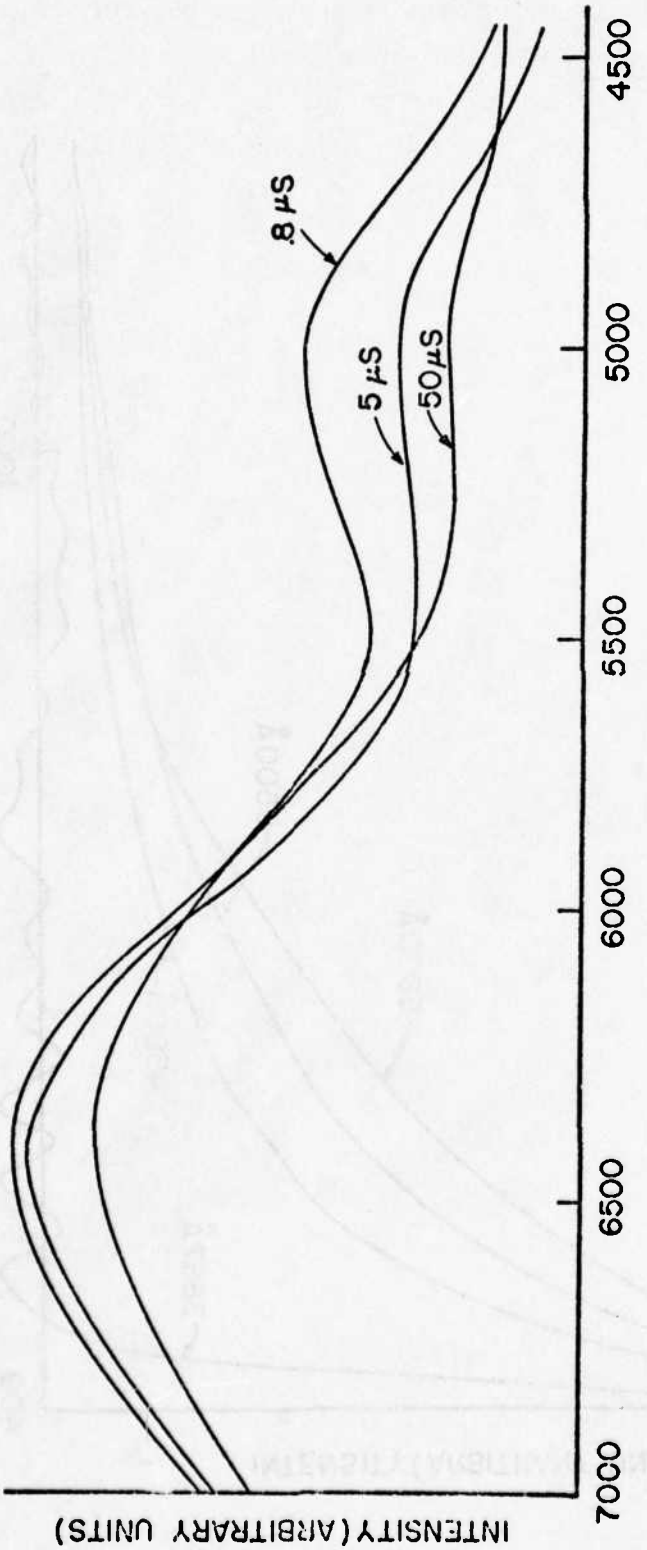

Figure 53. Time-Resolved Spectrum of a Hot Li Implant

Variable temperature luminescence was obtained from a variety of baked and unbaked samples of ZnO using the photoluminescence system. In all cases the ultraviolet luminescence of these samples exhibited the same spectra as those obtained previously using cathodoluminescence. No significant changes were induced in the spectra by varying the intensity of the excitation with neutral density filters.

d. Summary of Results

The significant results obtained from this study of Li, Na, N, P, and Ne implants in ZnO were:

(1) A discolored layer is produced near the surface of the implanted samples, and the degree of discoloration becomes stronger as the dose is increased.

(2) All implanted samples exhibit a previously unobserved series of phonon-coupled peaks in the violet region of the spectrum. This series appears very strongly in RT implants of Li and Ne which have been annealed at 475°C for two hours and appears very weakly in hot implants and implants of P. The series of violet peaks appears to be shifted approximately 10 Å toward longer wavelengths in samples which have been implanted with P.

(3) Samples which have been implanted with a low dose ($<10^{13}/cm^2$) of Li exhibit a large number of new lines in the region near 3690 Å, and such an implant also produces new structure near 3770 Å. Implants of P show a new peak near 3693 Å.

(4) All hot implants into previously vacuum-baked substrates exhibit a peak near 6500 Å immediately after implantation. This red peak is removed from the spectrum after a subsequent anneal for two hours at 900°C.

(5) A shallow donor level (E_d = .024 eV) is observed in hot implants of Li which have been subsequently annealed at 900°C for two hours. In comparison, a hot P implant which has undergone a similar annealing treatment exhibits a somewhat deeper donor center (.080 eV).

(6) The decay time of the red-orange peak near 6500 Å in a hot Li implant is long compared to that of the green peak. In an unimplanted sample the entire green peak decays with a single time constant of approximately 100 nanoseconds, and the decay time of the ultraviolet peaks is on the order of a few nsec.

SECTION V

CONCLUSIONS AND RECOMMENDATIONS

The results of this study have led to a number of conclusions, which are based on a plausible series of arguments discussed in the previous section. Further work would be required to provide more positive proof of all of these assertions. One conclusion seems clear, however, and that concerns the utility of cathodoluminescence as a means of investigating implanted layers. It is apparent from the results achieved that cathodoluminescence provides a method which is very useful for probing implanted layers in luminescent materials. The semiquantitative technique may be scaled for any substrate material, and the energetic electrons will excite any luminescent substrate, regardless of its bandgap. Since the luminescence is a sensitive indicator of impurity content and the extent of damage, the method described herein can be one of great utility.

1. CONCLUSIONS

Based upon the analysis of the results as presented in the preceding section the following conclusions have been reached concerning the properties of ion implanted layers in ZnO substrates:

(1) Optical evidence of a shallow acceptor center has been seen in ZnO for the first time, and since the violet bands appear in all implanted samples to some degree it may be concluded that the acceptor center is induced by damage. The shallow acceptor may be a complex involving Li, however, since Li was present in all samples.

(2) Further evidence of complexes involving Li is observed in samples implanted with Li, which have an increased number of sharp, bound exciton lines believed to be produced by associated donor-acceptor pairs. These samples also exhibit sharp structure near 3770 Å which may be produced by excitons bound to acceptor centers.

(3) Phosphorus implants lead to the formation of a donor complex upon annealing. This is evidenced by the appearance of a unique luminescence line in the region of peaks due to excitons bound to neutral donors. In addition, the violet bands shift toward longer wavelength (as they would be expected to do if they are donor-acceptor pair bands and if the donor involved in the luminescence is exchanged for one with higher ionization energy). This is also supported by the electrical measurements which show evidence of a deeper donor in phosphorus implanted samples.

(4) A new luminescence peak is observed near 6500 Å in all hot (475°C) implants; and since it is removed from the spectrum by a subsequent anneal at 900°C for two hours, it has been attributed to the formation of a damage center. Time-resolved measurements show that this peak has a much longer decay time than the characteristic green ZnO emission peak indicating a different recombination mechanism (possibly donor-acceptor pairs involving a deep center).

2. RECOMMENDATIONS

Several of the conclusions reached in the foregoing section are new assertions based upon results obtained from ZnO for the first time because of the unique nature of the ion implantation process. Further study is required to investigate these assertions in detail, and the following recommendations are made concerning an approach to further work in this area:

(1) Provide the capability to pulse the electron beam in the cathodoluminescence system so that time-resolved techniques may be used to examine the spectra obtained at various depths within the sample.

(2) Examine the violet luminescence bands created by implantation in detail-using time-resolved spectroscopy and variable excitation intensity to determine whether or not these peaks are a result of donor-acceptor pair recombination.

(3) Develop a technique for etching ZnO to remove a layer of prescribed thickness, and use this technique in conjunction with various measurements to profile the implants more carefully.

(4) Evaluate Si_3N_4 as an alternative to SiO_2 in protecting the implanted layers during annealing.

(5) Investigate the red peak using polarization, time-resolved spectroscopy, and variable intensity to provide a better indication of the type of center and the luminescence mechanism which produces the peak.

(6) Use a two-meter instrument to examine the bound exciton emission with more care and, if possible, determine correlations between specific lines and the particular impurities or native defects responsible for the lines.

APPENDIX A

PENETRATION OF VARIOUS IONS IN ZnO

LITHIUM

KEV	PR RANGE	DELTA	HALF	ONE	FOUR	E NUCLEAR
20.	828.7	386.4	456.0	828.9	1657.8	8.0
25.	1034.6	479.3	565.5	1028.0	2096.1	9.1
30.	1237.0	544.8	642.9	1168.5	2337.2	10.0
35.	1435.7	600.2	708.3	1287.5	2375.1	10.8
40.	1830.4	649.2	766.0	1392.5	2384.9	11.4
45.	1821.1	693.1	617.8	1486.5	2973.3	12.1
50.	2007.9	732.9	364.8	1572.0	3144.1	12.6
55.	2191.0	769.3	907.7	1650.1	3300.2	13.1
60.	2370.4	802.7	947.2	1721.3	3263.7	13.6
65.	2546.4	833.6	983.7	1788.1	3576.2	14.0
70.	2719.2	582.3	1017.5	1849.6	3599.3	14.4
75.	2888.9	889.0	1049.0	1906.9	3813.9	14.7
80.	3055.7	914.0	1078.5	1960.5	3921.0	15.1
85.	3219.7	937.4	1105.1	2010.7	4021.3	15.4
90.	3381.0	859.3	1132.0	2057.8	4115.6	15.7
95.	3539.7	980.1	1156.5	2102.2	4204.4	16.0
100.	3696.0	999.6	1179.5	2144.1	4288.3	16.2
105.	3850.0	1018.1	1201.3	2183.8	4367.6	16.5
110.	4001.7	1035.6	1222.0	2221.4	4442.7	16.7
115.	4151.2	1052.2	1241.6	2257.0	4514.1	16.9
120.	4298.6	1068.0	1260.3	2291.0	4581.9	17.1
125.	4444.1	1083.1	1278.1	2323.3	4646.5	17.4
130.	4587.6	1097.5	1295.0	2354.1	4708.2	17.5
135.	4729.3	1111.2	1311.2	2383.5	4767.0	17.7
140.	4869.2	1124.3	1326.7	2411.7	4823.4	17.9
145.	5007.4	1136.9	1341.5	2438.6	4877.3	18.1
150.	5143.9	1148.9	1355.8	2464.5	4929.0	18.2
175.	5803.3	1202.5	1418.9	2579.3	5158.6	19.0
200.	6428.5	1247.0	1471.5	2674.9	5349.8	19.6

LITHIUM (CONT'D)

KEV	PR RANGE	DELTA	HALF	ONE	FOUR	E NUCLEAR
225.	7024.1	1284.9	1516.1	2756.0	5512.1	20.1
250.	7593.8	1317.5	1554.6	2826.0	5652.0	20.6
275.	8140.8	1345.9	1588.2	2887.1	5774.1	21.0
300.	8657.5	1371.1	1617.9	2841.0	5881.9	21.4
325.	9176.0	1393.5	1644.3	2989.0	5978.0	21.7
350.	9668.0	1413.6	1668.0	3032.1	6064.1	22.0
375.	10145.0	1431.7	1689.4	3071.0	6142.0	22.3
400.	10808.3	1448.2	1708.9	3106.4	6212.8	22.5
425.	11058.9	1463.3	1726.7	3138.8	6277.5	22.8
450.	11497.9	1477.2	1743.0	3168.5	6337.0	23.0
475.	11926.1	1489.9	1758.1	3195.9	6391.8	23.2
500.	12344.3	1501.8	1772.1	3221.3	6442.6	23.4
525.	12753.1	1512.8	1785.1	3244.9	6489.8	23.5
550.	13153.0	1523.0	1797.2	3266.9	6533.8	23.7
575.	13544.9	1531.5	1807.2	3285.1	6570.3	23.9
600.	13929.0	1539.6	1816.7	3302.3	6604.7	24.0
625.	14305.8	1547.1	1825.6	3318.6	6637.2	24.1
650.	14675.7	1554.3	1831.1	3334.0	6667.9	24.3
675.	15039.0	1561.1	1842.1	3348.5	6697.0	24.4
700.	15396.0	1567.5	1849.7	3392.4	6724.7	24.5
725.	15747.2	1573.7	1856.9	3375.5	6751.0	24.6
750.	16082.7	1579.5	1863.8	3366.0	6776.1	24.8
875.	17743.9	1607.3	1896.6	3447.7	6895.4	25.2
1000.	19286.5	1629.6	1923.0	3495.5	5991.1	25.6
1125.	20739.4	1648.0	1944.7	3535.0	7070.0	26.0

SODIUM

M2	M1	Z1	Z2	ND	RK	EK
46.85	22.99	11.00	19.00	.7279E-01	.2722E+03	.3006E
5.	61.0	0.0	0.0	0.0	0.0	4.2 0

SODIUM (CONT'D)

KEV	PR RANGE	DELTA	HALF	ONE	FOUR	E NUCLEAR	
10.	110.3	54.5	64.3	116.9	233.8	8.4	112
15.	159.6	78.4	92.5	168.2	336.3	12.4	162
20.	209.8	101.9	120.2	218.5	437.0	16.2	214
25.	260.9	124.7	147.1	267.4	534.9	19.9	266
30.	313.0	146.9	173.4	315.2	630.3	23.5	320
35.	365.9	168.7	199.0	361.8	723.6	26.9	374
40.	419.5	189.9	224.1	407.4	814.8	30.2	428
45.	473.8	210.7	248.7	452.0	904.1	33.5	483
50.	528.8	231.1	272.7	495.8	991.5	36.6	539
55.	584.2	251.1	293.6	538.6	1077.2	39.6	594
60.	640.2	270.7	319.4	580.6	1161.1	42.5	651
65.	696.6	289.8	342.0	621.7	1243.4	45.4	707
70.	753.3	308.6	364.2	662.0	1324.1	48.1	764
75.	810.4	327.1	386.0	701.6	1403.2	50.8	821
80.	867.7	345.2	407.3	740.4	1480.7	53.4	878
85.	925.3	362.9	428.2	778.4	1556.8	55.9	935
90.	983.1	380.3	448.8	815.7	1631.5	58.4	992
95.	1041.1	397.4	468.9	852.4	1704.7	60.3	1050
100.	1099.2	414.1	488.7	888.3	1776.6	63.1	1107
105.	1157.4	430.6	508.1	923.6	1847.2	65.4	1165
110.	1215.8	446.7	527.1	958.2	1916.4	67.6	1222
115.	1274.2	462.6	545.8	992.2	1984.4	69.8	1280
120.	1332.6	478.1	564.2	1025.6	2051.2	71.9	1338
125.	1391.1	493.4	582.2	1058.4	2116.7	74.0	1395
130.	1449.7	508.4	599.9	1090.6	2181.1	76.0	1453
135.	1508.2	523.2	617.3	1122.2	2244.4	78.0	1511
140.	1566.7	537.7	634.4	1153.3	2306.5	79.9	1568
145.	1625.2	551.9	651.2	1183.8	2367.6	81.8	1626
150.	1683.7	565.9	667.7	1213.8	2427.6	83.6	1683
175.	1975.0	632.3	746.2	1356.4	2712.7	92.3	1969
200.	2264.2	693.5	818.4	1487.6	2975.2	100.1	2253
225.	2550.4	750.1	885.1	1608.9	3217.7	107.3	2533
250.	2833.3	802.5	946.9	1721.3	3442.6	113.8	2810

SODIUM (CONT'D)

KEV	PR RANGE	DELTA	HALF	ONE	FOUR	E NUCLEAR	
275.	3112.6	851.2	1004.4	1825.9	3651.7	119.9	3084
300.	3388.2	896.7	1058.1	1923.4	3846.9	125.5	3354
325.	3660.0	939.3	1108.3	2014.7	4029.4	130.7	3621
350.	3928.1	979.2	1155.5	2100.4	4200.8	135.6	3883
375.	4192.6	1016.8	1199.8	2181.0	4362.0	140.2	4143
400.	4453.5	1052.2	1241.6	2257.0	4514.0	144.5	4399
425.	4710.9	1085.7	1281.1	2328.9	4657.7	148.5	4652
450.	4964.9	1117.4	1318.6	2396.9	4793.8	152.4	4902
475.	5215.7	1147.5	1354.1	2461.4	4922.8	156.0	5148
500.	5463.2	1176.1	1387.8	2522.7	5045.4	159.4	5392
525.	5707.6	1203.3	1419.9	2581.0	5162.1	162.7	5632
550.	5949.0	1229.2	1450.5	2636.6	5273.3	165.8	5870
575.	6187.4	1253.9	1479.6	2689.7	5379.4	168.8	6105
600.	6423.0	1277.6	1507.5	2740.4	5480.7	171.6	6338
625.	6655.7	1300.2	1534.2	2788.9	5577.7	174.4	6567
650.	6885.8	1321.8	1559.8	2835.3	5670.7	177.0	6794
675.	7113.3	1342.6	1584.3	2879.9	5759.7	179.5	7019
700.	7338.2	1362.5	1607.8	2922.6	5845.3	181.9	7241
725.	7560.6	1381.7	1630.4	2963.7	5927.5	184.2	7461
750.	7780.6	1400.1	1652.1	3003.2	6006.5	186.4	7678
875.	8847.0	1482.6	1749.4	3180.1	6360.3	196.5	8734
1000.	9862.4	1552.1	1831.5	3329.3	6658.7	205.1	9740
1125.	10833.2	1611.7	1901.9	3457.2	6914.4	212.5	10703

NITROGEN

M2	M1	Z1	Z2	ND	RK	EK
46.85	14.01	7.00	19.00	.7279E-01	.3031E+03	.5735E-
5.	83.8	0.0	0.0	0.0	0.0	3.5 0.
10.	155.7	0.0	0.0	0.0	0.0	6.5 0.

NITROGEN (CONT'D)

KEV	PR RANGE	DELTA	HALF	ONE	FOUR	E NUCLEAR	
15.	227.4	117.1	138.2	251.1	502.3	9.2	231
20.	298.9	147.4	173.9	316.1	632.2	11.5	303
25.	370.2	174.7	206.2	374.8	749.5	13.6	374
30.	441.4	199.8	235.8	428.7	857.3	15.5	444
35.	511.5	223.1	263.3	478.5	957.1	17.2	514
40.	581.3	244.7	288.8	524.9	1049.9	18.8	583
45.	650.4	264.9	312.6	568.3	1136.6	20.3	651
50.	719.0	283.9	335.0	608.9	1217.8	21.7	718
55.	786.8	301.7	356.0	647.1	1294.3	23.0	784
60.	853.9	318.5	375.8	683.2	1366.3	24.2	850
65.	920.4	334.4	394.6	717.2	1434.4	25.3	915
70.	986.1	349.4	412.3	749.5	1499.0	26.4	980
75.	1051.1	363.7	429.2	780.1	1560.2	27.4	1043
80.	1115.5	377.3	445.2	809.2	1618.5	28.4	1106
85.	1179.1	390.2	460.4	837.0	1673.9	29.3	1168
90.	1242.1	402.5	475.0	863.4	1726.9	30.1	1230
95.	1304.4	414.3	488.9	888.7	1777.4	30.9	1291
100.	1366.0	425.6	502.2	912.9	1825.8	31.7	1351
105.	1427.0	436.4	514.9	936.1	1872.1	32.5	1411
110.	1487.4	446.8	527.2	958.3	1916.6	33.2	1470
115.	1547.2	456.7	538.9	979.6	1959.2	33.9	1528
120.	1606.4	466.3	550.2	1000.1	2000.3	34.5	1586
125.	1664.9	475.5	561.0	1019.9	2039.7	35.2	1644
130.	1723.0	484.3	571.5	1038.9	2077.8	35.8	1701
135.	1780.4	492.9	581.6	1057.2	2114.4	36.4	1757
140.	1837.3	501.1	591.3	1074.9	2149.8	37.0	1813
145.	1893.7	509.1	600.7	1092.0	2183.9	37.5	1868
150.	1949.6	518.8	609.8	1108.5	2217.0	38.0	1923
175.	2221.5	551.7	651.0	1183.4	2366.9	40.5	2190
200.	2482.2	581.8	686.5	1247.9	2495.9	42.6	2446
225.	2733.0	608.0	717.5	1304.2	2608.5	44.5	2693
250.	2974.9	631.2	744.8	1353.9	2707.9	46.1	2932

NITROGEN (CONT'D)

KEV	PR RANGE	DELTA	HALF	ONE	FOUR	E NUCLEAR	
275.	3208.8	651.8	789.2	1398.2	2796.4	47.6	3163
300.	3435.3	670.4	791.0	1437.9	2875.9	48.9	3387
325.	3655.2	687.1	810.8	1473.9	2947.7	50.1	3804
350.	3868.9	702.4	828.8	1506.6	3013.1	51.2	3816
375.	4076.9	716.3	845.2	1536.5	3072.9	52.3	4022
400.	4279.7	729.1	860.3	1563.9	3127.9	53.2	4223
425.	4477.6	740.9	874.3	1589.3	3178.6	54.1	4420
450.	4671.0	751.9	887.2	1612.8	3225.5	54.9	4612
475.	4860.1	762.1	899.2	1634.6	3269.2	55.7	4800
500.	5045.2	771.6	910.4	1655.0	3310.0	56.4	4984
525.	5226.6	780.4	920.9	1674.0	3348.1	57.1	5164
550.	5404.4	788.8	930.7	1691.9	3383.8	57.7	5341
575.	5578.9	796.6	940.0	1708.7	3417.4	58.3	5515
600.	5750.2	804.0	948.7	1724.5	3449.1	58.9	5685
625.	5918.5	811.0	956.9	1739.5	3479.0	59.5	5853
650.	6083.9	817.6	964.7	1753.7	3507.3	60.0	6018
675.	6246.7	823.8	972.1	1767.1	3534.2	60.5	6180
700.	6406.9	829.8	979.1	1779.8	3559.7	61.0	6339
725.	6564.5	835.4	985.5	1792.0	3583.9	61.4	6497
750.	6719.9	840.8	992.2	1803.5	3607.1	61.9	6651
875.	7464.5	864.3	1019.9	1854.0	3708.0	63.8	7394
1000.	8162.3	883.5	1042.5	1895.0	3790.0	65.5	8092
1125.	8822.5	899.4	1061.3	1929.3	3858.6	66.9	8751
1250.	9449.2	913.0	1077.3	1958.4	3918.7	68.1	

PHOSPHORUS

M2	M1	Z1	Z2	ND	RK	EK
46.85	30.97	15.00	19.00	.7279E-01	.2745E+03	.1891E-

KEV	PR RANGE	DELTA	HALF	ONE	FOUR	E NUCLEAR	
5.	47.5	13.5	16.0	29.0	58.1	4.1	47
10.	84.2	34.3	40.5	73.6	147.2	8.4	84
15.	119.2	50.8	60.0	109.0	218.0	12.6	120
20.	154.0	66.1	78.1	141.9	283.8	16.7	155

PHOSPHORUS (CONT'D)

KEV	PR RANGE	DELTA	HALF	ONE	FOUR	E NUCLEAR	
25.	188.9	80.9	95.5	173.5	347.0	20.7	191
30.	224.1	95.3	112.4	204.4	408.8	24.6	227
35.	259.7	109.4	129.1	234.7	469.3	28.4	263
40.	295.5	123.3	145.4	264.4	528.8	32.1	300
45.	331.8	136.9	161.5	293.7	587.3	35.7	337
50.	368.3	150.3	177.4	322.5	645.0	39.2	374
55.	405.2	163.6	193.0	350.9	701.8	42.7	412
60.	442.3	176.6	208.4	378.9	757.8	46.1	449
65.	479.8	189.5	223.6	406.5	813.1	49.4	487
70.	517.5	202.2	238.6	433.8	867.5	52.7	525
75.	555.4	214.7	253.4	460.6	921.3	55.9	564
80.	593.6	227.1	268.0	487.1	974.3	59.0	602
85.	632.0	239.3	282.4	513.3	1026.6	62.1	641
90.	670.6	251.3	296.6	539.1	1078.2	65.1	679
95.	709.3	263.2	310.6	564.6	1129.1	68.1	718
100.	748.2	274.9	324.4	589.7	1179.4	71.0	757
105.	787.3	286.5	338.0	614.5	1229.0	73.9	796
110.	826.5	297.9	351.5	639.0	1277.9	76.7	835
115.	865.8	309.1	364.8	663.1	1326.2	79.4	875
120.	905.3	320.3	377.9	687.0	1374.0	82.1	914
125.	944.8	331.2	390.9	710.5	1421.1	84.8	954
130.	984.5	342.1	403.7	733.8	1467.6	87.4	993
135.	1024.2	352.8	416.3	756.7	1513.5	90.0	1033
140.	1064.0	363.4	428.8	779.4	1558.8	92.5	1072
145.	1103.9	373.8	441.1	801.8	1603.6	95.0	1112
150.	1143.8	384.1	453.3	823.9	1647.8	97.5	1151
175.	1344.2	433.8	511.9	930.4	1860.9	109.2	1350
200.	1545.0	480.5	567.0	1030.7	2061.5	120.0	1549
225.	1745.8	524.6	619.0	1125.3	2250.6	130.0	1747
250.	1946.1	566.2	668.2	1214.6	2429.1	139.4	1944
275.	2145.4	605.6	714.6	1299.0	2598.1	148.3	2141
300.	2343.7	642.9	758.6	1379.0	2758.1	156.5	2336
325.	2540.6	678.3	800.4	1454.9	2909.9	164.3	2529

PHOSPHORUS (CONT'D)

KEV	PR RANGE	DELTA	HALF	ONE	FOUR	E NUCLEAR	
350.	2736.0	711.9	840.1	1527.0	3054.1	171.7	2722
375.	2929.9	743.9	877.8	1595.7	3191.3	178.7	2912
400.	3122.1	774.4	913.8	1661.1	3322.1	185.3	3101
425.	3312.6	803.5	948.1	1723.4	3446.9	191.6	3289
450.	3501.4	831.3	980.9	1783.0	3566.1	197.6	3474
475.	3688.5	857.8	1012.2	1840.1	3680.1	203.4	3659
500.	3873.8	883.3	1042.3	1894.7	3789.3	208.8	3841
525.	4057.4	907.7	1071.1	1947.0	3894.0	214.1	4022
550.	4239.3	931.1	1098.7	1997.3	3994.6	219.1	4201
575.	4419.6	953.7	1125.3	2045.6	4091.2	224.0	4378
600.	4598.2	975.3	1150.9	2092.1	4184.1	228.6	4554
625.	4775.2	996.2	1175.5	2136.8	4273.6	233.1	4728
650.	4950.6	1016.3	1199.2	2179.9	4359.9	237.4	4901
675.	5124.5	1035.7	1222.1	2221.6	4443.1	241.6	5073
700.	5296.9	1054.4	1244.2	2261.7	4523.4	245.6	5242
725.	5467.7	1072.5	1265.6	2300.5	4601.0	249.5	5411
750.	5637.1	1090.0	1286.2	2338.0	4676.1	253.2	5578
875.	6463.0	1169.4	1379.9	2508.3	5016.7	270.3	6394
1000.	7256.1	1237.7	1460.5	2654.8	5309.7	285.1	7178
1125.	8019.6	1297.2	1530.7	2782.5	5565.1	298.0	7933
1250.	8756.1	1349.7	1582.6	2895.1	5790.2	309.5	

NEON

M2	M1	Z1	Z2	ND	RK		EK
46.85	20.18	10.00	19.00	.7279E-01	.2785E+03		.3489E
5.	162.8	0.0	0.0	0.0	0.0	4.0	0
KEV	PR RANGE	DELTA	HALF	ONE	FOUR	E NUCLEAR	
10.	158.8	53.3	62.9	114.4	228.7	7.9	143
15.	196.8	100.3	118.4	215.2	430.5	11.6	189
20.	244.1	129.3	152.5	277.3	554.5	15.0	241
25.	295.0	154.2	182.0	330.8	661.6	18.3	295
30.	348.1	177.1	209.0	379.9	759.8	21.4	350

NEON (CONT'D)

KEV	PR RANGE	DELTA	HALF	ONE	FOUR	E NUCLEAR	
35.	402.4	198.7	234.5	426.3	852.6	24.3	406
40.	457.7	219.5	259.0	470.8	941.5	27.2	462
45.	513.6	239.5	282.6	513.7	1027.3	29.9	518
50.	570.1	258.8	305.4	555.1	1110.3	32.5	575
55.	626.9	277.5	327.5	595.3	1190.7	34.9	632
60.	684.0	295.7	349.0	634.4	1268.7	37.3	689
65.	741.2	313.4	369.8	672.3	1344.6	39.6	748
70.	798.7	330.6	390.1	709.1	1418.3	41.8	803
75.	856.2	347.3	409.8	745.0	1490.0	44.0	860
80.	913.8	363.6	429.0	779.9	1559.8	46.0	917
85.	971.3	379.4	447.7	813.9	1627.8	48.0	970
90.	1028.9	394.9	465.9	847.0	1693.9	49.9	1031
95.	1086.4	409.9	483.7	879.2	1758.4	51.8	1087
100.	1143.8	424.5	501.0	910.6	1821.3	53.5	1144
105.	1201.2	438.8	517.8	941.3	1882.6	55.3	1200
110.	1258.4	452.8	534.3	971.2	1942.4	57.0	1257
115.	1315.5	466.4	550.3	1000.4	2000.7	58.6	1313
120.	1372.4	479.6	566.0	1028.8	2057.7	60.2	1361
125.	1429.2	492.6	581.3	1056.6	2113.3	61.7	1427
130.	1485.8	505.3	596.2	1083.8	2167.6	63.2	1485
135.	1542.3	517.6	610.8	1110.3	2220.6	64.7	1535
140.	1598.6	529.7	625.1	1136.2	2272.4	66.1	1596
145.	1654.6	541.5	639.0	1161.6	2323.1	67.5	1648
150.	1710.5	553.1	652.6	1186.3	2372.7	68.8	1700
175.	1983.8	607.2	716.5	1302.4	2604.8	75.1	1971
200.	2257.8	656.0	774.0	1407.0	2814.0	80.7	2237
225.	2523.2	700.2	826.2	1501.9	3003.9	85.7	2497
250.	2783.2	740.6	873.9	1588.5	3177.0	90.2	2751
275.	3037.8	777.6	917.5	1667.9	3335.8	94.4	3001
300.	3287.3	811.7	957.8	1741.0	3482.1	98.2	3246
325.	3532.0	843.2	995.0	1808.7	3617.4	101.8	3486
350.	3772.0	872.5	1029.6	1871.6	3743.2	105.0	3722
375.	4007.7	899.8	1061.8	1930.2	3860.3	108.1	3954

NEON (CONCLUDED)

KEV	PR RANGE	DELTA	HALF	ONE	FOUR	E NUCLEAR	
400.	4239.1	925.4	1091.9	1984.9	3969.8	110.9	4182
425.	4466.4	949.3	1120.2	2036.2	4072.5	113.6	4408
450.	4690.0	971.8	1146.7	2084.4	4168.9	116.1	4628
475.	4909.8	992.9	1171.7	2129.9	4259.7	118.5	4848
500.	5126.1	1012.9	1195.3	2172.7	4345.4	120.7	5057
525.	5339.1	1031.8	1217.6	2213.3	4426.5	122.9	5267
550.	5548.7	1049.7	1238.7	2251.7	4503.4	124.9	5474
575.	5755.3	1066.7	1258.7	2288.1	4576.3	126.8	5679
600.	5958.9	1082.9	1277.8	2322.8	4645.6	128.6	5880
625.	6159.7	1098.3	1296.0	2355.8	4711.6	130.4	6079
650.	6357.7	1113.0	1313.3	2387.3	4774.6	132.1	6275
675.	6353.0	1127.0	1329.8	2417.4	4334.7	133.7	6468
700.	6745.8	1140.4	1345.6	2446.1	4892.2	135.2	6659
725.	6936.1	1153.2	1360.8	2473.6	4947.2	136.7	6848
750.	7124.0	1165.5	1375.3	2500.0	5000.0	138.1	7034
875.	8030.9	1220.0	1439.6	2617.0	5234.0	144.4	7934
1000.	8889.0	1265.4	1493.2	2714.3	5428.6	149.8	8787
1125.	9705.4	1303.9	1538.6	2796.8	5593.7	154.5	9599
1250.	10485.4	1337.0	1577.7	2868.0	5735.9	158.5	1037

APPENDIX B

PENETRATION OF ELECTRONS IN ZnO

E_B (keV)	X_R (mg/cm^2)	X_R (Å)	I_B (uA)	$\frac{I_B E_B}{X_R}$
1	.0037	66		
2	.0129	286		
3	.0269	477		
4	.0455	806		
5	.0680	1205	.57	23.5
6	.0940	1666		
7	.1250	2216		
8	.1600	2836		
9	.1990	3527		
10	.2400	4254	1.00	23.5
11	.2850	5051		
12	.3350	5938		
13	.3860	6842		
14	.4430	7852		
15	.5000	8862	1.39	23.5
16	.5600	9926		
17	.6300	11166		
18	.7000	12407		
19	.7700	13648		
20	.8400	14888	1.75	23.5
21	.9200	16306		
22	1.0000	17724		
23	1.0900	19319		
24	1.1800	20915		
25	1.2650	22421	2.10	23.5

REFERENCES

1. M. Neuberger, II-VI Semiconducting Compound Data Tables. Electronic Properties Information Center, Hughes Aircraft Company. Culver City, California.

2. S. C. Abrahams and J. L. Bernstein, "Remeasurement of the Structure of Hexagonal ZnO." Acta Crystallographics, B 25:1233 - 1236 (1969).

3. J. C. Phillips, "Ionicity of the Chemical Bond." Reviews of Modern Physics, 42:317-356 (July 1970).

4. D. L. Denburg and G. L. Dybwad. "Diagnostic Rate Monitoring of Sputtered ZnO Films." Journal of Applied Physics, 44:2724-2729 (June 1973).

5. H. W. Lehmann and R. Widmer. "RF Sputtering of ZnO Shear-Wave Transducers." Journal of Applied Physics, 44:3868-3879 (September 1973).

6. F. S. Hickernell and J. W. Brewer, "Surface-Elastic-Wave Properties of DC-Triode-Sputtered Zinc Oxide Films." Journal of Applied Physics, 44:389-391 (January 1973).

7. J. M. Hammer, et al. "Low-Loss Epitaxial ZnO Optical Waveguides." Journal of Applied Physics, 44:358-360 (January 1973).

8. J. M. Hammer, et al. "Fast Electro-Optic Waveguide Deflector Modulator." Applied Physics Letters, 23:176-177 (15 August 1973).

9. James F. Gibbons, "Ion Implantation in Semiconductors - Part I Range Distribution in Semiconductors." Proceedings of the IEEE, 56:295-319 (March 1968).

10. Lewis T. Chadderton, Radiation Damage in Crystals. New York: Barnes and Noble, Inc., (1965).

11. G. Dearnaley, "Ion Penetration." in Proceedings of the European Conference on Ion Implantation. Stevenage, Herts., England: Peter Peregrinus Ltd., (1970).

12. G. J. Dienes and G. H. Vineyard. Radiation Effects in Solids. New York: Interscience Publishers, Inc., (1957).

13. G. Dearnaley, et al. Ion Implantation. Amsterdam: North Holland Publishing Company, (1973).

14. R. M. Eisberg, Fundamentals of Modern Physics. New York: John Wiley and Sons, Inc., (1961).

15. R. B. Leighton, Principles of Modern Physics. New York: McGraw Hill Book Co., (1959).

REFERENCES (CONT'D)

16. W. S. Johnson and J. F. Gibbons. Projected Range Statistics in Semiconductors. Stanford, California: Stanford University Bookstore, (1970).

17. J. W. Mayer et al. Ion Implantation in Semiconductors. New York: Academic Press, (1970).

18. G. D. Watkins, "Irradiation Effects in II-VI Compounds." Radiation Effects, 9:105-113 (1971).

19. W. E. Vehse, et al. "Radiation Damage in ZnO Single Crystals." Physical Review, 167:828-836 (15 March 1968).

20. D. R. Locker and J. M. Meese. "Displacement Thresholds in ZnO." IEEE Transactions on Nuclear Science, NS-19:237-242 (December 1972).

21. J. M. Meese and D. R. Locker. "Oxygen Displacement Energy in ZnO." Solid State Communications, 11:1547-1550 (1972).

22. B. R. Appleton and L. C. Feldman. "Investigation of Interstitial Zn Concentrations in Additively Colored ZnO Using the Unidirectional Channeling and Blocking Technique." Journal of Physics and Chemistry of Solids, 33:507-517 (1972).

23. L. C. Feldman and B. R. Appleton. "Unidirectional Channeling and Blocking: A New Technique for Defect Studies." Applied Physics Letters, 15:305-307 (9 February 1970).

24. J. M. Smith and W. E. Vehse. "ESR of Electron Irradiated ZnO: Confirmation of the F Center." Physics Letters, 31A:147-148 (9 February 1970).

25. G. H. Kinchin and R. S. Pease. "The Displacement of Atoms in Solids by Radiation." Reports on Progress in Physics, XVIII: 1-51 (1955).

26. R. Heckingbottom and T. Ambridge. "Ion Implantation in Compound Semiconductors - An Approach Based on Solid State Theory." Radiation Effects, 17:31-36 (1973).

27. R. M. Allen, "Implantation of Compound Semiconductors." in Proceedings of the European Conference on Ion Implantation. Stevenage, Herts., England: Peter Peregrinus Ltd., (1970).

28. G. Carter, et al. "Radiation Damage by Implanted Ions in GaAs and GaP." in Ion Implantation, edited by Fred H. Eisen and Lewis T. Chadderton. London: Gordon and Breach, (1971).

29. Naguib, et al. "On the Damage Induced in GaP Single Crystals by Te Ion Bombardment." Radiation Effects, 18:279-281 (1973).

REFERENCES (CONT'D)

30. A. B. Campbell, et al. "Tellurium Implants into GaP at Elevated Temperatures - Atom Site Location and Damage." Radiation Effects, 17:19-24 (1973).

31. S. A. Armitage, "Damage Studies in Ion - Implanted CdS." in Proceedings of the European Conference on Ion Implantation. Stevenage, Herts., England: Peter Peregrinus Ltd., (1970).

32. J. A. Olley, et al. "Radiation Damage in II-VI Semiconductors." in Proceedings of the European Conference on Ion Implantation. Stevenage, Herts., England: Peter Peregrinus Ltd., (1970).

33. James A. Hutchby, "Optical Reflection Studies of Lattice Disorder in Iodine Implanted CdS." Radiation Effects, 16:1-4 (1972).

34. J. A. Hutchby, et al. "Lattice Disorder in Br, Cl, and F Implanted CdS - Optical Reflection Study." in Ion Implantation in Semiconductors and Other Materials, edited by Billy L. Crowder. New York: Plenum Press, (1973).

35. W. E. Miller, et al. "Lattice Disorder in Cl, Br, and F Implanted CdS - Channeling Study." in Ion Implantation in Semiconductors and Other Materials, edited by Billy L. Crowder, New York: Plenum Press, (1973).

36. V. V. Makarov, "Cathodoluminescence of SiC Crystals of Various Modifications Containing Defects." Soviet Physics - Solid State, 9: 457-460 (August 1967).

37. C. E. Barnes, et al. "Photoluminescence, Optical Absorption, and Cathodoluminescence in Ion Implanted CdS." in Ion Implantation in Semiconductors and Other Materials, edited by Billy L. Crowder. New York: Plenum Press, (1973).

38. C. B. Norris, et al. "Depth-Resolved Cathodoluminescence in Undamaged and Ion-Implanted GaAs, ZnS, and CdS." Journal of Applied Physics, 44:3209-3221 (July 1973).

39. W. Ehrenberg and J. Franks. "The Penetration of Electrons into Luminescent Materials." Proceedings of the Physical Society, LXVI: 1057-1066 (1953).

40. W. Ehrenberg and D. E. N. King. "The Penetration of Electrons into Luminescent Materials." Proceedings of the Royal Society, 81: 751-766 (1963).

41. Marvin Rosenstein, et al. "Electron Depth-Dose Distribution Measurements in Finite Polystyrene Slabs." Journal of Applied Physics, 43:3191-3202 (July 1972).

REFERENCES (CONT'D)

42. A. E. Grun, "Lumineszenz-photometrische Messungen der Energieabsorption im Strahlungsfeld von Elektronenquellen Eindimensionaler Fall in Luft." Zeitschrift fur Naturforschung, 12a:89-95 (1957).

43. J. R. Fiebiger and R. S. Muller. "Pair-Production Energies in Silicon and Germanium Bombarded with Low-Energy Electrons." Journal of Applied Physics, 43:3202-3207 (July 1972).

44. F. S. Goulding and Y. Stone. "Semiconductor Radiation Detectors." Science, 170:280-289 (October 1970).

45. G. Y. Gergely, "Surface Recombination and Diffusion Processes in Cathodoluminescence and Electron Bombardment Induced Conductivity." Journal of Physics and Chemistry of Solids, 17:112-116 (1960).

46. G. Y. Gergely, "Space Charge Effects in Ambipolar Diffusion of Charge Carriers Induced by Electron Bombardment in Photoconducting Insulator Crystals." Journal of Physics and Chemistry of Solids, 21:105-109 (1961).

47. Mitsuhashi, et al. "Dislocation Effects on Luminescence of CdS Crystals." in II-VI Semiconducting Compounds, edited by D. G. Thomas. New York: W. A. Benjamin, Inc., (1967).

48. Shigeo Shionoya. "Luminescence of Lattices of the ZnS Type ." in Luminescence of Inorganic Solids, edited by Paul Goldberg. New York: Academic Press, (1966).

49. R. E. Halsted, "Radiative Recombination in the Band Edge Region." in Physics and Chemistry of II-VI Compounds, edited by M. S. Aven and J. S. Prener. Amsterdam: North Holland Publishing Co., (1967).

50. D. Curie and J. S. Prener. "Deep Center Luminescence." in Physics and Chemistry of II-VI Compounds, edited by M. S. Aven and J. S. Prener. Amsterdam: North Holland Publishing Co., (1967).

51. S. Shionoya, "Optical Properties of Defects in II-VI Compounds." in II-VI Semiconducting Compounds, edited by D. G. Thomas. New York: W. A. Benjamin, Inc., (1967).

52. S. Shionoya, "Review of Luminescence in II-VI Compounds." in Luminescence, edited by Ferd E. Williams. Amsterdam: North Holland Publishing Co., (1970).

53. G. F. J. Garlick, "Recombination Emission in Inorganic Solids." Reports on Progress in Physics, XXX:491-561 (1967).

54. P. J. Dean, "Junction Electroluminescence." Applied Solid State Science, I 2-140 (1969).

REFERENCES (CONT'D)

55. M. A. Lampert, "Mobile and Immobile Effective - Mass - Particle Complexes in Nonmetallic Solids." Physical Review Letters, 1: 450-453 (December 15, 1968).

56. J. R. Haynes, "Experimental Proof of the Existence of a New Electronic Complex in Silicon." Physical Review Letters, 4: 361-363 (April 1, 1960).

57. R. E. Halsted and M. Aven. "Photoluminescence of Defect-Exciton Complexes in II-VI Compounds." Physical Review Letters, 14:64-65 (18 January 1965).

58. J. J. Hopfield, et al. "Pair Spectra in GaP." Physical Review Letters, 10:162-164 (1 March 1963).

59. P. J. Dean and J. L. Merz. "Pair Spectra and Edge Emission in Zinc Selenide." Physical Review, 178:1310-1318 (15 Feburary 1969).

60. C. H. Henry, et al. "Double - Donor - Acceptor Pair Lines and the Chemical Identification of the I_1 Lines in CdS." Physical Review Letters, 24:820-822 (13 April 1970).

61. D. G. Thomas, et al. "Light from Distan Pairs." in Radiative Recombination in Semiconductors, edited by M. Hulin. Paris: Dunod, (1964).

62. J. S. Prener and F. E. Williams. "Associated Donor - Acceptor Luminescent Centers." Physical Review, 132:1427-1438 (February 1956).

63. E. F. Gross and D. S. Nedzvetsky. "Fine Structure of Decay Time and the Dependence of Luminescence Spectrum on the Exciting Light Intensity in GaP Crystals." in Radiative Recombination in Semiconductors, edited by M. Hulin. Paris: Dunod, (1964).

64. K. Colbow, "Free - to - Bound and Bound - to - Bound Transitions in CdS." Physical Review, 141:742-749 (January 1966).

65. G. Dresselhaus, "Effective Mass Approximation for Excitons." Journal of Physics and Chemistry of Solids, 1:14-22 (1956).

66. R. Englman and B. Barnett. "Quantitative Theory of Luminescent Centers in a Configurational Coordinate Model. I. Description of the Method." Journal of Luminescence, 3:37-55 (1970).

67. B. Barnett and R. Englman. "Quantitative Theory of Luminescent Centers in a Configurational Coordinate Model II. Results and Their Interpretation." Journal of Luminescence, 3:55-74 (1970).

68. C. C. Klick and J. H. Schulman. "Luminescence in Solids." Solid State Physics, 5:97-172 (1957).

REFERENCES (CONT'D)

69. D. Curie, Luminescence in Crystals. Paris: Dunod, (1960).

70. R. P. Messmer and G. D. Watkins. "Linear Combination of Atomic Orbital - Molecular Orbital Treatment of the Deep Defect Level in a Semiconductor: Nitrogen in Diamond." Physical Review Letters, 25:656-659 (7 September 1970).

71. G. D. Watkins and R. P. Messmer. "An LCAO - MO Treatment for a Deep Defect Level in a Semiconductor." Tenth International Conference on Physics of Semiconductors, August 17-21, 1970 Cambridge Massachusetts Conference - 700801 National Technical Info Service, Springfield, Va. (October 1970).

72. E. B. Moore and C. M. Carlson. "Calculation of the Physical Properties of Solids by the Extended Huckel Theory." Physical Review B, 4:2063-2065 (15 September 1971).

73. G. D. Watkins and R. P. Messmer. "Calculation of the Physical Properties of Solids by Extended Huckel Theory: A Reply." Physical Review B, 4:2065-2067 (15 September 1971).

74. R. P. Messmer and G. D. Watkins. "Molecular-Orbital Treatment for Deep Levels in Semiconductors: Substitutional Nitrogen and the Lattice Vacancy in Diamond." Physical Review B, 7:2568-2590 (15 March 1973).

75. R. H. Bube. Photoconductivity of Solids. New York: John Wiley and Sons, Inc., (1960).

76. D. C. Reynolds, et al. "Zeeman Effects in the Edge Emission and Absorption of ZnO." Physical Review, 140:A1726-A1734 (29 November 1965).

77. G. Heiland, et al. "Electronic Processes in ZnO." Solid State Physics, 8:193-326 (1959).

78. H. E. Brown, Zinc Oxide Rediscovered. New York: New Jersey Zinc Co., (1957).

79. Ch. Solbrig and E. Mollwo. "Der Einfluss Von Temperatur and Uniavialer Verspannung auf das Linienspektrum von Zinkoxyd - Kristallen." Solid State Communications, 5:625-631 (1967).

80. Ya. M. Zelikin and A. P. Zhukovskii. "The Yellow Luminescence of Zinc Oxide." Optics and Spectroscopy, 11:212-215 (1961).

81. O. F. Schirmer and D. Zwingel. "The Yellow Luminescence of Zinc Oxide." Solid State Communications, 8:1559-1563 (1970).

82. Yu. M. Gerbshtein and Ya. M. Zelikin. "On the Nature of Yellow-Orange Luminescence Centers in Zinc Oxide." Optics and Spectroscopy, 27:275-276 (1969).

REFERENCES (CONT'D)

83. V. V. Osiko, "The Low Temperature Luminescence of ZnO in the Red Region of the Spectrum." Optics and Spectroscopy, 7:454-457 (1959).

84. Yu. M. Gerbshtein and Yu. M. Zelikin. "On the Red Luminescence Band of Zinc Oxide." Optics and Spectroscopy, 28:521-522 (1970).

85. R. B. Lauer "The I.R. Photoluminescence Emission Band in ZnO." Journal of Physics and Chemistry of Solids, 34:249-253 (1973).

86. F. H. Nicoll, "Ultraviolet ZnO Laser Pumped by an Electron Beam." Applied Physics Letters, 9:13-15 (1 July 1966).

87. F. H. Nicoll, "Zinc Oxide Crystals for Electron-Beam Pumped Lasers."

88. J. M. Hvam, "Electron-Beam Pumped Laser Action in ZnO from 15°K to 250°K." Tenth International Conference on Physics Of Semiconductors, August 17-21, 1970 Cambridge Massachusetts Conference - 700801 National Technical Info Service, Springfield, Va. (October 1970).

89. J. Shewchun, et al. "Lasing Action in Electron-Beam-Pumped ZnO." Journal of Applied Physics, 43:545-549 (February 1972).

90. W. D. Johnston, Jr. "Characteristics of Optically Pumped Platelet Lasers of ZnO, CdS, CdSe, and $CdS_{.6}Se_{.4}$ Between 300°K and 80°K." Journal of Applied Physics, 42:2731-2740 (June 1971).

91. T. Goto and D. W. Langer. "Stimulated Emission and Excited States of the I_6 Donor Electron in ZnO." Journal of Applied Physics, 42:5066-5071 (November 1971).

92. R. L. Weiher and W. C. Tait. "Contributions of Excitons to the Edge Luminescence in Zinc Oxide." Physical Review, 166:791-796 (15 February 1968).

93. I. Filinski and T. Skettrup. "Ultraviolet E Mission Spectrum of ZnO." Solid State Communications, 6:223-237 (1968).

94. T. Skettrup and L. R. Lidholt. "Decay Times of the Ultraviolet and Green Emission Lines in ZnO." Solid State Communications, 6:589-592 (1968).

95. D. C. Reynolds and T. C. Collins. "Excited Terminal States of a Bound Exciton-Donor Complex in ZnO." Physical Review, 185: 1099-1103 (15 September 1969).

96. R. L. Weiher and W. C. Tait. "Observation of Mixed-Mode Excitons in the Photoluminescence of Zinc Oxide." Physical Review, 185:1114-1116 (15 September 1969).

REFERENCES (CONT'D)

97. D. C. Reynolds, et al. "Phonon Sidebands on Bound Exciton Transitions in CdS and ZnO." Tenth International Conference on Physics of Semiconductors, August 17-21, 1970 Cambridge Massachusetts Conference - 700801 National Technical Info Service Springfield, Va. (October 1970). 519-524.

98. D. G. Thomas and J. J. Hopfield. "Bound Exciton Complexes." Physical Review Letters, 7:316-319 (15 October 1961).

99. D. G. Thomas and J. J. Hopfield. "Optical Properties of Bound Exciton Complexes in Cadmium Sulfide." Physical Review, 128: 2135-2148 (1 December 1962).

100. D. C. Reynolds and C. W. Litton. "Edge Emission and Zeeman Effects in CdS." Physical Review, 132:1023-1028 (June 1963).

101. D. C. Reynolds, et al. "Edge Emission and Magneto-Optical Effects in CdSe." Physical Review, 156:881-896 (15 April 1967).

102. R. G. Wheeler and J. C. Miklosz. "Exciton Structure and Zeeman Effects in Zinc Sulfide." in Radiative Recombination in Semiconductors, edited by M. Hulin. Paris: Dunod, (1964).

103. C. H. Henry and Nassau. "Lifetimes of Bound Excitons in CdS." Physical Review B, 1:1628-1634 (15 February 1970).

104. C. H. Henry and Nassau. "Lifetimes of Bound Excitons in CdS." in Luminescence, edited by Ferd Williams. Amsterdam: North Holland Publishing Co., (1970).

105. R. Dingle, "Luminescent Transitions Associated with Divalent Copper Impurities and the Green Emission from Semiconducting Zinc Oxide." Physical Review Letters, 23:579-581 (15 September 1969).

106. R. E. Dietz, et al. "Electronic Structure of Copper Impurities in ZnO." Physical Review, 132:1559-1569 (15 November 1963).

107. D. Zwingel, "Trapping and Recombination Processes in the Thermoluminescence of Li-Doped ZnO Single Crystals." Journal of Luminescence, 5:385-405 (1972).

108. O. F. Schirmer, "The Structure of the Paramagnetic Lithium Center in Zinc Oxide and Beryllium Oxide." Journal of Physics and Chemistry of Solids, 29:1407-1429 (1968).

109. J. L. Merz, et al. "Ion Implantation of Bismuth into GaP I. Photoluminescence." in Ion Implantation, edited by F. H. Eisen and L. T. Chadderton. New York: Gordon and Breach, Science Publishers, Inc., (1971).

REFERENCES (CONT'D)

110. L. C. Feldman, et al. "Implantation of Bi into GaP II. Channeling Studies." in Ion Implantation, edited by F. H. Eisen and L. T. Chadderton. New York: Gordon and Breach, Science Publishers, Inc., (1971).

111. J. S. Harris and F. H. Eisen. "The Annealing of Damage in Ion Implanted Gallium Arsenide." in Ion Implantation, edited by F. H. Eisen and L. T. Chadderton. New York: Gordon and Breach, Science Publishers, Inc., (1971).

112. J. S. Harris, et al. "Influence of Implantation Temperature and Surface Protection on Tellurium Implantation in GaAs." Applied Physics Letters, 21:601-603 (15 December 1972).

113. B. Tell, et al. "Ion Implantation of Sodium, Lithium, and Neon in Cadmium Sulfide." Applied Physics Letters, 17:315-318 (15 October 1970).

114. B. Tell, "Properties of the Alkalis in CdS." Journal of Applied Physics, 42:2919-2924 (June 1971).

115. C. H. Henry, et al. "Optical Studies of Shallow Acceptors in CdS and CdSe." Physical Review B, 4:2453-2463 (15 October 1971).

116. J. J. Santiago, et al. "Annealing Studies of Broad-Band Luminescence from Ion-Implanted ZnSe." in Ion Implantation in Semiconductors and Other Materials, edited by Billy L. Crowder. New York: Plenum Press, (1973).

117. E. H. Putley, The Hall Effect and Semiconductor Physics, New York, Dover, (1960).

118. L. J. van der Pauw, "Specific Resistivity of Flat Samples of Arbitrary Shape." Philips Research Reports, 13:1-9 (February 1958).

119. P. M. Hemenger, "Measurement of High Resistivity Semiconductors Using the van der Pauw Method." Review of Scientific Instruments, 44:698-700 (June 1973).

120. J. P. McKelvey, Solid State and Semiconductor Physics. New York, Harper and Row, (1966).

121. D. G. Thomas and J. J. Lander. "Hydrogen as a Donor in Zinc Oxide." The Journal of Chemical Physics, 25:1136-1142 (December 1956).

122. D. G. Thomas, "Interstitial Zinc in Zinc Oxide." Journal of Physics and Chemistry of Solids, 3:229-237 (1957).

REFERENCES (CONT'D)

123. D. G. Thomas, "The Diffusion and Precipitation of Indium in Zinc Oxide." Journal of Physics and Chemistry of Solids, 9:31-42 (1958).

124. J. J. Lander, "Reactions of Lithiumas a Donor and Acceptor in ZnO." Journal of Physics and Chemistry of Solids, 15:324-334 (1960).

125. A. R. Hutson, "Hall Effect Studies of Doped Zinc Oxide Single Crystals." Physical Review, 108:222-230 (15 October 1957).

126. A. R. Hutson, "Electronic Properties of ZnO." Journal of Physics and Chemistry of Solids, 8:467-472 (1959).

127. J. W. Mayer, et al. "Ion Implantation of Silicon II. Electrical Evaluation Using Hall Effect Measurements." Canadian Journal of Physics, 45:4073-4089 (1967).

128. N. G. E. Johansson, et al. "Technique Used in Hall Effect Analysis of Ion Implanted Si and Ge." Solid State Electronics, 13:317-335 (1970).

129. R. G. Hunsperger and O. J. Marsh. "Electrical Properties of Cd, Zn, and S Ion-Implanted Layers in GaAs." in Ion Implantation, edited by F. H. Eisen and L. T. Chadderton. New York: Gordon and Breach, Science Publishers, Inc., (1971).

130. J. D. Sansbury and J. F. Gibbons. "Properties of Implanted Silicon, Sulfur, and Carbon in Gallium Arsenide." in Ion Implantation, edited by F. H. Eisen and L. T. Chadderton. New York: Gordon and Breach, Science Publishers, Inc., (1971).

131. P. M. Hemenger and B. C. Dobbs. "Zinc Ion Implantation of Sulfur Doped GaP." Applied Physics Letters, 23:462-464 (15 October 1973).

132. W. W. Anderson and J. T. Mitchell. "Phosphorous-Ion-Implanted CdS." Applied Physics Letters, 12:334-336 (15 May 1968).

133. S. L. Hou and J. A. Marley Jr. "Photoelectronic Properties of Ion-Implanted CdS." Applied Physics Letters, 16:467-469 (1 June 1970).

134. H. Sugimoto, et al. "New Electron Paramagnetic Resonance in Nitrogen-Ion-Implanted CdS." Applied Physics Letters, 18: 461-463 (15 May 1971).

135. Y. S. Park and B. K. Shin. "Ion-Implanted ZnSe p-n Junction Devices." in Proceedings of Solid State Devices Conference. Tokyo (1973).

REFERENCES (CONT'D)

136. Y. S. Park and C. H. Chung. "Type Conversion and p-n Junction Formation in Lithium-Ion-Implanted AnSe." Applied Physics Letters, 16:99-102 (1 February 1971).

137. S. L. Hou, et al. "Properties of Fluorine-Implanted ZnTe." Applied Physics Letters, 14:151-153 (1969).

138. J. Marine, "Properties of Ion Implanted ZnTe."

139. J. Marine and H. Rodot. "Properties of Ion Implanted ZnTe." Applied Physics Letters, 17:352-354 (1970).

140. F. Chernow, et al. "High Conductivity p-Type CdS." Applied Physics Letters, 12:339-341 (15 May 1968).

141. B. K. Shin, et al. "Electrical Characteristics of Aluminum-Implanted Zinc Selenide." Applied Physics Letters, 24:435-436 (May 1974).

142. B. W. Thomas and D. Walsh. "Anneal Characteristics of Ion-Implanted ZnO." Journal of Physics D, 6:612-615 (1973).

143. R. A. Laudise and A. A. Ballman. "Hydrothermal Synthesis of Zinc Oxide and Zinc Sulfide." Journal of Physical Chemistry, 64:688-691 (1960).

144. J. W. Nielsen and E. F. Dearborn. "The Growth of Large Single Crystals of Zinc Oxide." Journal of Physical Chemistry, 64: 1762-1763 (1960).

145. R. A. Laudise, et al. "Hydrothermal Growth of Large Sound Crystals of Zinc Oxide." Journal of the American Ceramic Society, 47:9-12 (1964).

146. E. D. Kolb and R. A. Laudise. "Properties of Lithium-Doped Hydrothermally Grown Single Crystals of Zinc Oxide." Journal of the American Ceramic Society, 48:342-345 (1965).

147. F. W. Sears, Thermodynamics. Reading: Addison - Wesley Publishing Co., Inc., (1950).

148. C. E. Bleil and J. G. Gay. "Exciton Line Widths and the Phonon Interaction in CdS." in II-VI Semiconducting Compounds, edited by D. G. Thomas. New York: W. A. Benjamin, Inc., (1967).

149. V. Segall, "Thermal Broadening of Exciton Levels in II-VI Compound Semiconductors." in Proceedings of IX International Conference on the Physics of Semiconductors. Leningrad: Nauka Publishing House, (1968).

REFERENCES (CONT'D)

150. F. J. Bryant, et al. "Interpretation of Asymmetric Band Shapes in Terms of Bound Exciton Complexes." Journal of Physics C, 6: 1316-1324 (1973).

151. V. L. Broude, et al. "Luminescence Kinetics of Free and Bound Excitons in CdS Crystals." Soviet Physics-Solid State, 14: 2971-2976 (June 1973).

152. D. C. Reynolds, et al. "Sharp Line Emission Due to Preferential Pairing in ZnO Crystals." Journal of the Physical Society of Japan, 21 (supplement):143-147 (1966).

153. C. W. Litton and D. C. Reynolds. "The Lasing Transitions of CdS." in II-VI Semiconducting Compounds, edited by D. G. Thomas, New York: W. A. Benjamin, Inc., (1967).

154. L. S. Pedrotti and D. C. Reynolds. "Energy Model for Edge Emission in Cadmium Sulfide." Physical Review, 120:1664-1669 (1 December 1960).

155. N. Hammond, et al. "Copper and Native Defects in Zinc Telluride." Journal of Physics and Chemistry of Solids, 34:1069-1073 (1973).

156. U. Flesch, et al. "Exciton Luminescence of Cubic ZnS Crystals." Journal of Luminescence, 3:137-142 (1970).

157. C. H. Henry, et al. "Donor-Acceptor Pair Lines in Cadmium Sulfide." Physical Review, 183:798-806 (15 July 1969).

158. S. Shionoya, et al. "Nature of Luminescence Transitions in ZnS Crystals." Journal of the Physical Society of Japan, 19:1157-1167 (July 1964).

*U.S.Government Printing Office: 1977 — 757-001/67

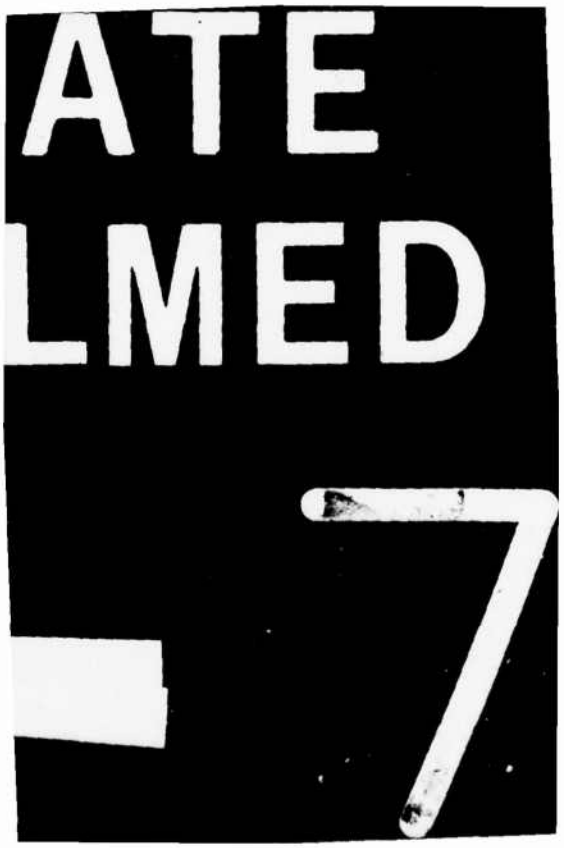
ATE
LMED
7